POLYMER-FILLER INTERACTIONS IN POLYETHER BASED THERMOPLASTIC POLYUREATHANE/SILICA NANOCOMPOSITES

by
ÖZGE HEİNZ

Submitted to the Graduate School of Engineering and Natural Sciences
in partial fulfillment of
the requirements for the degree of
Doctor of Philosophy

Sabancı University
Spring 2013

POLYMER-FILLER INTERACTIONS IN
POLYETHER BASED THERMOPLASTIC POLYUREATHANE/SILICA
NANOCOMPOSITES

APPROVED BY:

Prof. Dr. Yusuf Z. Menceloğlu .....

(Dissertation Supervisor)

Prof. Dr. İskender Yılgör .....

Prof. Dr. Yaşar Gürbüz .....

Assoc. Prof. Dr. Melih Papila .....

Asst. Prof. Dr. Burç Mısırlıoğlu .....

DATE OF APPROVAL: 07.06.2013

© Özge Heinz 2013

All Rights Reserved

POLYMER-FILLER INTERACTIONS IN
POLYETHER BASED THERMOPLASTIC POLYUREATHANE/SILICA
NANOCOMPOSITES

ABSTRACT

Thermoplastic polyurethaneureas (TPU) are a unique class of materials that are used in a broad range of applications due to their tailorable chemistry and morphology that allow engineering materials with targeted properties. The central theme of this dissertation is to develop an understanding on polymer-filler interfacial interactions and related reinforcing mechanism of silica nanoparticles in polyether based TPU/silica nanocomposites. Prior to our investigation on nanocomposite materials, the growth of silica nanoparticles in different solvents was studied by monitoring the temporal changes in tetraethyl orthosilicate concentration and in the average diameter of silica particles during initial hydrolysis of tetraethyl orthosilicate in C1-C4 alcohols. Stable silica sols in iso-propanol, which is a common solvent for studied TPU copolymers, were prepared in a controlled manner.

Nanocomposites consisting of TPU and silica nanoparticles of various size (20-250 nm) and filler loadings (1-40 weight%) were prepared by solution blending and characterized. TPU copolymer was based on a cycloaliphatic diisocyanate and hydroxyl terminated poly(tetramethylene oxide) or poly(ethylene oxide) with number average molecular weight of 2000 g/mol and 2-methyl-1,5-diaminopentane chain extender. Even distribution of silica in copolymer matrices led to higher modulus and tensile strength of the nanocomposites, and elastomeric properties were retained. The improvements in tensile properties of the nanocomposites mainly stemmed from the hydrogen-bonding between silanol groups on the surface of silica nanoparticles and ether linkages of the polyether segments of the copolymers. It was demonstrated that polyether based TPU/silica nanocomposites with a range of mechanical properties can be prepared by a simple technique.

Keywords: Nanocomposites, polyether based thermoplastic polyurethaneurea, silica, solution blending, polymer-filler interfacial interaction.

POLYMER-FILLER INTERACTIONS IN
POLYETHER BASED THERMOPLASTIC POLYUREATHANE/SILICA
NANOCOMPOSITES

ÖZET

Termoplastik poliüretanüre (TPU), hedeflenen özellikler doğrultusunda uyarlanabilen kimyası ve morfolojisi nedeniyle geniş bir uygulama aralığına sahip, bilimsel ve ticari açıdan önemli bir polimer sınıfıdır. Bu tezin ana teması, polieter bazlı TPU/silika nanokompozitlerde polimer/silika arayüzey etkileşiminin incelenmesi ve buna bağlı olarak gelişen morfolojik, termal ve mekanik özelliklerin tespit edilmesidir. Bu şekilde, TPU/silika nanokompozitlerde yapı/özellik ilişkisine bir anlayış getirilmesi hedeflenmektedir. Nanokompozit sistemler üzerindeki inceleme öncesinde, silika nanopartiküllerin içinde büyümesi ve tetraetil ortosilikat hidroliz reaksiyonu C1-C4 alkolleri içinde izlenmiştir. Kararlı silika soller, çalışılan TPU kopolimerler için ortak bir çözücü olan izo-propanol ortamında kontrollü bir şekilde hazırlanmıştır.

Çeşitli boyut (20-250 nm) ve dolgu yüklerine (ağırlıkça % 1-40) sahip TPU/silika nanokompozit filmler hazırlanmış ve karakterize edilmiştir. Polieter bazlı TPU, moleküler ağırlığı <Mn> 2,000 g/mol olan hidroksil sonlu poli(etilen oksit) ya da poli(tetrametilen oksit), halkalı alifatik diizosiyanat ve zincir uzatıcı olan kullanılan diaminden oluşmaktadır. Ortak çözücüde karıştırma tekniği ile silika nanopartiküllerin polieter bazlı TPU kopolimerde homojen dağılımı sağlanmıştır. Silika ilavesi ile kopolimerin elastomerik özellikleri korunurken daha yüksek elastik modül ve gerilme mukavemetine sahip nanokompozitler elde edilmiştir. Bunun yanı sıra, camsı geçiş sıcaklığında bir değişim gözlenmemiştir. Nanokompozit sistemlerin gerilme özelliklerindeki iyileşme, silika yüzeyindeki silanol grupları ile kopolimerlerin yumuşak kısımlarındaki eter gruplarının hidrojen bağı kurarak etkileşmelerinden kaynaklanmıştır. Bu çalışma ile üstün ve/veya istenilen mekanik özelliklere sahip polieter bazlı TPU/silika nanokompozit sistemlerin sunulan ortak çözücüde karıştırma tekniği ile hazırlanmasının mümkün olduğu gösterilmiş ve elde edilen iyileşmenin nedenleri sunulmuştur.

Anahtar Kelimeler: Nanokompozit, polieter bazli termoplastik poliuretanure, silika, çözeltide karıştırma, polimer-dolgu arayüzey etkileşimi.

ACKNOWLEDGEMENTS

I would like to thank my Ph.D. advisor Professor Yusuf Z. Menceloğlu for his guidance and enduring support throughout my time at Sabancı University. I am deeply grateful for his patience and understanding over the years.

Our collaborators Professor İskender Yılgör and Emel Yılgör at Koç University are highly appreciated for their contributions to this work, as well as their graduate student Çağla Koşak for polymer synthesis and characterization. I would like to thank Oğuzhan Oğuz for his friendship and help in the preparation and characterization of materials. Burçin Yıldız has been instrumental for the NMR studies and interpretation of data.

I am further grateful to the members of my dissertation committee, Professors Yaşar Gürbüz, Melih Papila, and Burç Mısırlıoğlu, for their time and advise.

During my time at Sabancı University, the support and advise of Professors Mehmet Ali Gülgün and Cleva Ow-Yang was very essential. I would also thank my labmates for their support and friendship, making my life enjoyable at SU.

I am eternally grateful to my father Ziya Kaşlı, my mother Esin Kaşlı and my brother Tahir Emre Kaşlı for their unconditional love and support.

I extend heartfelt thanks to my husband Hendrik Heinz. His love and support carried me through roughest times. And my little son Leonard Ege Heinz, thanks for being my sunshine.

TABLE OF CONTENTS

LIST OF FIGURES X

LIST OF TABLES XIV

LIST OF ABBREVIATIONS XV

1. INTRODUCTION 1

2. LITERATURE REVIEW 4

2.1. PART I: Silica 4

2.1.1. Synthesis of Silica by Sol-Gel Route: Stöber Method 7

2.1.2. Proposed Models for Growth Mechanism of Stöber Silica 11

2.1.3. Control over Particle Size and Polydispersity 12

2.1.4. Polymer/Silica Nanocomposites 14

2.2. PART II: Thermoplastic Polyurethanes 16

2.2.1. The Evolution of Thermoplastic Elastomers 16

2.2.2. Block Copolymers 18

2.2.3. Chemistry and Properties of Thermoplastic Polyurethanes 21

2.3. PART III: Thermoplastic Polyurethane Composites 29

2.3.1. TPU/Organoclay Nanocomposites 31

2.3.2. TPU/Silica Nanocomposites 32

3. METHODS 35

3.1. Experimental 35

3.1.1. Silica Sol Preparation 35

3.1.2. TPU Synthesis 36

3.1.3. TPU/Silica Composite Preparation 37

3.2. Characterization 38

3.2.1. Dynamic Light Scattering 38

3.2.2. Spectroscopy 39

3.2.2.1. Nuclear Magnetic Resonance Spectroscopy 39

3.2.2.2. Fourier Transform Infrared Spectroscopy (FT-IR) 40

3.2.3. Imaging 41

3.2.3.1. Scanning Electron Microscopy 41

3.2.3.2. Transmission Electron Microscopy 41

3.2.3.3. Atomic Force Microscopy 42
3.2.4. Thermal Analyses 42
3.2.4.1. Differential Scanning Calorimetry 42
3.2.4.2. Thermal Gravimetric Analysis 43
3.2.5. Mechanical Analysis 44
3.2.5.1. Tensile Testing 44
3.2.5.2. Nanoindentation 45

4. TEOS HYDROLYSIS KINETICS AND CONTROLLED SYNTHESIS OF SILICA NANOPARTICLES IN LOW MOLECULAR WEIGHT ALCOHOLS 47
4.1. Introduction 47
4.2. Chemical Reactions Kinetics of Stöber Systems 50
4.3. Experimental Section 52
4.3.1. Materials 52
4.3.2. Methods 52
4.4. Results and discussion 55
4.4.1. NMR Experiments 55
4.4.2. Dynamic Light Scattering Experiments 65
4.4.3. TEOS Hydrolysis Rate versus Silica Particle Size 71
4.4.3.1. Effect of TEOS, Ammonia and Water Concentration 71
4.4.3.2. Effect of Solvent 75
4.5. Conclusions 81

5. POLYURETHANEUREA-SILICA NANOCOMPOSITES: PREPARATION AND INVESTIGATION OF THE STRUCTURE-PROPERTY BEHAVIOR 82
5.1. Introduction 82
5.2. Experimental 84
5.2.1. Materials 84
5.2.2. Synthesis Polyurethaneurea Copolymer 84
5.2.3. Preparation and Characterization of Silica Sol 85
5.2.4. Preparation of Nanocomposites 86
5.2.5. Characterization of Nanocomposites 87
5.3. Results and Discussion 88
5.3.1. Preparation and Properties of the Colloidal Silica 88
5.3.2. Composition and the Morphology of the Nanocomposites 93
5.3.3. FTIR Studies on Nanocomposites 96
5.3.4. Thermal Analyses by DSC and TGA 99

5.3.5. Stress-Strain Behavior 102
5.3.6. Influence of Soft Segment Chemistry on Nanocomposite Properties 108
5.4. Conclusions 117
REFERENCES 119

LIST OF FIGURES

Figure 2-1: Two-dimensional representation of random versus regular packing of [Si-O_4]$^{4-}$ tetrahedra: amorphous (left) and crystalline silica [2]. 4
Figure 2-2: (a) Different types of surface silanol groups [7] and (b) aggregate formation between fumed silica particles through H-bonds [8]. 5
Figure 2-3: Illustration of various stages, end-products and applications of sol-gel processing [18]. The numbers refer to the processing stages. 7
Figure 2-4: Polymerization pathway of aqueous silicates according to Iler [19]. 9
Figure 2-5: Effects of pH on the sol stability (gel-time) of the colloidal silica-water system [19]. 10
Figure 2-6: Urethane linkage formed by the reaction of isocyanate and hydroxyl groups. 16
Figure 2-7: Block copolymer architectures. 18
Figure 2-8: Schematic representation of polyurethane structures at various temperatures: (a) room temperature phase-separated morphology and (b) most dissociated structures at high temperature [72]. 20
Figure 2-9: Schematic representation of a TPU composed of diisocyanate, long-chain diol, and chain extender [63]. 22
Figure 2-10: Chemical Composition of commercial thermoplastic polyurethanes [60]. 23
Figure 2-11: TPU synthesis via prepolymer method by the use of diol type chain extender [74]. 26
Figure 2-12: Hydrogen bonding in TPUs. 27
Figure 3-1: Tetraethyl orthosilicate (TEOS) molecule. 35
Figure 3-2: Chemical structures of the chemicals that constitute TPU. 37
Figure 4-1: Silica sols prepared in ethanol, n-propanol, iso-propanol and n-butanol after one month. 52
Figure 4-2: Hydrolysis of TEOS under basic conditions. 55
Figure 4-3: In-situ liquid ^{29}Si-NMR spectra of reaction mixture in (a) ethanol, (b) n-propanol, (c) iso-propanol, (d) n-butanol and (e) methanol. 58
Figure 4-4: (a) Time-dependent TEOS consumption in different solvents and generation of singly hydrolyzed species in (b) methanol, (c) ethanol and n-butanol, (d) n-propanol and iso-propanol. 61

Figure 4-5: Proposed hydrolysis mechanism for TEOS under basic conditions [19]. ... 62
Figure 4-6: The typical ^{29}Si-NMR spectra of the reaction solution S7 with respect to time (inset) and the time dependent concentrations of soluble Si species (main)..... 64
Figure 4-7: The time dependent concentrations of soluble Si species for the solutions with molar ratio of TEOS/H_2O/NH_3 at S2: 1/8.5/3, S3: 1/4.2/1.5, S5: 1/8.5/1.5, S6: 1/3.2/1.1. 65
Figure 4-8: Change in the hydrodynamic radii of silica nanoparticles for S3 measured by DLS up to 10 days. 66
Figure 4-9: Average hydrodynamic diameter of silica particles as a function of time during synthesis in different solvents, analyzed by DLS. The solvents include methanol, ethanol, n-propanol, iso-propanol and n-butanol. The error bars indicate the width of the size distribution of the particles (full width at half maximum). 69
Figure 4-10: Tapping Mode AFM height images of silica nanoparticles synthesized in methanol, ethanol, n-propanol, iso-propanol, n-butanol and t-butanol (1x1μm). 70
Figure 4-11: Time-dependent TEOS monomer concentration in ethanol media: (a) [TEOS]:0.8 (S1), 0.32 (S3), 0.16 (S2); [NH_3]:0.48; [H_2O]:1.35, (b) [TEOS]: 0.32; [NH_3]:0.48 (S3), 0.36 (S8), 0.10 (S9); [H_2O]:1.35 , (c) [NH_3]: 0.48; [TEOS]:0.32; [H_2O]:1.35 (S3), 2.09 (S4), 2.74 (S5). (d) [TEOS]: 0.32; [NH_3]:0.48, [H_2O]: 1.35 (S3); [NH_3]:0.36, [H_2O]: 1.02 (S6); [NH_3]:2.39, [H_2O]: 6.77 (S7). The slope of straight line is the pseudo first-order rate constant of TEOS hydrolysis. 72
Figure 4-12: SEM images of silica particles synthesized by Stöber method. 74
Figure 4-13: TEOS hydrolysis rate versus particles size of silica particles in ethanol media prepared under various experimental conditions. 75
Figure 4-14: Effect of solvent alcohol chain length on hydrolysis rate of TEOS given by time dependent precursor consumption. The slope of straight line gives the pseudo first-order rate constant. 76
Figure 5-1: Time dependent TEOS consumption (main) and change in molarity (inset) in isopropanol for S2. 86
Figure 5-2: Tapping Mode AFM height images and profiles of (a) S1 (0.5x0.5 μm), (b) S2 and (c) S3 (2x2 μm). 90

Figure 5-3: TEM images of (a) S1, (b) S2 and (c) S3. 92
Figure 5-4: FTIR-ATR spectra of dried colloidal silica designated as S1, S2 and S3. .. 93
Figure 5-5: TEM image of TPU-PTMO-20-S2-20 blend dried on carbon coated Lacey formvar film supported in 300 mesh copper TEM grids. 95
Figure 5-6: SEM micrographs of TPU/silica nanocomposite cross-sections. 50 kX magnification: (a) TPU-PTMO-20 neat polymer, (b) TPU-PTMO-20-S1-20 (c) TPU-PTMO-20-S2-20 , (d) TPU-PTMO-20-S3-20, (e) TPU-PTMO-20-S2-40 and 20kX magnification: (f) TPU-PTMO-20-S3-20. 96
Figure 5-7: FTIR investigation of (a) N-H and (b) carbonyl regions of virgin TPU-20 and silica nanocomposites as a function of the amount of silica filler. 97
Figure 5-8: Comparative FTIR spectra of the ether region for TPU-PTMO-20 and its nanocomposites with S2. 98
Figure 5-9: Comparative FTIR spectra of the ether region for TPU-PTMO-20 and its nanocomposites with 20% by weight S1, S2 and S3. 99
Figure 5-10: DSC curves of PTMO, PTMO-S2-20, TPU-PTMO-20 and TPU-PTMO-20-S2-20. 100
Figure 5-11: TG curves of TPU/silica nanocomposites as a function of silica content. Dashed lines indicate the increase in thermal degradation temperature for 50%weight loss in the presence of silica particles. 102
Figure 5-12: Stress-strain curves of TPU-PTMO-20 and its nanocomposites containing 1 to 40wt% of S2 colloidal silica. 103
Figure 5-13: Stress-strain curves of TPU-PTMO-20 and nanocomposites containing 20 weight% S1, S2 and S3 colloidal silica. 104
Figure 5-14: SEM images of tensile-fractured surfaces of (a) TPU-PTMO-20 and (b) TPU-PTMO-20-S2-20. 106
Figure 5-15: SEM micrograph of a surface fracture on TPU-PTMO-20-S2-20. 107
Figure 5-16: Representation of hydrogen bonding in polyether based TPUs. 109
Figure 5-17: SEM micrographs of TPU-PEO-30-S2-20 at 100 kX magnification: (a) cross-section and (b) surface. 110
Figure 5-18: ATR-IR investigation of carbonyl region of the neat copolymer (TPU-PEO-30) and corresponding nanocomposites with filler loadings of 1-20wt%. 111
Figure 5-19: ATR-IR investigation of ether region of the neat copolymer (TPU-PEO-30) and corresponding nanocomposites with filler loadings of 1-20wt%. 112

Figure 5-20: DSC traces of neat copolymer (TPU-PEO-30) and corresponding nanocomposites with filler loadings of 1-20wt%. 113
Figure 5-21: Stress-strain curves of the neat copolymer (TPU-PEO-30) and corresponding nanocomposites with filler loadings of 1-20wt%. 114

LIST OF TABLES

Table 2-1: Various types of silica-polymer nanocomposites reported in the literature with the details on filler size, content and selected results. 15
Table 2-2: Chemical structure of various precursors utilized in PU chemistry [77]. 25
Table 2-3: Composition and preparation methods of thermoplastic polyurethane composites over the last decade..... 30
Table 4-1: Initial Stöber reactant compositions in different solvent media. 53
Table 4-2: Initial Stöber reactant compositions in ethanol media. 53
Table 4-3: Liquid ^{29}Si-NMR chemical shift (δ). 59
Table 4-4: Experimental conditions and results of *in-situ* liquid state ^{29}Si-NMR analyses (hydrolysis rate constant) and DLS measurements (hydrodynamic diameter of particles). 73
Table 4-5: Effect of solvents on hydrolysis rate and particle diameter. 77
Table 4-6: Solubility parameters of solvents at 25°C and contribution of various components [152]. 79
Table 5-1: Properties of the colloidal silica (and sols) incorporated in TPU/silica nanocomposites. 89
Table 5-2: Compositions of TPU/colloidal silica composites. 93
Table 5-3: Thermal properties of the TPUs/silica nanocomposites. 101
Table 5-4: Tensile properties of TPU-20 and silica nanocomposites..... 105
Table 5-5: Nanomechanical properties of nanocomposites containing 20 weight% silica 105
Table 5-6: Compositions of TPU-PEO/colloidal silica composites. 108
Table 5-7: Tensile properties of TPU polymers with various soft segment components with molecular weight of 2000 g/mol and hard segment ratio. 109
Table 5-8: Mechanical test results of neat polymer and corresponding nanocomposites. 114
Table 5-9: Comparison of mechanical properties of PTMO and PEO based TPU/silica nanocomposites based on percent increase/decrease in Young's modulus (M), ultimate tensile strength (TS) and elongation at break (E). Percent changes were given in comparison with the corresponding properties of the neat polymers..... 115

LIST OF ABBREVIATIONS

AFM	Atomic force microscopy Chain extender
ATR	Attenuated transmission reflectance
DLS	Dynamic light scattering
DMF	N,N-Dimethyl formamide
DSC	Differential scanning calorimetry
FT-IR	Fourier transform infrared spectroscopy
GPC	Gel permeation chromatography
HMDI	Bis(4-isocyanatocyclohexyl)methane
IPA	Isopropanol
<Mn>	Number average molecular weight
NMR	Nuclear Magnetic Resonance
PdI	Polydispersity index (DLS)
PDMS	Poly(dimethylsiloxane)
PEO	Poly(ethylene oxide)
PTMO	Poly(tetramethylene oxide)
SAXS	Small-angle X-ray scattering
SEM	Scanning electron microscope
SLS	Static light scattering
TEM	Transmission electron microscope
TEOS	Tetraethyl orthosilicate
T_g	Glass transition temperature
TGA	Thermogravimetric analysis
THF	Tetrahydrofuran
TMOS	Tetramethyl orthosilicate
TPE	Thermoplastic elastomer(s)
TPU	Thermoplastic polyurethane(s)

1. INTRODUCTION

There is a growing interest in polymeric nanocomposite materials due to their improved characteristics and expanding fields of applications. This interest originates from the increased need for superior materials and the recent advances in characterization techniques of materials. Polymeric nanocomposites are mostly produced by homogeneous dispersion of nano-scaled inorganic building blocks within an organic polymer matrix. The purpose of organic/inorganic nanocomposites is to develop novel and superior materials by combining the characteristics of organic polymers such as flexibility, ductility, low-density and processibility with the characteristics of inorganic materials such as scratch resistance, hardness and thermal stability. Additionally, improvements in gas permeability characteristics and flame retardancy of materials are aimed.

Polyurethanes are produced in very high amounts throughout the world and are used in foam, coating and adhesive industries. Polyurethane chemistry is a very broad field and encompasses a large number of chemical reactions of diisocyanates with various active hydrogen-containing compounds allowing a wide range of end-products adaptable to various applications. Polymer chains in polyurethanes are composed of alternating hard and soft segments, which are linked by urethane linkages. Crosslinking in polyurethanes are provided by chemical or physical processes. Chemical crosslinking occurs when a tri- or more functional monomers are used and this leads to the formation of a network structure, which cannot be disrupted by heat treatment. Therefore, such polyurethane elastomers show thermoset polymer characteristics. On the other hand, crosslinking in thermoplastic polyurethanes (TPU) occurs by a physical process as a result of their microheterogeneous, two-phase morphology, which arises from the incompatibility between the hard and soft segments. TPUs, as a subclass of thermoplastic elastomers, combine the service properties of elastomers and the processing properties of thermoplastics with the possibility of recycling and reuse. TPUs can also be defined as linear-segmented multiblock copolymers with alternating

hard and soft segments. One type of block, hard segment, is formed by addition of chain extender, a low molecular weight diol or diamine, to the diisocyanate. The copolymer is named as polyurethaneurea when diamine is used as the chain extender. The other type is the soft segment, which is usually a high molecular weight macroglycol (e.g. polyether, polyester) that establishes the interconnection between two hard segments.

Thermoplastic polyurethanes are used in applications such as wire insulation, automobile fascia, footwear, wheels and adhesives. However, there is a growing interest to broaden the range of applications for TPUs beyond the current limits. The outstanding performance of TPUs is their resistance to abrasion and low coefficient of friction against other surfaces with tailorable hardness and low temperature flexibility characteristics. TPUs are very versatile materials with tailorable chemistry and commercial availability of a very large number of starting materials for their synthesis. For instance, mechanical properties of polyether based TPUs are somewhat lower than the polyester based counterparts, whereas they show superior low temperature flexibility and hydrolytic stability.

Until recently, fillers are not normally used in polyurethanes to bulk out the product. Nanoparticles and nano-sized organoclays are now being investigated and used to provide improved characteristics to TPUs. Commercially available TPUs and most of the academic work on TPUs and TPU nanocomposites have been mainly carried on polyester based materials. On the other hand, silica nanoparticles has been extensively used as fillers to reinforce several different polymeric matrices.

The central theme of this dissertation is to develop an understanding on polymer-filler interfacial interactions and related reinforcing mechanism of silica nanoparticles in polyether based TPU/silica nanocomposites. By this way, it would be possible to design TPU/silica nanocomposites with improved mechanical and thermal properties for several specific applications. The expected impact of this approach is to gain control over design parameters, and hence over ultimate properties of the TPU/silica nanocomposite materials by establishing a structure/property relation.

In *Chapter 2*, a broad overview of both silica and segmented copolymer literature is presented. A more comprehensive literature review of each topic is reserved for the appropriate chapter.

Experimental procedures and characterization techniques are briefly introduced in *Chapter 3*. Detailed explanations of the experimental sections are presented in the following chapters.

Chapter 4 includes the work on formation and growth of silica particles in low molecular weight alcohols (methanol, ethanol, n-propanol, isopropanol, n-butanol) and controlled synthesis of silica particles in ethanol as the parent alcohol. In the first part of this chapter, TEOS hydrolysis kinetics is monitored by using *in-situ* liquid ^{29}Si-NMR and dynamic light scattering to investigate the effects of concentration of reaction ingredients and type of solvent on hydrolysis rate and particle size, respectively. Solvent effects on initial hydrolysis kinetics, size and polydispersity of silica particles were discussed in terms of polarity and hydrogen-bonding characteristics of the solvents. The following part presents the preparation and characterization of colloidal silica in ethanol, where the effects of initial concentration of TEOS, ammonia and water were investigated.

Structure-property behavior of polyether based TPU with respect to filler size and loading as well as soft segment chemistry is presented in *Chapter 5*. Initially, the properties of silica nanoparticles prepared in isopropanol, which is the common solvent used for the preparation of TPU/silica nanocomposites, were introduced. First part of this chapter includes the effect of filler size and loading in poly(tetramethylene oxide) based TPU/silica nanocomposites. Finally, TPU/silica nanocomposites with poly(ethylene oxide) soft segments were investigated in order to demostrate the effect of soft segment chemistry on the morphology as well as mechanical and thermal properties of resultant TPU/silica nanocomposites. The effect of particle loading was studied for poly(ethylene oxide) based TPU/silica nanocomposites and the results were discussed in comparison with the results of the poly(tetramethylene oxide) based TPU/silica nanocomposites.

2. LITERATURE REVIEW

2.1. PART I: SILICA

Silicon, at 27.8 % by weight, is the second most abundant element after oxygen (46.6 % by weight) and it is the main component of the earth's crust [1]. In nature, silicon is almost always bonded to oxygen, either to oxygen alone as in silicon dioxide, silica (SiO_2), or as in the silicates with additional elements (e.g. bentonites such as montmorillonite and wollastonite). The natural silicates are mostly used as raw materials for the production of cement, glass, porcelain, brick, etc.

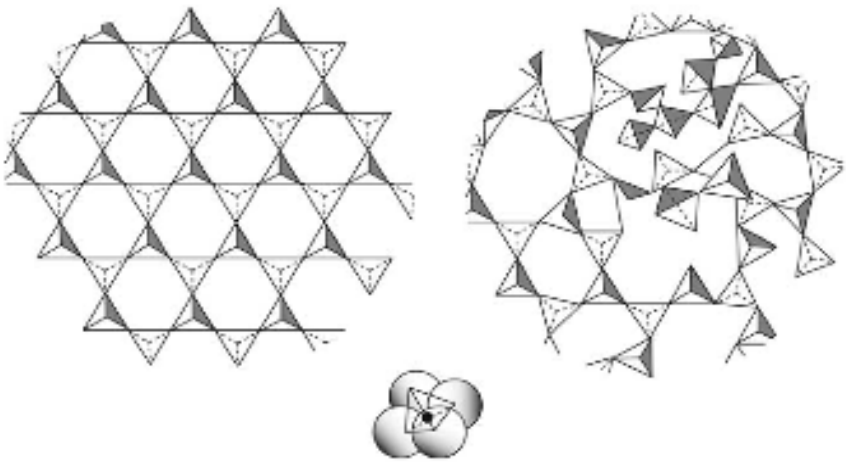


Figure 2-1: Two-dimensional representation of random versus regular packing of $[Si\text{-}O_4]^{4-}$ tetrahedra: amorphous (left) and crystalline silica [2].

The building block of silica and the silicate structures is the SiO_4 tetrahedron, four oxygen atoms at the corners of a regular tetrahedron with a silicon ion at the center cavity or centroid [3]. Silica can be natural or synthetic, crystalline or amorphous. All forms of silica contain the Si-O bond, which is the most stable of all Si-X element bonds. The Si-O bond length is about 0.162 nm, which is considerably smaller than the sum of the covalent radii of silicon and oxygen atoms (0.191 nm) [4]. Familiarity with

the structure of crystalline silica is helpful in understanding the bulk and surface structure of amorphous silica. In amorphous silica, the bulk structure is determined, as opposed to the crystalline silicas, by a random packing of $[SiO_4]^{4-}$ units, which results in a nonperiodic structure as shown by Figure 2-1 [5]. As a result of the structural differences the various silica forms have different densities (2-3 g/mol at 273 K) [2].

Surface chemistry of silica is a subject of intensive studies since many of the absorption, adhesion, chemical and catalytic properties of silicas depend on the chemistry and geometry of their surfaces. At the surface, silicas end in siloxane groups (Si-O-Si) and one of the several forms of silanol groups (Si-OH) lead to hydrophilic nature of the particles. Silanol groups on the surface may exist as free (isolated), vicinal or geminal silanols as shown in Figure 2-2 (a). The silanol groups residing on adjacent particles may form hydrogen bonds and to formation of aggregates as illustrated in Figure 2-2 (b). Silanol groups may also be found within the structure of colloidal particles and they are designated as internal silanols or structurally bound water. The silica surface OH groups are the main absorption and reaction centers. The average concentration silanol groups was found to be 4.9 OH groups per square nanometer as a result of 231 independent measurements, which is in good agreement with the numerical value (4.6 OH groups per square nanometer) obtained by Zhuravlev [6].

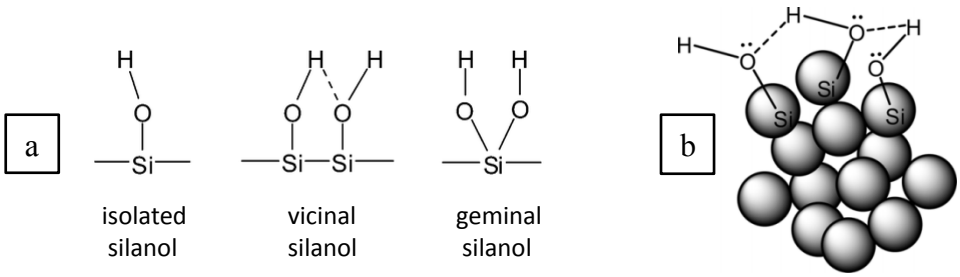


Figure 2-2: (a) Different types of surface silanol groups [7] and (b) aggregate formation between fumed silica particles through H-bonds [8].

Advances in nanotechnology have led to the production of nanosized silica (nanosilica), which has been widely used in many fields of colloid and materials science. Silica obtained from natural resources is non-reinforcing and has been used to reduce cost. It is also not favorable for advanced scientific and industrial applications since it contained metal impurities. Therefore, the synthetic silica (colloidal silica, silica

gels, pyrogenic silica, and precipitated silica), which is mostly in amorphous powder, has gained importance. There exist two main approaches to obtain silica particles: top-down and bottom-up. In the first case, which is a physical approach, special size reduction techniques are used to reduce the dimension of a bulk material. Bottom-up or chemical approach works in the opposite direction and the material is obtained starting from the atomic or molecular precursors. In general, three bottom-up methods have been used for the synthesis of silica nanoparticles: flame decomposition, precipitation, reverse micro-emulsion and sol-gel routes. These methods offer certain advantages with some limitations.

The commercially prominent method for the silica production is the high-temperature hydrolysis of silicon tetrachloride ($SiCl_4$) in the O_2/H_2 flame [1]. This continuous combustion process results in amorphous, large surface area fumed silica and the by-products steam and HCl. The nanometer-sized primary particles quickly form into aggregates that is followed by the formation of agglomerates [9]. In this way, so-called "fumed silica" is formed. Difficulty to control the size and morphology of the particles is the major drawback of this method.

Precipitated silicas are formed by consecutive coagulation and precipitation from silica solutions and defined as dry silicas with no long or short distance characteristic structure [10]. Precipitated silica is not as common as fumed silica in the preparation of nanocomposites because it has much higher tendency for agglomeration due to higher number of surface silanol groups compared to that of fumed silica.

In reverse microemulsion systems, nanodrops (3-30 nm) of the aqueous phase are trapped within aggregates (micelles) of 50-100 surfactant molecules dispersed in an external oil phase [11]. This method has been used for the surface modification of silica nanoparticles with different functional groups specifically for biotechnological applications [12-14]. In addition to the ease of surface modification, size and polydispersity of the particles could be successfully controlled by this technique. However high cost and difficulties in removing the surfactant molecules and the solvent represent the major limitations.

Alternatively, the sol-gel method introduced by Stöber [15] is widely utilized for the production of pure silica particles. This method offers an easy route to synthesize (5-2000 nm) colloidal silica at mild conditions yet limited by the polydispersity of the particles especially below 50 nm. Research has been focused on the use of colloidal silica due to its homogeneous dispersion and tailorable surface properties. Colloidal

silica particles exist in the form of sols within water or alcohol as the dispersing medium [16].

2.1.1. Synthesis of Silica by Sol-Gel route: Stöber Method

The term *sol-gel* was introduced in 1950s to refer to the art of manufacturing materials by the preparation of a sol, gelation of the sol, and removal of the solvent. Later, sol-gel processing was formally defined by Brinker [17] as: Growth of colloidal particles and their linking together to form a gel. Today sol-gel processing covers all liquid based processes for the preparation of ceramic materials in various forms such as films, fibers and particles. As illustrated in Figure 2-3, even the synthesis of unaggregated particles may not involve the gelation step or the sol may be composed of polymers instead of particles through fiber spinning, all formations are considered as sol-gel processes.

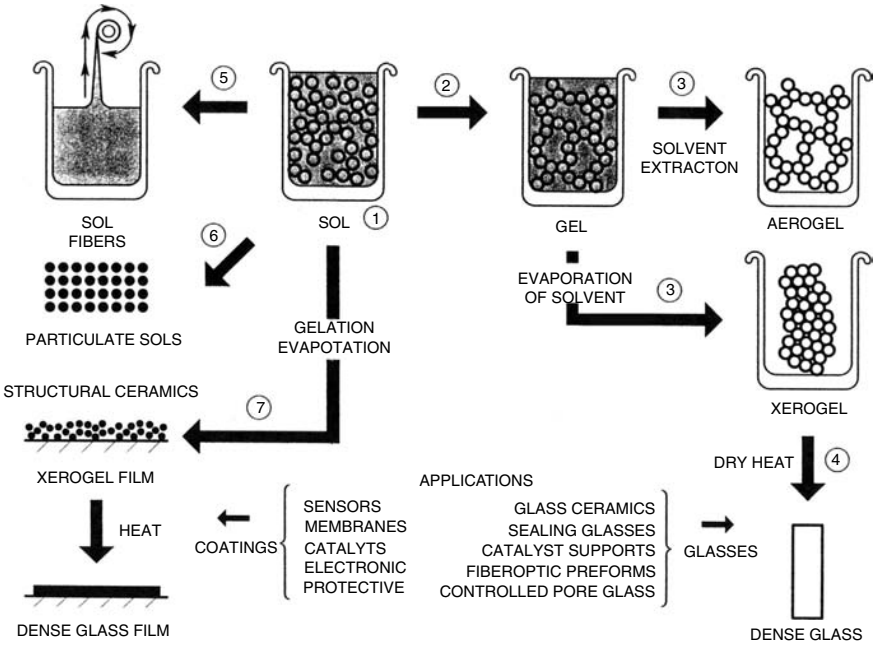


Figure 2-3: Illustration of various stages, end-products and applications of sol-gel processing [18]. The numbers refer to the processing stages.

Preparation of silica via sol-gel route basically involves hydrolysis and condensation of inorganic salts such as sodium silicate, Na_2SiO_3, or monomeric, tetrafunctional metal alkoxide $Si(OR)_4$ (R = alkyl) in the presence of a mineral acid (e.g., HCl) or base (e.g. NH_3) as a catalyst .

The general sol-gel reactions (hydrolysis and condensation) of silicon alkoxides that leads to the formation of silica are as follows [17]:

$$\equiv Si - OR + H_2O \underset{\text{esterification}}{\overset{\text{hydrolysis}}{\rightleftharpoons}} \equiv Si - OH + ROH \tag{2.1}$$

$$\equiv Si - OR + HO - Si \equiv \underset{\text{alcoholysis}}{\overset{\text{alcohol condensation}}{\rightleftharpoons}} \equiv Si - O - Si \equiv + ROH \tag{2.2}$$

$$\equiv Si - OH + HO - Si \equiv \underset{\text{hydrolysis}}{\overset{\text{water condensation}}{\rightleftharpoons}} \equiv Si - O - Si \equiv + H_2O \tag{2.3}$$

The hydrolysis reaction (Eq. 2.1) forms silanol groups as alkoxide groups (OR) is replaced with hydroxyl (OH). Subsequent condensation reactions involving silanol groups produce siloxane bridges (Si-O-Si) and the by-products alcohol (Eq. 2.2) and water (Eq. 2.3). Tetramethoxysilane (TMOS), $Si(OCH_3)_4$, and tetraethoxysilane (TEOS), $Si(OCH_2CH_3)_4$, are the most commonly used metal alkoxide precursors in sol-gel processing of silicates (where silicate refers to any hydroxylated or alkoxylated forms of silica). A mutual solvent, generally the parent alcohol, is used to provide homogeneity since water and alkoxides are immiscible.

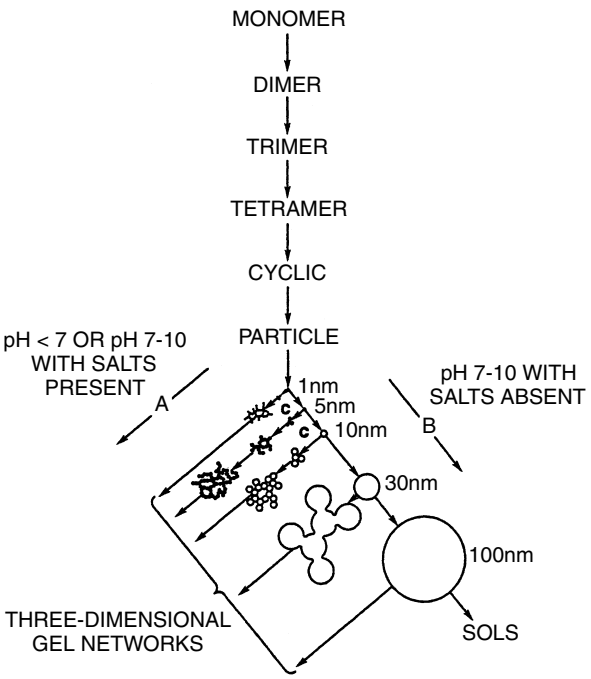


Figure 2-4: Polymerization pathway of aqueous silicates according to Iler [19].

The structural evolution of silicates are affected by several parameters: pH (catalyst type and amount), solvent, water-to-silicon ratio (R) and monomer. As illustrated in Figure 2-4 and reported by numerous studies on silicates, pH has the prominent effect on hydrolysis and condensation of silicates. The general trend shows that acid-catalyzed hydrolysis with low R produces weakly branched 'polymeric sols', whereas based-catalyzed hydrolysis with large R produces highly condensed 'particulate sols' [17]. pH-dependence of sol-gel silicate systems suggests that for more highly cross-linked systems, protonated and deprotonated silanols are involved in the acid- and base-catalyzed condensation mechanism at pH<2 and pH>2, respectively. Under more basic conditions, where the gel times are observed to increase (Figure 2-5), condensation reactions process but gelation does not occur. In this regime, particles are formed that, after reaching a critical size, become stable toward gelation due to mutual repulsion effects. This high-pH region represents the condition in which so-called Stöber silica particles are formed.

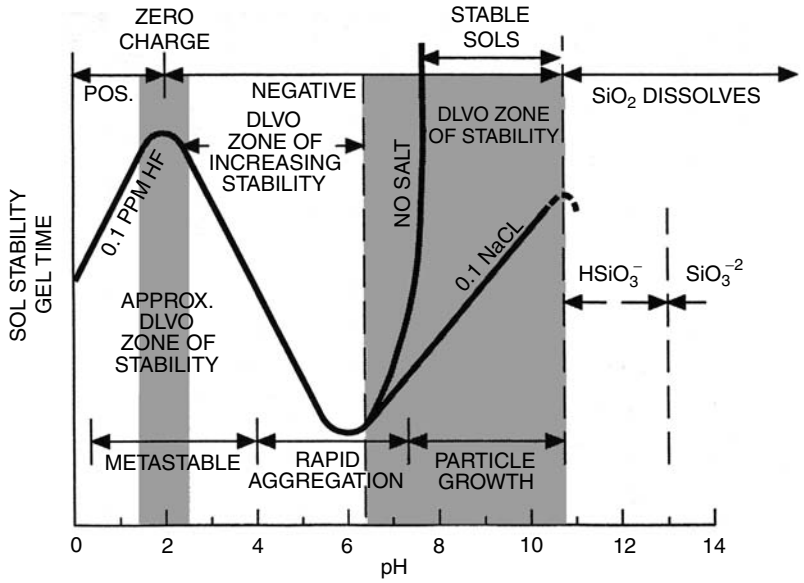


Figure 2-5: Effects of pH on the sol stability (gel-time) of the colloidal silica-water system [19].

In 1956, Kolbe [20] was the first to introduce the formation of silica particles by reacting tetraethyl silicate in alcoholic solution with water in the presence of certain bases. Stöber et al. [15] were the first to systematically show that remarkably uniform silica particles with sizes ranging from 50 nm to >1μm in diameter could be synthesized by hydrolyzing silicon alkoxides in aqueous alcoholic solutions containing ammonia. In a typical Stöber process, TEOS is introduced into a batch reactor with ethanol, water and ammonia. The lower parent alcohol, e.g. ethanol, acts as a co-solvent for silicon alkoxides (e.g. TEOS), which is immiscible with water. Ammonia catalyzes both hydrolysis and condensation by dissociating the water molecules, and provides the spherical shape of the silica particles with a negative, stabilizing charge in the alcohol solutions [15, 21].

In addition to various scientific and industrial applications, the research on Stöber silica has been focused on two major subjects:

(i) Growth mechanisms of silica in basic media

(ii) Empirical prediction and control on the final particle size based on the concentration of reagents and reaction temperature

2.1.2. Proposed Models for Growth Mechanism of Stöber Silica

There are two extreme kinetic models that have been proposed to explain the mechanisms yielding highly monodisperse Stöber silica particles: (i) monomer addition, (ii) controlled aggregation. By these models, silica formation is basically divided into two events: nucleation and growth [22]. Nucleation, the formation of the first nuclei or primary particles, occurs at the early stages. Subsequently, the particles grow to achieve a final size distribution.

Monomer addition model is also called 'growth-only' model and is based on LaMer's synthesis of monodispersed colloidal particles by homogeneous precipitation [23]. Matsoukas and Gulari [24-26] argue that there is a burst of identical primary particles – a LaMer-like burst – which grow by the addition of monomers. Therefore, the monodispersity is preserved through later stages. This model neglects aggregation and holds a brief 'burst' of nucleation, followed by diffusion-limited growth (as the addition of soluble species directly to the particle surface).

On the other extreme, controlled aggregation model is also called 'aggregation only' model that is proposed by Bogush and Zukoski [27, 28]. By this model they claim that initially a broad size distribution of primary particles exist in the solution and nucleation occurs throughout the reaction. These primary particle or nuclei aggregate with themselves or with larger aggregates by the preferential growth of larger particles at the expense of small ones, assuring a narrow size distribution of the particles at later stages. In their assessment of Stöber synthesis, McCormick et al. reported consistent trends with the aggregation model and they reported that nucleation is rate-limited by the hydrolysis of the singly-hydrolyzed monomer [29].

Byers et al. [30] and van Blaaderen et al. [31] claimed both mechanisms are responsible during the formation of particles. Both groups of researchers believed that nucleation is controlled by the aggregation of soluble species and occurs for much of the reaction, however subsequent growth is controlled by monomer addition that smoothens the colloid surface. Byers et al. proposed that nucleation occurs over most of the reaction, although the greater portion of the silicic acid precipitates on the surface of the silica. On the other hand, van Blaaderen et al. experimentally showed that monomer addition is responsible for an increase in particle size toward later stages by suggesting

that the final particle size is strongly dependent on the colloidal stability of the primary and intermediate particles.

This combined model was refined by considering that the final particle growth occurs via both monomer addition and aggregation of primary particles [32]. Both models are based upon dynamic and static light scattering (DLS and SLS) and transmission electron microscopy (TEM) measurements of the particles relative to time. There is still uncertainty about the size and structure of the initial nuclei and primary particles due to insufficiencies of these monitoring tecniques. In the monomer addition model of Matsoukas and Gulari [26], primary particle was defined as the combination of two hydrolyzed TEOS monomers. This suggests that the primary particle must be within molecular domain [22]. In addition to these, Bailey and Mecartney [33] used cryo-TEM that is the fast-freezing of a sample with liquid ethane to avoid the effects of drying encountered using regular TEM. They observed low density mass fractals (26 nm) in the early stages of formation and proposed a collapse mechanism for particle densification their observations. On the other hand, Boukari et al. [34-36] employed small-angle X-ray scattering (SAXS), an in-situ method that can probe molecular (0.1-0.2 nm) to colloidal (1-20 nm) length scales. The SAXS results showed that the primary particles possess the same size (methanol-$R_g \approx 4$ nm; ethanol-$R_g \approx 8$ nm) and low-density structure independent of ammonia and water concentrations. Ultimately, The common result of these groups was the presence of an induction period where no particles were detected. Later, Green et al. [37] indicated that this induction period before particle formation represents the build-up of singly hydrolyzed monomers that form the initial low-density open polymeric structures, possible through the self-assembly of these monomer molecules.

2.1.3. Control over Particle Size and Polydispersity

There are numerous studies aiming at controlling Stöber particle size and polydispersity. These studies generally focuses on how particle synthesis, and hence particle size and size distribution, is affected by temperature and relative amounts of reagents used. The reagents could be listed as:

(i) Tetraesters of silicic acid (tetraalkyl silicates) as monomer
(ii) Ammonia as catalyst
(iii) Water as reactant
(iv) Low molecular weight alcohol as solvent

In their pivotal work, Stöber et al. indicated that an increase in ammonia concentration caused larger particles [15]. In addition, they showed that ammonia influences the morphology of the particles and played the key role for the preparation of spherical particles. It was also stated that using higher alcohols as solvents or increasing molecular weight of the esters as monomers could slow the reaction down. However, the particle sizes could not be precisely reproduced, and resulted in high standard deviation in size distribution. Following this pioneering work, diverse results with respect to control over particle size were reported in literature. For instance, Stöber et al. found that there was no effect of TEOS on the final particle size. In contrast to Bogush et al. [38] who reported larger particles due to increasing TEOS concentrations, van Helden et al. [21] showed that the particle size decreased.

On the other hand, over the years, novel techniques have been introduced to control the size and size distribution of silica particles. Rao et al. reported a sequential method to prepare monodisperse and uniform silica particles using ultrasonification and defined the particle size ranges regarding to reagent concentrations [39]. Bagwe et al. used reverse microemulsion technique to control size and size distribution of dye-doped silica nanoparticles [13]. Recently, Yokoi et al. introduced a novel method for the formation of the silica nanospheres with a size of 12−23 nm and with a well-ordered arrangement [40]. Analogous to Stöber method, basic amino acid monomers (lysine) were used in place of ammonia under weakly basic conditions. In a similar study, Hartlen et al. used arginine as a base catalyst and silica particle stabilization, and achieved remarkable control in particle size in the range of 15-200 nm [41].

2.1.4. Polymer/Silica Nanocomposites

One of the prominent applications of silica nanoparticles is as fillers in polymeric matrices for the preparation of advanced nanocomposite materials. The small size of the fillers leads to a dramatic increase in interfacial area, which creates a significant volume fraction of interfacial polymer with properties different from the bulk polymer even at low loadings [42, 43]. For instance, Zhou et al. reported that nanosilica particles could more effectively improve hardness, abrasion resistance, and scratch resistance of acrylic based polyurethane nanocomposites than microsilica or fumed silica particles [44]. Wu et al. reported that silica nanoparticles could simultaneously provide polypropylene with stiffening, strengthening and toughening effects at a rather low filler content (typically 0.5% by volume) as demonstrated by the applied tensile tests [45]. On the other hand, it was shown by Manna et al. that both storage modulus and T_g of epoxidized natural rubber increased through addition of silica [46]. As shown in Table 2-1, silica particles in various size and weight percentage have been used to improve the properties of different types of polymer. Silica particle reinforcement in certain polymer matrices can lead to significant property improvements, whereas adverse effects could also be observed.

Properties of the nanocomposite materials can be tailored by changing the volume/weight fraction, size and surface chemistry of nanosilica. However, the most important aspect that has significant impact on the properties of the nanocomposites is the dispersion of the nanosized filler material, which essentially depends on the degree of interfacial interaction [16]. Chemical modification of the silica surface is one of the most frequently applied methods to enhance the compatibility between the polymer and the nanosilica [47]. Nanocomposite preparation method is also crucial and several different methods have been applied to achieve homogeneous dispersion. Solution blending, in-situ polymerization and melt mixing are commonly used techniques for the preparation of polymer/silica nanocomposites. Solution blending and in-situ polymerization processes generally produce higher levels of nanoparticle dispersion, however the melt process finds favor due to its compatibility with current industrial compounding facilities [48].

Table 2-1: Various types of silica-polymer nanocomposites reported in the literature with the details on filler size, content and selected results.

Polymer Matrix	Silica Size (nm)	Silica Content	Major Property Changes (with increasing filler content)	Ref.
Polystyrene	25-200	5-10 wt%	(i) Increased DTA peak at low concentrations (ii) Strong interaction between silane groups with polymer chain	[49]
Polypropylene	50-110	1-5 wt%	(i) Larger thermal degradation stabilization (ii) Higher elastic modulus	[50]
Polyurethane	175-730	1-10 wt%	Constant T_g at different particle size and concentartions	[51]
Polyurethane	14-260	1-4 wt%	T_g increased with particle size up to 66 nm and then decreased	[52]
Thermoplastic Polyurethane	7	10 wt%	(i) Decreased T_g (ii) Increased storage modulus	[53]
Polyimide	20	10-50 wt%	(i) Increased dielectri constant (ii) Enhanced thermal stability	[54]
Acrylic polymer	15-20	10-50 wt%	(i) Enhanced thermal stability (ii) Enhanced hardness (iii) Excellent optical transparency	[55]
Epoxy (Diglycidylether of bisphenol A)	10-20	10-70 wt%	(i) Decreased T_g (ii) Increased thermal stability	[56]
Epoxy (Diglycidylether of bisphenol A)	400	50-70 wt%	(i) Decreased CTB and increased T_g (ii) Increased brittleness	[57]

2.2. PART II: THERMOPLASTIC POLYURETHANES

2.2.1. The Evolution of Thermoplastic Elastomers

Polyurethanes, also called *urethanes* are among the most important class of specialty polymers. In most general terms, polyurethanes is defined as a large family of polymers, based on the reaction products of an organic isocyanate with active hydrogen-containing compounds as shown in Figure 2-6 below [58].

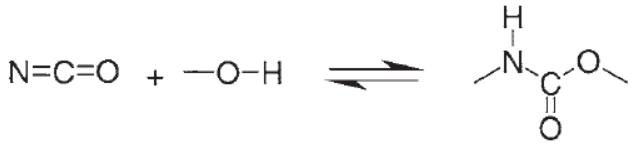


Figure 2-6: Urethane linkage formed by the reaction of isocyanate and hydroxyl groups.

Besides pularity of urethane groups, typical polyurethane may contain aliphatic and aromatic hydrocarbons, esters, ethers, amides, urea, and isocyanurate groups. Thus, polyurethanes are a heterogeneous family of polymers unlike polyethylene, polyvinyl chloride or polystyrene, which have a fairly simple chemical structure [59]. On the other hand, polyurethanes may be linear, branched, or networked, and they may exist as homopolymers or copolymers with variable molecular weight and structure. Hence, polyurethanes comprise an array of different products, ranging from rigid foams to soft, millable gums [60].

Polyurethane was first developed by Otto Bayer and his co-workers in 1937 while they were synthesizing polymer fibers to compete with nylon [61]. By subsequent recognition of its elastomeric properties, polyurethane production on industrial scale started in 1940s [62]. Early polyurethane elastomers consisted of three basic components [63]:

(i) A polyester or polyether macrodiol
(ii) A chain extender, e.g. water, a short-chain diol, or a diamine.
(iii) A bulky diisocyanate, e.g. naphthalene-1,5-diisocyanate (NDI).

Thermoplastic properties was introduced to polyurethane elastomers by the work of Schollenberger et al. (B.F. Goodrich) in 1958 [64]. This progress was established when NDI was replaced by diphenylmethane-4,4'-diisocyanate (MDI). Thermoplastic polyurethane elastomers (TPUs) were the first, homogeneous, thermoplastically processable elastomers [63] and the development of TPUs were the first appearance of a new class of polymeric materials called thermoplastic elastomers.

Thermoplastic elastomers (TPE) can be simply defined as a class of polymers, which combine the service properties of elastomers and the processing properties of thermoplastics with the possibility of recycling and reuse [65]. Prior to the introduction of TPEs, there was a distinct division between rubbers and plastics; former being soft, flexible and elastic, and latter being hard and rigid. TPEs bridge the gap between conventional rubbers and thermoplastics. Crosslinking in conventional elastomers is chemical; it is achieved by the formation of chemical bonds between polymer chains. Crosslinking of thermoplastic elastomers occurs by a physical process as a result of their microheterogeneous, two-phase morphology [66].

Over the past three decades, the literature on TPEs has grown progressively. TPEs may be classified into the following classes according to their chemistry and morphology [67]:

1. Block Copolymers
    a. Styrenic block copolymers
    b. Thermoplastic copolyesters (COPE)
    c. Thermoplastic polyurethanes (TPU)
    d. Thermoplastic polyamides (COPA)
2. Blends and Elastomeric alloys
    a. Elastomeric rubber-plastic blends
    b. Thermoplastic vulcanizates (TPVs)
    c. Melt processable rubber
3. Crystalline-amorphous block copolymers (Polyolefin elastomers with distinct crystalline and amorphous blocks)
4. Ionomers
    a. Sulfonated ethylene-propylene-diene monomer rubber (S-EPDM)
    b. Zn or Na salt of ethylene acrylic acids
5. Miscalleneous (e.g. Metallocene elastomers-TPEs)

A number of other polymers have the characteristics and some are available commercially. According to the study of Freedonia Group, global demand for TPEs was forecast to increase 6.2% per year through 2009, reaching 3.1 million metric tons. The study, "World Thermoplastic Elastomers," claimed that TPEs would continue to find the majority of their use as replacements for natural and synthetic rubber, as well as for rigid thermoplastics. TPEs are expected to gain new applications in which they are over-molded onto rigid plastic or metal components to enhance ergonomic or soft touch features on a wide range of products [68].

2.2.2. Block Copolymers

Copolymer synthesis offers the ability to alter the properties of a homopolymer in a desired direction by the introduction of an appropriately chosen second repeating unit. Different types of copolymers (e.g. alternating, statistical, block) are possible with regard to sequencing of the two repeating units relative to each other [69]. Block copolymers are a particular class of polymers that, independent of procedure of synthesis, can simply be considered as being formed by two or more chemically homogeneous polymer fragments (blocks) joined together by covalent bonds [70]. In simplest case of two distinct monomers (termed as A and B), linear diblock (AB), triblock (ABA), multiblock or star-block copolymers can be prepared (Figure 2-7). Several techniques such as living anionic polymerization and step-growth polymerization can be used to prepare block copolymers.

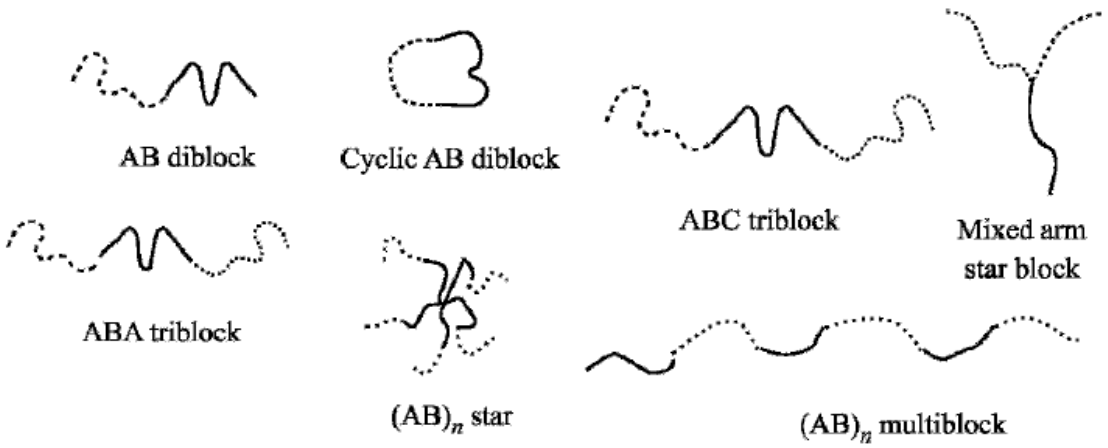


Figure 2-7: Block copolymer architectures.

Almost any type of block copolymer can be synthesized by selecting the synthetic method that is best suited for a particular target. Block copolymers consisting of monomer units with opposing properties, for instance thermoplastics (styrenes, methacrylates) versus elastomers (dienes, siloxanes), crystallizable blocks (ethylene oxide) versus amorphous ones (styrene, dienes), water soluble blocks (ethylene oxide, acrylic acid) versus hydrophobic blocks (dienes, styrene), etc. can be designed. Diversity in both synthesis routes and the starting materials allow the tailoring of block copolymers with complementary properties for ultimate applications.

Numerous experimental and theoretical studies on block copolymers have been concentrated on phase behavior of diblock copolymers. Pioneer work on statistical thermodynamic theory of linear block copolymers was done by D.J. Meier based on confined chain model of linear diblock copolymers [71]. In this approach, domain structure by random flight chains was constrained by barrier. The barrier represents the effect of incompatibility between the components and the resulting restriction of the components to region of space. Current theories mostly deal with $(A\text{-}B)_n x$ type star-block copolymers.

Microphase separation, which is a self-assembly process, is driven by an unfavorable mixing enthalpy and a small entropy, while covalent bond connecting the blocks prevents macroscopic phase separation. The phase behavior of block copolymers of is determined by three experimentally controllable factors [63, 70]:

(i) The overall degree of polymerization, N ($=N_A+N_B$)
(ii) Architectural constraints characterized by n and composition (f_A and f_B being fractions of the constituents blocks)
(iii) The Flory-Huggins interaction parameter, χ, which is a measure of incompatibility between two blocks

The first two factors are regulated through the polymerization stoichiometry and affect the translational and configurational entropy, while the magnitude of χ, mostly enthalpic, is determined by the selection of the A-B monomer pair.

Interaction parameter has the temperature dependence $\chi \approx \alpha T^{-1}+\beta$ where $\alpha>0$ and β are constants for given values of f and n. This parameter describes the free energy cost per monomer of conducts between A and B and constitutes the driving force for phase separation. At equilibrium, monodisperse diblock copolymers are in a highly ordered,

minimum free configuration. When the temperature is decreased (therefore χ is increased, positive), repulsion occurs between the A and B: thus A-B monomer contacts are reduced, whereas a negative value of χ signifies mixing of unlike monomers. Another parameter that strongly influences the block copolymer behavior is the total degree of polymerization, *N*. For large *N* the loss of translational and configurational entropy leads to a reduction of the A-B monomer contacts and thus to local ordering. Such local compositional ordering/local segregation is often referred as *microphase separation*. Figure 2-8 represents a phase-separated and a phase-mixed polyurethane at room temperature and at high temperatures, respectively.

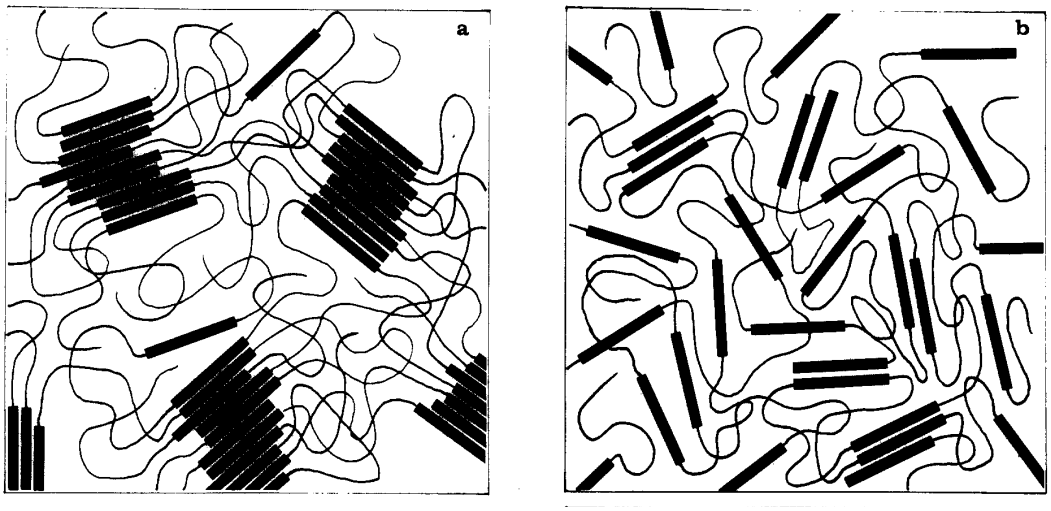


Figure 2-8: Schematic representation of polyurethane structures at various temperatures: (a) room temperature phase-separated morphology and (b) most dissociated structures at high temperature [72].

Besides the major parameters χN and *f*, extent of microphase separation is also affected by presence of strong secondary interactions (e.g. hydrogen bonding in polyurethanes), crystallizability of hard and/or soft segments and inherent polydispersity (c.a. 2 for step-growth polymerization). Recently, it was also demonstrated by Sheth et al. that backbone symmetry and chain architecture have distinct effects on microphase separation [73]. Microphase separation in block copolymers has been the major concern among researchers since micro-domain structure as a consequence of microphase separation determines the processability and performance of block copolymers.

2.2.3. Chemistry and Properties of Thermoplastic Polyurethanes

Polyurethane chemistry is a very broad field and encompasses a large number of chemical reactions of isocyanates with various active hydrogen-containing compounds allowing a wide range of end-products adaptable to various applications. Polyurethane elastomers developed up to 1960s differs from TPUs since their melting temperature was higher than the decomposition temperature of the urethane linkages [63]. TPU was first described by Schollenberger et al. as a polyurethane based on MDI instead of NDI, which was used for the development of polyurethane elastomers [64]. This progress led to the development of phase-separated systems of TPU multiblock polymers.

In terms of processing, polyurethanes are classified as: TPU, castable PU and cross-linked PU. TPU is supplied as a polymer chain extended to a suitable length with terminal groups that do not allow any further chain extension. Castable polyurethanes are supplied as a prepolymer with an active terminal isocyanate group to the polymer chain. These isocyanate groups are reacted with either a diamine or a diol. In castable polyurethanes, the actual chains will break down on heating before the physical chemical bonds give way. The material therefore cannot be reformed after the chain extension is complete. In cross-linked polyurethanes, there are actual chemical bonds formed in a three-dimensional manner. The main difference is that with the castable polyurethanes the actual chemical structure consists of two major zones, a hard zone and a soft zone. This is not as pronounced in the crosslinked polyurethanes. A typical example is the addition of TMP (trimethylol propane) to polyurethane to make it softer. This curative agent will make the material much softer as it breaks the hard segment zoning up to a certain degree [74].

TPUs can be defined as linear-segmented multiblock copolymers with alternating hard and soft segments (Figure 2-9). One type of block, hard segment, is formed by addition of chain extender, a low molecular weight diol, to the diisocyanate, e.g. MDI. The other type is the soft segment, which is usually a high molecular weight macroglycol (e.g. polyether, polyester) that establishes the interconnection between two hard segments.

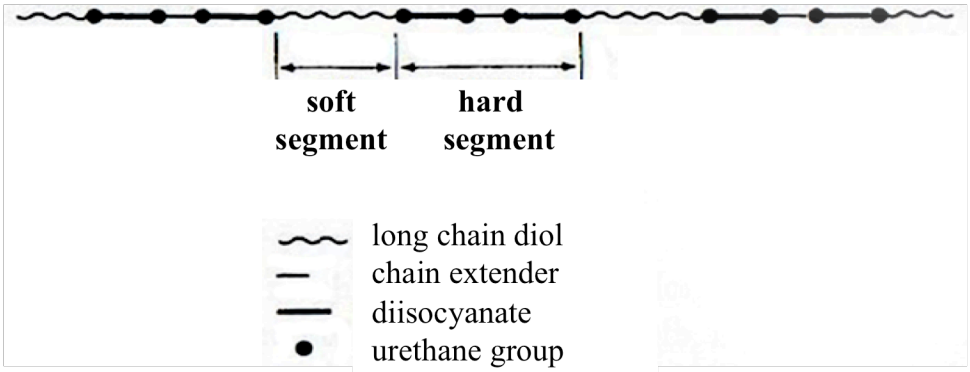


Figure 2-9: Schematic representation of a TPU composed of diisocyanate, long-chain diol, and chain extender [63].

Crosslinking in conventional elastomers is chemical; it is achieved by the formation of chemical bonds between copolymer chains. As stated earlier, crosslinking of thermoplastic elastomers occurs by a physical process as a result of their microheterogeneous, two-phase morphology, which arises from the incompatibility between hard and soft segments. This is a consequence of morphological differences between the two different blocks in the multiblock copolymer [69]. The hard rigid segment segregates into a glassy or semicrystalline domain, and the polyol soft segments form amorphous or rubbery matrices in which the hard segments are dispersed [59]. The rigidity of the polyurethane blocks is due to crystallinity (and hydrogen bonding). For other thermoplastic elastomers such as those based on styrene and 1,3-dienes, the rigidity of the hard polystyrene blocks is due to their glassy nature. The hard blocks from different copolymer molecules aggregate together to form rigid domains at ambient temperature. These rigid domains (hard segments) comprise a minor, discontinuous phase dispersed in the major, continuous phase composed of the rubbery blocks (soft segments) forming the elastomer matrix. Hard segments act as multifunctional tie points that function as physical crosslinks and reinforcing fillers. Physical crosslinking, unlike chemical crosslinking, is thermally reversible since heating over the T_m of the hard blocks softens the rigid domains and the copolymer flows. Cooling reestablishes the rigid domains, and the copolymer again behaves as a crosslinked elastomer [60, 63, 69]. That's the reason why TPU network was called as "virtually crosslinked" [64]. To ensure thermoplasticity high molecular weight linear chains with no or only very few branch points should be provided. Therefore, the

average functionalities of the starting materials (prepolymer or monomer) should be close to 2.

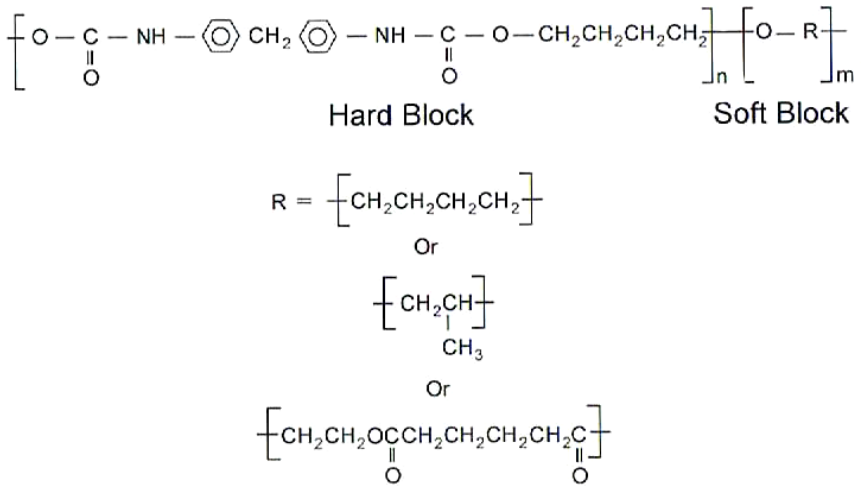


Figure 2-10: Chemical Composition of commercial thermoplastic polyurethanes [60].

Multiblock polyurethanes are often referred to as segmented polyurethanes. The long flexible soft segment, mostly consisting of long-chain polyols with an average molecular weight of 600 to 4000, governs the lower temperature properties, the resistance to solvents, and weather resistant properties (Figure 2-10). Hydroxyl terminated polyesters and polyethers are the two types of flexible segments of importance (Table 2-2). Polydimethylsiloxanes (PDMS), with respect to its unique nature of flexible Si-O bonds, are also used [75]. As polar solvents, TPUs are very resistant to non-polar fluids. In aqueous solutions, TPUs with polyether soft segments (e.g. polytetramethylene oxide (PTMO) and polyethylene oxide (PEO), polypropylene oxide) possess superior resistance to hydrolysis than polyester soft blocks (e.g. polycaprolactones), both being comparable to copolyesters (COPs) in terms of hydrolytic stability. In general, the polyester-based TPU is tougher and has better oil resistance while the polyether-based TPUs show better low temperature flexibility and better hydrolytic stability. Mixtures of polyethers and polyesters have been claimed to be advantageous to combine the useful properties of both classes of materials [63, 76]. The uses of each polyol with variable characteristics (e.g. molecular weight), or combinations of these polyols impart different properties to the final product. As explained earlier, the characteristics of the soft segment determines the lower service

temperature range of TPUs, and it is characterized by T_e, lower end of glass transition temperature. Low-temperature flexibility is provided by the soft segments that are incompatible with the hard segments, and it can be adjusted by increasing the molecular weight of the soft segments.

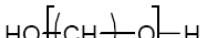
Diisocyanates governing the hard segments can be either aromatic or aliphatic. Mostly used diisocyante is the 4-4′-diphenylmethane diisocyanate (MDI) that has a symmetric aromatic structure. Other aromatic diisocyanates being used are toluene diisocyanate (TDI), para-phenylene diisocyanate (pPDI), meta-phenylene diisocyanate (mPDI). Aromatic diisocyanates are mostly more reactive due to resonance stabilization of the phenyl ring, whereas being symmetric provides crystallizability and therefore formation of more cohesive hard domains [73]. Aliphatic linear diisocyanates utilized are hexamethylene diisocyanate (HDI), hydrogenated diphenylmethane diisocyanate (HMDI) with cycloaliphatic diisocyanates, such as cyclohexyl diisocyanate (CHDI) are more UV stable than their aromatic counterparts.

The choice of the chain extender and diisocyanate (Table 2-2) determines the characteristics of the hard segments and to a large extent the physical properties of TPU. The most important chain extenders for TPU are linear diols such as ethylene glycol and 1,4-butanediol (BD). These glycols react with diisocyanates forming urethane linkages, which can be well crystallized and melt without decomposition on thermoplastic processing. Ethylenediamine (EDA), which forms urea linkages between isocyanate end-capped prepolymer and hard segment, is also used as a chain extender. However, urea linkages are not appropriate for high temperature processing since urea groups melt below the processing range of TPUs. Spandex with a trade name Lycra® based on MDI is a typical example of this type of material. Spandex fibers can undergo large, reversible deformations and are used in the manufacture of undergarments. It differs from conventional TPU in containing urea linkages instead of urethane in the hard blocks. These are obtained by using a diamine (instead of diol) to chain-extend isocyanate-terminated polyurethane prepolymers (synthesized from macroglycol and excess diisocyanate) and the resulting polymer is called thermoplastic polyurethaneurea or segmented polyurethane-urea copolymer.

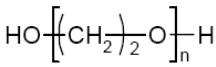
Table 2-2: Chemical structure of various precursors utilized in PU chemistry [77].

Soft Segments

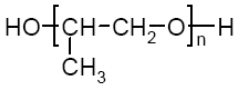
Polyethers



PTMO

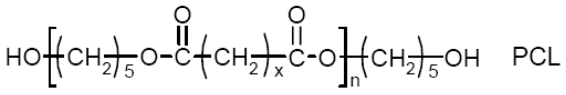


PEO



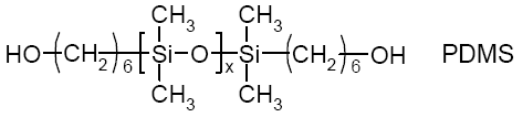
PPO

Polyesters



PCL

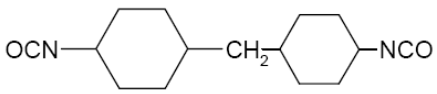
Polysiloxane



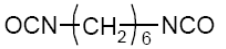
PDMS

Diisocyanates

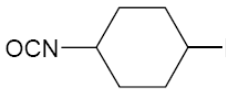
Aliphatic



HMDI

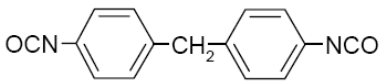


HDI

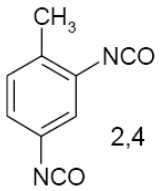


CHDI

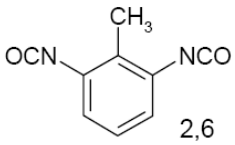
Aromatic



MDI

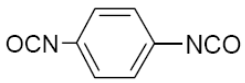


2,4

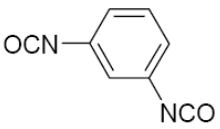


2,6

TDI



*p*PDI



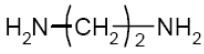
*m*PDI

Chain Extenders

Diol

BD or BDO

Diamine



EDA

Segmented polyurethane synthesis can be carried out in either one-step or two-step method, which are equally applicable [58]. One-prepolymer method (also called "one-shot method") involves mixing all the ingredients together. In the two-step method (also called "prepolymer method"), the polyol is reacted with diisocyanate to give an isocyanate containing prepolymer [65]. The prepolymer chains extend by the reaction of terminal isocyanate groups (-NCO) with the diol (Figure 2-11). The mole reaction ratio of the diol to diisocyanate is normally kept in the range of one mole diol to 1.6 to 2.25

moles of the diisocyanate. A reaction ratio of one mole diol to one mole diisocyanate will produce a linear material. This type of polyurethane is normally thermoplastic. The molecular weight of the prepolymer is too low to form an elastic polymer. The overall molecular weight must be increased by joining prepolymer chains using either diols or diamines. When the prepolymer chain is extended with a diol, the polymer formed has only urethane linkages. The polymer formed with the diamine chain extender is strictly a polyurethane-urea.

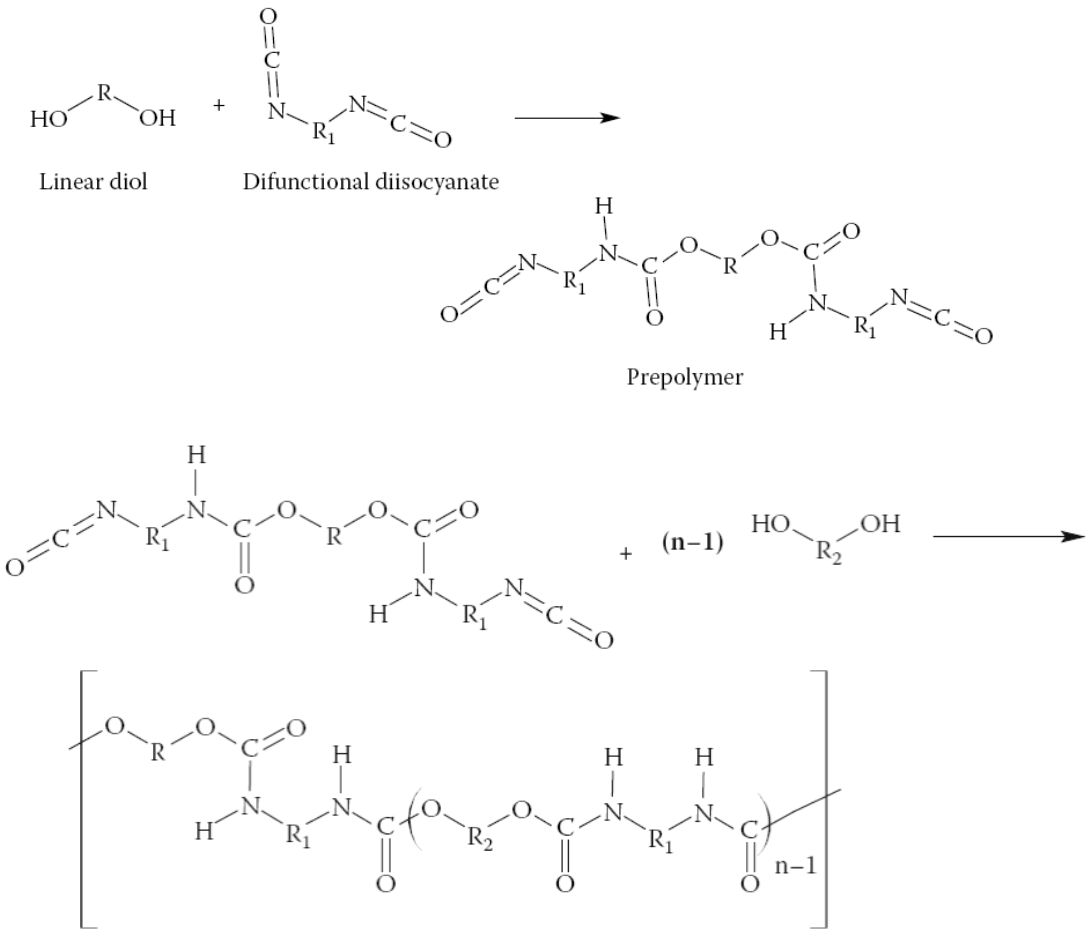


Figure 2-11: TPU synthesis via prepolymer method by the use of diol type chain extender [74].

The melting point of the hard segments determines the theoretical upper temperature limit of a TPU, whereas glass transition point of soft segments determines the lower temperature limit. In TPUs, involving hard segments from the isocyanate chemistry, the cohesiveness of the hard domains is further enhanced by the ability of

these hard segments to establish a hydrogen-bonded network (Figure 2-12). As postulated by Bonart et al., hard domains are arranged that provided optimum bonding to exist in a crystalline state [78]. It has been reported that in addition to the packing capability of the hard segments, H-bonding capability plays a major role in microphase separation.

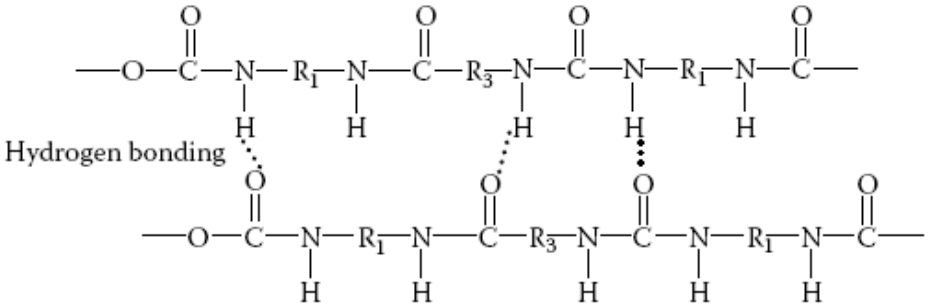


Figure 2-12: Hydrogen bonding in TPUs.

It was demonstrated by Sheth et al. that hard segment symmetry and the nature of hydrogen bonding had a pronounced effect on the processability and performance of segmented polyurethanes. Following this, important factors affecting microphase separation, and hence morphology of TPUs, have been summarized by Yilgor et al. as follows [79]:

1. Chemical structure, number average molecular weight and molecular weight distribution of soft segments.

2. Chemical structure and symmetry of the diisocyanate.

3. Chemical structure of the chain extender, average chain length and length distribution of hard segments.

4. Hard/soft segment ratio in the copolymer.

5. Crystallizability of hard and soft segments.

6. Extent of competitive hydrogen bonding between hard–hard and hard–soft segments.

7. Inherent solubility between hard and soft segments.

8. Method/polymerization procedure used during the synthesis, which can be a one-step or two-step (prepolymer method).

9. The nature of the interfacial region between the soft segment matrix and hard segment domains.

In the same study based on a single diisocyanate molecule with no chain extenders, it was quantitatively determined that the kinetics of hydrogen bonding between polyurethane hard segments governing the microphase separated morphology has a strong dependence on the chemical structure and symmetry of the diisocyanate, and these two parameters control the extent of microphase separation.

In general, elastomeric TPUs contain 60-70% by weight of soft segments. Hard segment to soft segment ratio is one of the key parameters that affect the processability and performance. Good microphase separation of these segments results in the formation of TPUs with excellent mechanical properties. As reviewed earlier, microphase separated morphology is a consequence of chemical incompatibility between the hard and soft segments, and the crystallizability of the hard segments. When the hard segment content is raised above 25%, the connectivity between the hard domains increases leading to a percolation in the elastomer matrix. This results in an increase in hardness with an increase in the glass transition temperature of the matrix, which reduces the low temperature flexibility. At levels of over 60% by weight of hard segment, overall behavior of the elastomeric matrix changes into a high modulus, brittle plastic [80]. On the other hand, miscibility between the segments plays an important role. It was reported by Coleman et al. that amorphous urethane hard segments show complete miscibility with amorphous polyethers at every composition resulting in poor elastomeric properties [81]. Yilgor et al. demonstrated that three different states of urethane hard segments exist in the equilibrium morphology of TPUs and these are: (a) well-microphase separated (pure) and strongly hydrogen bonded hard segments, (b) loosely hydrogen bonded hard segments, and (c) non-hydrogen bonded (polyether mixed) hard segments [79].

Thermoplastic polyurethanes, which are mostly polyester based, are used in applications such as wire insulation, automobile fascia, footwear (lifts, ski boots, football cleats), wheels (industrial, skateboard), and adhesives. Mechanical properties of polyether based TPUs are somewhat lower than the polyester based counterparts, whereas they show superior low temperature flexibility and hydrolytic stability. There is a growing interest to broaden the range of applications for polyether based TPUs beyond the current limits by playing with the listed parameters that affect the morphology of these materials. This means producing TPUs with lower hardness and greater heat resistance as well as TPUs with higher hardness that retains good low temperature properties. Since the development of new blocks is rather limited, major

improvement will be achieved by a deeper understanding of morphology, resulting in optimized performance of these types of materials. For instance, to gain the desired softness desired by marketplace, TPUs are softened by the addition of plasticizers or compounded by other softer materials. However, these applications come at a cost of reduced mechanical or thermal properties such as reduced deflection temperature under load with respect to reduced hard segment to soft segment ratio [82]. New line of TPUs is expected to be based on a soft, fast crystallizing ether soft segments, which would increase the incompatibility between the phases and therefore enhance the microphase separation. It was recently reported for a segmented non-chain extended polyether based polyurea system that an increase in soft segment molecular weight leads to increased formation of soft segment crystallites at low temperatures. This morphological change in the system increased the tensile modulus of the polyureas, whereas adversely shortened the service window as a result of decrease in the long-range connectivity of hard segments [83].

On the other hand, there is also growing effort to improve the properties of TPUs by the addition of nanosized fillers. Recent few studies show that mechanical and thermal properties of TPUs can be optimized by the interaction of the fillers and the polyurethane matrix. However, most of the studies are based on polyester based TPU polymers, where organoclays or nanosilica were used as fillers.

2.3. PART III: THERMOPLASTIC POLYURETHANE COMPOSITES

Until recently fillers are not normally used in polyurethanes to bulk out the product, because they reduce the properties too drastically. This is in contrast to conventional elastomers, where they can be used to reinforce the product. Nanoparticles are now being investigated and used to provide improved characteristics to TPUs.

Table 2-3: Composition and preparation methods of thermoplastic polyurethane composites over the last decade.

Group	Year	HS	SS	Filler	Ref.
Bistricic et al.	2010	MDI	Polyether	Fumed Silica	[84]
Zhou et al.	2008	MDI	Polyester (PCL)	Stöber silica	[85]
Aso et al.	2007	Hytrel (commercial TP, polyester-ether mixture)		Fumed silica	[86]
Chen et al.	2007	HDI	Acrylic polyol	Stöber silica	[87]
Vega-Baudrit et al.	2007 2006	MDI	Polyester	Fumed silica	[53]
Kim et al.	2006	HMDI	Polyether	Fumed silica	[88]
Chen et al.	2005	HDI	Acrylic polyol	Stöber silica	[89]
Pattanayak et al.	2005	MDI	Polyether+ester	Layered silicate	[90]
Cho et al.	2004	MDI	Polyether	Stöber silica	[91]
Chen et al.	2004	IPDI	Polyester	Stöber silica	[52]
Zhou et al.	2002	HDI	Acrylic polyol	Fumed silica	[44]
Nunes et al.	2001 2000	MDI	Polyester	Precipitated silica	[92, 93]
Tien & Wei	2001	MDI	Polyether	Layered silicate	[94]

MDI: 4-4′-diphenylmethane diisocyanate

HDI: 1,6-hexamethylene diisocyanate

HMDI: 4,4′-dicyclohexylmethane diisocyanate

IPDI trimer:isophorone diisocyanate

We can group the existing studies on TPU composites based on the type of the inorganic constituent, which is generally either layered clays, or spherical particles as listed in Table 2-3. A vast amount of research was related to the exfoliated layered clays within polyurethane nanocomposites, whereas papers dealing with segmented polyurethane nanocomposites reinforced with dispersed spherical nanocomposites are less common. The mostly studied TPU nanocomposites involved natural montmorillonite, which consists of layers made up of two silicate tetrahedrons fused to edge-shared octahedral sheets. Recently, carbon nanotubes [95], fumed and collidal silica were used as matrix modifiers (Table 2-3).

2.3.1. TPU/Organoclay Nanocomposites

Segmented polyurethane (PU)/clay nanocomposites was synthesized with nano-scale amine modified silicate layers of organoclay exfoliated in PU. It was reported that segmented structures of PTMO-MDI based PU was not affected by the presence of silicate layers in these nanocomposites as evidenced by glass transition temperature and degree of phase separation. However, two-fold increase in tensile strength and three-fold increase in elongation with enhanced thermo-degradation and water-absorption properties were obtained [96]. On the other hand, it was also pointed out that based on the functionality of the organoclay, it is possible to modify the interfacial interaction between the polymer and the organoclay, resulting in different mechanical property characteristics. The reinforcing effects were much stronger when the functionality of the amine modifier was higher. Increased tensile strength was explained by increased intermolecular force between PU molecules, where increase in elongation was attributed to the dispersion of exfoliated silicate layers between the soft and hard segments and the crosslinking effect. Subsequent study based on the same polymeric system showed that the degree of hydrogen bonding in the hard segments was reduced due to presence of silicate layers, which resulted in simultaneous enhancement in the maximal strength and elongation at break for an optimum 1wt% amine-modified organoclay loading, regardless of the hard segment ratio [94]. This was explained by the dangling chain conformation and the plasticizing effect of functional organoclays in polyurethane. On the other hand, higher loading was advantageous in terms of hardness in the expense of elongation loss due to poorer dispersion.

In a recent study the effect of amine based organoclays with different lengths and amounts of alkyl chains was investigated. It was suggested that organic treatment reduced platelet-platelet attraction and increased organoclay-polymer affinity. It was concluded that one long alkyl tail on the ammonium rather than two, hydroxyl ethyl groups on the amine rather than methyl groups, and longer alkyl tail lead to higher clay dispersion and therefore greater polyester based TPU (Pellethane®) matrix reinforcement [97]. This was attributed to higher affinity of the matrix to the modified organoclay and resultant enhanced hydrogen bonding between the organoclay and the polymer matrix. Contrarily, Pattanayak and Jana claimed that hydrogen bonding between clay and polymer matrix had no effect on mechanical properties and that clay particles showed no influence on hard segment hydrogen bonding in polyesterpolyols [90]. However, it was shown that clay particles caused strong improvement in thermal stability and mechanical properties, latter being explained by clay-polymer tethering.

2.3.2. TPU/Silica Nanocomposites

In recent years polymer/silica nanocomposites received much attention and have been employed in a variety of applications as reviewed in section 2.1.2. Related to elastomers, it is believed that colloidal silica is displacing carbon black as the filler of choice with respect to recent advances in the silane chemistry and silica modification [98]. Silica has increased in importance due to both its improved performance properties and environmental efficiency since it is not petroleum based. Although silica and carbon black have similarities in agglomeration, the causes of agglomeration and the ability to disagglomerate and disperse are slightly different. Carbon black and silica both experience filler-filler interactions through the relatively weak Van der Waals forces, which can be broken by mixing. These forces are strong enough to create agglomerates. In addition to Van der Waals forces, silica agglomerates contain hydrogen bonds, creating significant challenges in breaking small agglomerates through mixing [99]. Synthetic silica has particle size as small as carbon black besides an extremely reactive surface. In addition to these, theoretical treatment of the carbon black reinforcement phenomena is difficult with respect to its complexity, surface inhomogeneity and resultant large differences in energy of adsorption at different sites on the surface [100]. On the other hand, silica surface is much more clearly defined and tailorable, therefore reinforcement properties of the material can be much more easily studied.

Commonly, fumed silica nanoparticles are added to improve the thermal, rheological and mechanical properties of polyester based TPU adhesives [101-103]. The improved rheological properties of the PU composite containing hydrophilic fumed silica was ascribed to the creation of a network between the polyurethane chains and the silanol groups on the fumed silica surface. In the following studies, it was claimed that the network structure was the result of hydrogen bonding between the silanol groups on the nanosilica surface and the ester carbonyl groups of the polyester groups (soft segments) in the polyurethane, favoring the degree of phase separation [92, 93]. Vega-Baudrit et al. also demonstrated that the degree of phase separation in polyester based polyurethanes was increased due to creation of interaction between the silanol groups on the nanosilicas and the polyurethane [104]. They reported that the formation of these interactions decreased the crystallinity, and therefore melting enthalpies of polyurethane-silica nanocomposites, whereas increased the thermal stability due to the increase in degree of phase separation. The increase in both tensile strength and elongation at break were related to the silanol content and the dispersibility of nanosilica. It was pointed out by Nunes et al. that improvement in hardness could also be obtained in the expense of elongation [92]. They also reported that a maximum value for tensile strength at 1% loading, and reduction in tensile strength with filler concentration. This was attributed to the possibility of formation of voids in the polymer layer next to the filler surface that would cause tension concentration at the void vicinity generating the fractures as the filler concentration increases. Chen et al. suggests that there should be a maximum T_g value dependent on particle size, silanol content and particle dispersion for the polyester based TPU/nanosilica system [52]. They also showed that silica nanoparticles bearing high surface silanol content suffered from aggregation, and the agglomerate size increases by increasing the silanol content [104].

Aggregation leading to phase separation has been the most important problem affecting the resultant properties of polymer/silica nanocomposites since it ultimately decreases the interfacial interaction between the organic and inorganic phases resulting in diminished mechanical and thermal properties. The most frequently used method is to modify the surface of the silica nanoparticles to enhance the compatibility with polymer matrix and therefore to improve the dispersion of nanosized silica particles. Silane coupling agents (SCA) are generally selected as the modifing agents for colloidal silica particles since the hydroxyl groups on the surfaces of silica particles could react with siloxane groups of SCA. SCA molecules attached to the silica surface could inhibit

aggregation due to steric repulsion of the grafted organic groups leading to improved dispersion of the silica and increased interfacial interaction between the phases [57, 105-107].

Few studies involving TPU/modified silica composites exist in the literature, and most of these stduies are based on polyester based TPUs. Chen et al. reported that the abrasion resistance of polyester based polyurethanes containing nanosilicas modified with long-chain SCA molecules had better static mechanical properties and transparency, but lower storage modulus, than those with short-chain SCA molecules [89]. Further investigation on the same system demonstrated that the storage modulus of the nanocomposite depends on the surface properties of the silica particles, the crosslinking density and the interfacial interaction [87]. Aso et al. claimed that dimethyl dichlorosilane modification on silica surface had a dual positive effect on the TPU nanocomposite: the lack of large agglomerates hinders the formation of local stress concentrations where fracture is easy to start; secondly, the larger contact surface provides a better opportunity for the properties of the dispersed phase to be reflected in the TPU-silica nanocomposite [86].

3. METHODS

3.1. EXPERIMENTAL

3.1.1. Silica Sol Preparation

Silica sols containing particles within the range of 20-200 nm were prepared by Stöber method, which includes addition of alkyl silicate into saturated alcoholic ammonia solutions or in alcohol-ammonium hydroxide mixtures [15]. Tetraethyl orthosilicate (TEOS), $Si(OC_2H_5)4$, was used as the precursor (Figure 3-1). Initial studies aiming the optimization of silica particle size and size distribution were performed in the parent alcohol, ethanol. Following these studies, six different low molecular weight alcohols (methanol, ethanol, n-propanol, iso-propanol, n-butanol, t-butanol) were used to investigate the effect of solvent alcohol on TEOS hydrolysis rate and silica particle size. Finally, particle size and size distribution was studied in iso-propanol (IPA), which is a good solvent for the polyurethaneurea block copolymers used in this study. Aqueous ammonia solution (25% NH_3) was used as the source of both base catalyst and water for all experiments.

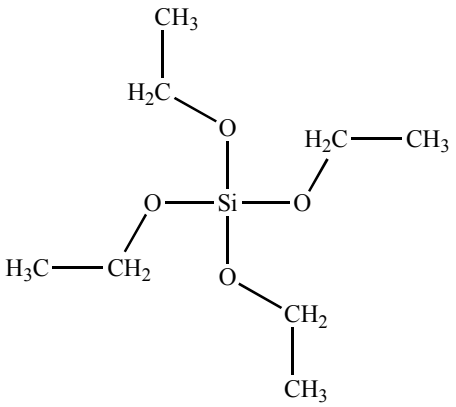
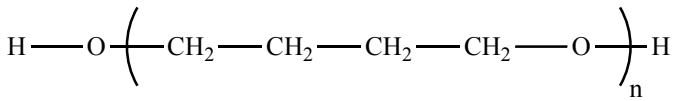


Figure 3-1: Tetraethyl orthosilicate (TEOS) molecule.

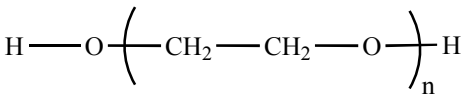
3.1.2. TPU Synthesis

Polyurethaneurea block copolymers with 20-30% by weight hard segment content was synthesized and provided by Polymer Science and Technology Laboratories at Koç University.

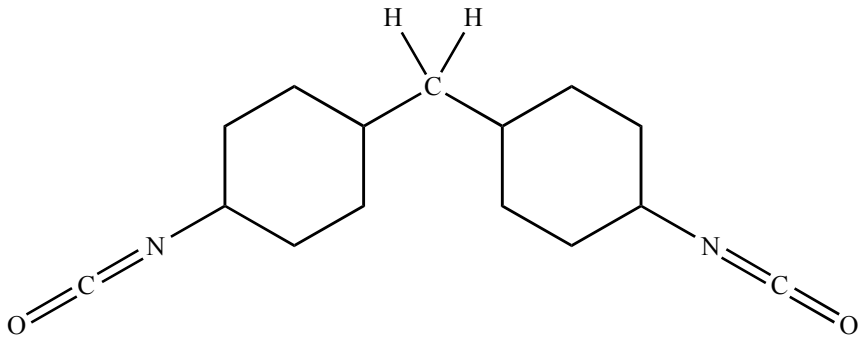
Poly(tetramethylene oxide) glycol (PTMO) and Poly(ethylene oxide) glycol (PEO) with <Mn> = 2,000 g/mol were used as the soft segment components. The hard segment was composed of an cycloaliphatic diisocyanate, bis(4-isocyanatocyclohexyl)methane (HMDI), chain extended with 2-methyl-1,5-diaminopentane (MDAP). The polymers were prepared by a two-step process in THF/IPA (1:1 v/v) and detailed explanation of the preparation method is given in Chapter V. Chemical structures of the chemicals and polyurethane-urea copolymer are provided in Figure 3-2.



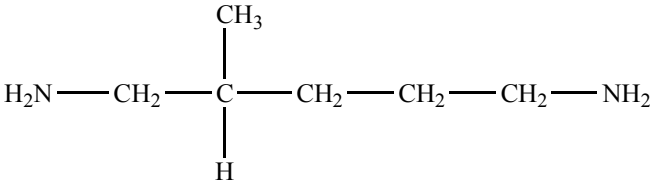
PTMO: Poly(tetramethylene oxide), Mn= 2,000 g/mol



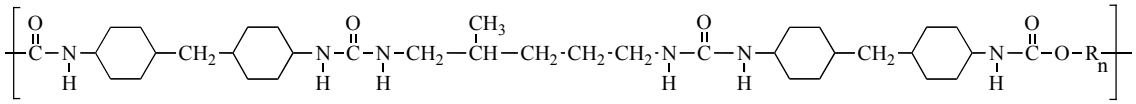
PEO: Poly(ethylene oxide), Mn= 2,000 g/mol



HMDI: Bis(4-cyclohexylmethane)diisocyanate



MDAP: (2-Methyl-1,5-diaminopentane)



TPU: Polyurethane-urea copolymer with R_n = PTMO (n=28) or PEO (n=46)
(Alkyl hydrogen atoms are not shown for simplicity)

Figure 3-2: Chemical structures of the chemicals that constitute TPU.

3.1.3. TPU/Silica Composite Preparation

Making a homogeneous dispersion of nanoparticles in a polymeric matrix is a very difficult task due to the strong tendency of nanoparticles to agglomerate. To overcome this difficulty, we utilized the fact that polyurethaneurea copolymer can be completely dissolved in IPA. Subsequently, we optimized the preparation of silica sols in IPA and used solution blending in this common solvent for the preparation of TPU/silica nanocomposites. By using silica sols "as-prepared", redispersion of silica nanoparticles in polymer solution could be avoided. In addition to the simplicity of this technique, we aimed to prevent agglomeration of silica nanoparticles, and hence to enhance the interfacial interaction between the copolymer matrix and the silica surface.

3.2. CHARACTERIZATION

In this section, the theory and applications of characterization techniques utilized in this dissertation is briefly reviewed.

3.2.1. Dynamic Light Scattering

Dynamic light scattering (DLS, also known as photon correlation spectroscopy or quasi-elastic light scattering) is a technique in physics that can be used to determine the size distribution profile of particles in the sub micron range [108]. DLS typically measures the Brownian motion of the particles (random movement of particles due to the bombardment by the surrounding solvent molecules) and relates this to the size of particles. This is done by measuring the rate, at which the intensity of the scattered light fluctuates when detected using a suitable optical arrangement. If the particles are small compared to the wavelength of the laser used, then the scattering from a particle illuminated by a vertically polarized laser will be essentially isotropic. The Rayleigh approximation defines that intensity of the scattered light is proportional to the sixth power of the particle diameter. When the size of the particles becomes roughly equivalent to the wavelength of the illuminating light, then a complex function of minima and maxima with respect to angle is observed (Mie Theory) [109].

The velocity of the Brownian motion is defined by the translational diffusion coefficient (D). The size of the particle is calculated from the translational diffusion coefficient by using Stokes-Einstein equation (3.1);

$$d(H) = \frac{kT}{3\pi\eta D} \qquad (3.1)$$

where *d(H)* is the hydrodynamic diameter, *k* is the Boltzmann constant and η is the viscosity. By definition, “DLS measured hydrodynamic diameter” is the diameter of a hypothetical hard sphere that diffuses with the same speed as the particle under examination.

Intensity weighted mean particle size and the width of the particle size distribution (polydispersity index, PdI) are calculated from a cumulants analysis of the

DLS measured intensity correlation function. The cumulants analysis is basically the fit of a polynomial to the log of the G1 correlation function:

$$Ln[G1] = a + bt + ct^2 + dt^3 + \ldots \quad (3.2)$$

The first cumulant or moment, b, is used to calculate mean particle size and the second moment, c, is used to calculate PdI when scaled as $2c/b^2$. The PDI, as an indication of variance in the sample, is given in the range [0,1]. Low PDI (usually less than 0.2) indicates that the sample is monodispersed, whereas with a broader distribution (PdI over 0.5) mean particle size calculation is not recommended [110].

DLS measurements were conducted to determine the mean particle size and the size distribution of silica particles in different solvents. Time dependent silica growth was also monitored by succeeding analyses.

3.2.2. Spectroscopy

3.2.2.1.Nuclear Magnetic Resonance Spectroscopy

Nuclear magnetic resonance spectroscopy, NMR, is a technique that exploits the magnetic properties of certain atomic nuclei to determine physical and chemical properties of atoms or the molecules in which they are contained. It relies on the phenomenon of nuclear magnetic resonance and can provide detailed information about the structure, dynamics, reaction state, and chemical environment of molecules [111].

According to the Pauli Exclusion principle, electrons have +½ and -½ spins. Same phenomenon is also valid for many atoms (e.g., ^{1}H, ^{13}C, ^{15}N, ^{31}P), and they have so-called "spin ½" nuclei, which have two quantum states that can be visualized as having the spin axis pointing "up" or "down" [112]. Since, the protons are electrically charged, they can generate their own magnetic field from the spin. In the absence of an external magnetic field, these two states have the same energy and one half of a large population of a nuclei will be in the "up" state and one half will be in the "up" state. When the external magnetic field is applied, the "up state", which is aligned with the magnetic filed, is lower in energy than the "down" state, which is opposed to the magnetic field. Because this is a quantum phenomenon, there are no possible states in between. NMR machines generate magnetic fields, which the nucleus of the molecule's magnetic field to align in two possible orientations. Since energy is required to flip from

one orientation to another, the NMR machine calculates these energy values and converts the data as "chemical shifts" signals [113].

Liquid ^{29}Si-NMR technology has been a very useful tool in sol-gel research to obtain valuable information about the chemistry of silicon alkoxides and their hydrolyzed species by allowing identification and quantification of soluble Si-containing species in solution without disturbing the evolving system. [37, 114]. In this study, we employed *in-situ* liquid ^{29}Si-NMR to monitor the hydrolysis reaction kinetics during the formation of silica particles.

3.2.2.2.Fourier Transform Infrared Spectroscopy (FT-IR)

FTIR spectrometry is widely used in organic synthesis, polymer science, petrochemical engineering, pharmaceutical industry and food analysis [115]. The range of Infrared region is 13000 ~ 10 cm^{-1}. It is divided into near-IR region (13000 ~ 4000 cm^{-1}), mid-IR region (4000 ~ 400 cm^{-1}) and far-IR region (400 ~ 10 cm^{-1}) [116].

Infrared spectra result form the transitions between quantized vibrational energy states. The energy difference for transitions between the ground state and the first excited state of most vibrational modes corresponds to the energy of radiation in the mid-infrared spectrum (4000 ~ 400 cm^{-1}) [115]. It is the most commonly used region for infrared absorption spectroscopy because the absorption radiation of most organic compounds and inorganic ions is within this region.

A common FTIR spectrometer consists of a source, interferometer, sample compartment, detector, amplifier, A/D convertor, and a computer. The source generates radiation, which passes the sample through the interferometer and reaches the detector. Then the signal is amplified and converted to digital signal by the amplifier and analog-to-digital converter, respectively. Eventually, the signal is transferred to a computer in which Fourier transform is carried out [111].

During this study, FTIR spectroscopy was used to monitor the presence and changes in the interaction between silanol groups and segments of copolymer in nanocomposites. In addition to this, it was used to detect the degree of unreacted ethoxy groups on the resulting silica nanoparticles.

3.2.3. Imaging

Several imaging techniques, scanning electron microscopy (SEM), transmission electron microscopy (TEM) and atomic force microscopy (AFM) were used to determine size and morphology of silica particles. SEM was also used to examine the cross-sections of the polymer and polymer/silica nanocomposites to determine the degree of dispersion of filler in the polymer matrix. In addition, TEM was used to image the particle dispersion in polymer solution.

3.2.3.1. Scanning Electron Microscopy

Scanning electron microscope (SEM) is a type of electron microscope that produces images of a sample by scanning it with a focused beam of electrons. The electrons interact with electrons in the sample, producing various signals (secondary, backscattered, etc.) that contain information about the sample's surface topography and composition. The electron beam is generally scanned in a raster scan pattern, and the beam's position is combined with the detected signal to produce an image [117].

For conventional imaging in the SEM, specimens must be electrically conductive, at least at the surface, and electrically grounded to prevent the accumulation of electrostatic charge at the surface. Nonconductive specimens tend to charge when scanned by the electron beam, and especially in secondary electron imaging mode, this causes scanning faults and other image artifacts.

3.2.3.2. Transmission Electron Microscopy

Transmission electron microscopy (TEM) is a microscopy technique whereby a high-energy electron beam is transmitted through a ultra-thin specimen to image and analyze the microstructure of the materials with atomic scale resolution. An image is formed from the interaction of the electrons transmitted through the specimen; the image is magnified and focused onto a fluorescent screen, or recorded on a film or digital camera [118].

TEMs are capable of imaging at a significantly higher resolution than light microscopes, owing to the small de Broglie wavelength of electrons. This enables the instrument's user to examine fine detail—even as small as a single column of atoms, which is tens of thousands times smaller than the smallest resolvable object in a light

microscope. Alternate modes of use allow for the TEM to observe modulations in chemical identity, crystal orientation, electronic structure and sample induced electron phase shift as well as the regular absorption based imaging. A TEM specimen must be approximately 1000Å or less in thickness based on the area of interest.

3.2.3.3.Atomic Force Microscopy

Atomic force microscopy (AFM) is a very high-resolution type of scanning probe microscopy, with demonstrated resolution on the order of fractions of a nanometer, more than 1000 times better than the optical diffraction limit.

The AFM consists of a cantilever with a sharp tip (probe) at its end that is used to scan the specimen surface. The cantilever is typically silicon or silicon nitride with a tip radius of curvature on the order of nanometers. When the tip is brought into proximity of a sample surface, forces between the tip and the sample lead to a deflection of the cantilever according to Hooke's law. Depending on the situation, forces that are measured in AFM include mechanical contact force, van der Waals forces, capillary forces, chemical bonding, electrostatic forces, magnetic forces, etc. [119]. The AFM can be operated in a number of modes, depending on the application. The primary modes of operation for an AFM are static mode and dynamic mode. In static mode, the cantilever is "dragged" across the surface of the sample and the contours of the surface are measured directly using the deflection of the cantilever. In the dynamic mode, the cantilever is externally oscillated at or close to its fundamental resonance frequency or a harmonic. The oscillation amplitude, phase and resonance frequency are modified by tip-sample interaction forces. These changes in oscillation with respect to the external reference oscillation provide information about the sample's characteristics. Contact, non contact and tapping mode are the major operating modes for AFM.

3.2.4. Thermal Analyses

3.2.4.1. Differential Scanning Calorimetry

Differential scanning calorimetry (DSC) is basically defined as the measurement of the change of the difference in the heat flow rate to the sample and to a reference sample while they are subjected to a controlled temperature program [120]. DSC is used widely to determine the thermal transitions in polymeric materials such as melting point

and glass transition temperature. Percent crystalline material and thermal degradation of polymers can also be studied by using this thermoanalytical technique.

DSC includes both a sample substance and a reference substance, residing in separate chambers. While the reference chamber contains only a solvent (such as water), the sample chamber contains an equal amount of the same solvent in addition to the substance of interest, of which the heat of reaction ($\Delta_r H$) is being determined. The $\Delta_r H$ due to the solvent is constant in both chambers, so any difference between the two can be attributed to the presence of the substance of interest. Each chamber is heated by a separate source in a way that their temperatures are always equal. This is accomplished through the use of thermocouples; the temperature of each chamber is constantly monitored and if a temperature difference is detected, then heat will be added to the cooler chamber to compensate for the difference. The heating rate used to maintain equivalent temperatures is logged as a function with respect to the temperature [121].

In this study, DSC was used to evaluate the thermal behavior of neat TPU copolymer and its silica nanocomposites in order to investigate the effect of silica incorporation on the thermal characteristics of TPU.

3.2.4.2. Thermal Gravimetric Analysis

Thermogravimetric analysis (TGA) measures the amount and the rate of weight changes in a material as a function of temperature or time in a controlled atmosphere. These measurements are used to obtain information about physical phenomena, such as second-order phase transitions (e.g. vaporization, sublimation, absorption) or chemical phenomena (e.g. chemisorption, dehydration, decomposition, oxidation, reduction) by making determinations about composition and thermal stability [121]

Thermogravimetric analysis relies on a high degree of precision in three measurements: mass change, temperature, and temperature change. Therefore, TGA is basically equipped with a precision balance including a pan loaded with the sample, and a programmable furnace. The furnace can be programmed either for a constant heating rate, or for heating to acquire a constant mass loss with time.

Thermogravimetric analyses were performed on the nanocomposites in order to investigate the effect of nanosilica on the thermal stability of the system and to determine the residual silica content of the nanocomposites.

3.2.5. Mechanical Analysis

3.2.5.1. Tensile Testing

In a broad sense, strength refers to the ability of a structure to resist loads without failure, which may occur due to excessive stressor deformation. Tensile testing, also known as tension testing, is a fundamental materials science test in which a sample is subjected to a controlled tension until failure [122]. Properties that are directly measured via a tensile test are ultimate tensile strength, maximum elongation and reduction in area. From these measurements the following properties can also be determined: Young's modulus of elasticity, Poisson's ratio, yield strength and strain hardening characteritics.

The test process involves placing the test specimen in the testing machine and applying tension to it until it fractures. During the application of tension, the elongation of the gauge section is recorded against the applied force. The data is manipulated so that it is not specific to the geometry of the test sample. The elongation measurement is used to calculate the *engineering (or nominal) stain*, ε, using the equation 3.3:

$$\varepsilon = \frac{\Delta L}{L_0} = \frac{L - L_0}{L_0} \tag{3.3}$$

where ΔL is the change in gauge length, L_0 is the initial gauge length, and L is the final length. The force measurement is used to calculate the *engineering (or nominal) stress*, σ, using equation (3.4):

$$s = \frac{F_n}{A} \tag{3.4}$$

where F is the force and A is the cross-section of the gauge section. When force-elongation data are converted to engineering stress and strain, a *stress-strain curve,* which is virtually independent of specimen dimensions, is obtained. The tensile strength (ultimate strength) is defined as the highest value of engineering stress. The slope of the strain-stress curve in the elastic region is defined as the Young's modulus of elasticity (Eqn. 3.5), which is a measure of the stiffness of the material.

$$E = \frac{\Delta\sigma}{\Delta\varepsilon} \tag{3.5}$$

Total elongation, which includes both elastic and plastic deformation, is the amount of uniaxial strain at fracture. Percent elongation at break is used to describe the ductility of a material. It is determined by removing the fractured specimen from the grips; fitting the broken ends together and measuring the distance between gage marks. Percent elongation at break reports the amount of plastic deformation only. If the amount of elongation is small, percent reduction of area is used to describe the ductility of a material. In this study, tensile testing was used to investigate the improvement in mechanical properties of nanocomposite systems with respect to filler size and loading.

3.2.5.2.Nanoindentation

Indentation testing essentially consists of touching a specimen whose mechanical properties (e.g. elastic modulus, hardness) are unknown with another material whose properties are known [123]. Nanoindentation is simply an indentation test in which the length scale of the penetration is measured in nanometers and an indenter with a geometry known to high precision (usually a Berkovich tip, which has a three-sided pyramid geometry) is employed. During the course of nanomechanical testing, the instrument performs nanoscale indents by applying a force (denoted as *P*) and the probe displacement (denoted as *h*) into the sample. A load versus displacement curve can then be generated from the collected data. The sample hardness (denoted as *H*)and reduced elastic modulus (denoted as E_r) can then be calculated from this curve. The reduced modulus is defined by the Eqn (3.6):

$$E_r = \frac{S\sqrt{\pi}}{2\sqrt{A}} \tag{3.6}$$

where *S* is the unloading stiffness and is defined by Eqn. (3.7):

$$S = \frac{dP}{dh} \tag{3.7}$$

and A is the projected contact area. The reduced modulus is related to the modulus of eleasticity (E) through the Eqn. (3.8):

$$\frac{1}{E_r} = \frac{(1 - v_i^2)}{E_i} + \frac{(1 - v_s^2)}{E_s} \tag{3.8}$$

where the subscript I corresponds to the indenter material, the subscript s corresponds to the indented sample material, and v is the Poisson's ratio. The unloading stiffness is calculated by fitting the unloading curve to the power law relation (Eqn 3.9),

$$P = A(h - h_f)^m \tag{3.9}$$

where A, h_f, and m are arbitrary fitting parameters. The stiffness can be calculated from the derivative of Equation (3.9),

$$S = \frac{dP}{dh}(h_{max}) = mA(h_{max} - h_f)^{m-1} \tag{3.10}$$

The hardness is defined by the ratio of the maximum load to the projected contact area by the following Eqn (3.11)

$$H = \frac{P_{max}}{A} \tag{3.11}$$

The contact area is determined from a probe calibration function $A(h_c)$ where h_c, the contact depth, is found by using the equation

$$h_c = h_{max} - \varepsilon \frac{P_{max}}{S} \tag{3.12}$$

To account for edge effects, the deflection of the surface at the contact perimeter is estimated by taking the geometric constant ε as 0.75. Nanoindentation testing was used to investigate the mechanical properties of TPU/silica nanocomposites.

4. TEOS HYDROLYSIS KINETICS AND CONTROLLED SYNTHESIS OF SILICA NANOPARTICLES IN LOW MOLECULAR WEIGHT ALCOHOLS

4.1. INTRODUCTION

Controlled fabrication of monodisperse silica particles is of great interest in many fields, including ceramics, optics, catalysis, electronics and biology. Sol-gel route combines the ability to control the growth of silica particles at molecular level with the possibility of processing the material at room temperature, such as casting into molds, spinning fibers. The synthesis basically consists of the hydrolysis of alkoxides dissolved in their parent alcohols with a mineral acid or a base catalyst (Eq. 4.1) and subsequent condensation reactions involving the silanol groups that produce siloxane bonds and the by-products, which are alcohol (Eq. 4.2) or water (Eq. 4.3), that lead to the formation of various forms of silica by the polymerization of silicic acid [17, 18].

$$\equiv Si - OR + H_2O \rightleftharpoons \equiv Si - OH + ROH \quad (4.1)$$

$$\equiv Si - OR + HO - Si \equiv \rightleftharpoons \equiv Si - O - Si \equiv + ROH \quad (4.2)$$

$$\equiv Si - OH + HO - Si \equiv \rightleftharpoons \equiv Si - O - Si \equiv + H_2O \quad (4.3)$$

The morphology of the end product is essentially controlled by the type of the catalyst used. Acid catalyzed reactions lead to a three-dimensional gel or a network structure [124, 125], whereas base-catalyzed reactions result in condensed spherical-shaped particles [126, 127].

Stöber et al. [15] were the first to show that remarkably uniform silica particles with sizes ranging from 50 nm to >1μm in diameter could be synthesized by hydrolyzing silicon alkoxides in aqueous alcoholic solutions containing ammonia. In a typical Stöber process, TEOS is introduced into a batch reactor with ethanol, water and ammonia. The lower parent alcohol, e.g. ethanol, acts as a co-solvent for silicon alkoxides (e.g. TEOS), which is immiscible with water. Ammonia catalyzes both hydrolysis and condensation by dissociating the water molecules, and provides the

spherical shape of the silica particles with a negative, stabilizing charge in the alcohol solutions [15, 21]. Since the reactions are carried out in high pH region (>7), particles formed are stable toward gelation with respect to repulsion effects.

Accordingly, the primary parameters that affect the reaction kinetics and the properties of resulting silica particles can be summarized as initial concentration of reactants (TEOS, water, ammonia), type of the alcohol used as the solvent and the reaction temperature. The reports regarding the effects of TEOS, ammonia and water especially on the size of silica particles are controversial. Rao et al. reported that the particle size decreased with increasing ammonia concentration (2.8-28.0 M) in the presence of 3.0-14.0 M water in a semi-batch sol-gel process [39]. They also found that particle size increased from 60 to 417 nm when TEOS concentration was increased from 0.012 to 0.12 M. Bagwe et al. observed that the increase in the amount of ammonia (0.16 to 0.64 M) yielded larger particles in a micro-emulsion process [13]. They also reported that there was no change in particle size when TEOS concentration was increased from 0.025 to 0.1 mM. Tan et al. tuned the size of particles and showed that the particle size decreases with reduced initial ammonia concentration [128].

The role of the solvent alcohol is rather complex compared to the other components in sol-gel systems. In addition to regulating the miscibility of the system, alcohol used during the synthesis could also play the role of a reactant through transesterification (alkoxy exchange) reactions (Eqn. 4.4):

$$Si(OR)_{4-z} + zR^*OH \underset{}{\overset{\text{transesterification}}{\rightleftharpoons}} (OR^*)_z Si(OR)_{4-z} + zROH \qquad (4.4)$$

Several studies show that alkoxy exchange is promoted in acidic environment while it could not be detected in basic media [129-133]. Recent work of Lim et al., however, has presented the possibility of fast alkoxy exchange at the early stage of hydrolysis of TEOS in basic media [134]. Under these circumstances, the reaction rate and the resulting particle size of silica are modified.

The role of the alcohol type and composition is also critical in terms of the solubility of the intermediates bearing polar and charged groups [135]. Since solvents may change the electrostatic and hydrogen bonding interactions, the choice of the solvent might alleviate or aggravate the reaction rate and/or change the solubility and stability of the intermediate products. Hydrolysis of silicon alkoxides has been reported

to be the rate-determining step by many researchers [29] during silica synthesis. However, in case of base-catalyzed reactions, nature of the solvent has been shown to have a stronger influence on the reaction rate compared to acidic systems [136].

Despite great interest in Stöber silica and its applications, few studies have included the role and effect of solvent type in basic media [30, 128, 137, 138]. Furthermore, observed dependencies were subjected to further investigation and related work was mostly focused on the effects of ammonia and water concentrations in limited number of solvent alcohols. In the study of Harris et al., early stages of Stöber silica particles were investigated by time-resolved ultra-small-angle X-ray scattering and slower growth rate was detected in ethyl alcohol when compared to growth rates in n-propyl and n-butyl alcohol when excess water was used [138]. Their recent work was directed towards the investigation of the reaction kinetics, leading to the first Stöber silica nanoparticles by using NMR and SAXS both in methanol and ethanol [37] and they proposed that the size of the primary particles is thermodynamically controlled by the interactions of the reaction intermediates and the solvents.

Main goal of this work is to determine the effect of each reagent on TEOS hydrolysis rate and silica particle size in ethanol in addition to the effect of alcohol molecular weight and structural isomerism under stoichiometric conditions in basic media. Thereby, a systematic approach is followed to produce uniform silica particles in different alcohols and to discuss the effects of different parameters (TEOS, ammonia, water, alcohol) are aimed. For this purpose, liquid ^{29}Si-NMR was used to monitor the nucleation and growth of Stöber silica by means of consumption of TEOS and generation of reaction intermediates at five polar aprotic solvents (C1-C4 alcohols). We mainly focused on the initial hydrolysis of TEOS, which has been reported as the rate-determining step for the Stöber synthesis [29]. In this chapter, we discuss the effect of initial TEOS, water and ammonia concentration along with alcohol type in hydrolysis kinetics. In addition, we also provide detailed analyses on the size of the silica particles formed and their size distribution based on the dynamic light scattering (DLS) measurements and atomic force microscopy (AFM) studies.

4.2. CHEMICAL REACTIONS KINETICS OF STÖBER SYSTEMS

Overall hydrolysis reaction of TEOS can be described by the following equation:

$$Si(OEt)_4 + xH_2O \rightarrow (OH)_x Si(OEt)_{4-x} + xEtOH \qquad (4.5)$$

The hydrolysis of TEOS runs simultaneously with condensation that results in a complex reaction mechanism. In literature, there are several sophisticated reaction models developed to explain the complex nature of Stöber synthesis [29, 30]. In this study, a simple hydrolysis model proposed by Green et al. [37] was used to calculate the hydrolysis rate constant for TEOS to be able to evaluate the effect of different solvents at the onset of the reaction. For all the solvent systems studied, it was shown that the precursor hydrolyzed through singly hydrolyzed monomer and this step is shown by Eqn. (4.6)

$$Q_0^0 + H_2O \xrightarrow{k_H} Q_1^0 + ROH \qquad (4.6)$$

The rate equation for reaction (4.7) is as follows:

$$r_{TEOS} = -d[Q_0^0]/dt = k_H [Q_0^0]^{\alpha} [NH_3]^{\beta} [H_2O]^{\gamma} \qquad (4.7)$$

where the exponents α, β and γ are the reaction orders with respect to TEOS, NH_3 and H_2O respectively. Since NH_3 is used as the catalyst and the change in water was reported as less than 5% of the initial level [139], they are both considered invariable. So we could define the pseudo first-order rate constant, k_H^*, as

$$k_H^* = k_H [NH_3]^{\beta} [H_2O]^{\gamma} \qquad (4.8)$$

thus the hydrolysis rate equation (4.7) can be simplified as;

$$r_{TEOS} = -d[Q_0^0]/dt = k_H^* [Q_0^0]^{\alpha} \qquad (4.9)$$

The integration of Eqn. (4.9) leads to:

$$\ln[Q_0^0] = \ln[Q_0^0]_0 - k_H^* t \qquad (4.10)$$

where ($\ln[Q_0^0]$) is plotted as a function of time, hydrolysis of TEOS is expected to follow a first order reaction kinetics (α=1) for all systems investigated.

4.3. EXPERIMENTAL SECTION

4.3.1. Materials

Silica sols were prepared from a solution of reagent grade ammonium hydroxide (25% NH_3), tetraethyl orthosilicate (TEOS, >99%) in an ethyl alcohol with >99.8% purity. All chemicals were obtained from Merck, Germany and were used as received.

4.3.2. Methods

All reactions were carried out in 100 mL Pyrex reactors with low to moderate mixing speeds at room temperature (25±2°C). All vessels were washed with 2% HF solution and then rinsed with deionized water several times before use. For practical purposes, we used 25% or 0.4 M ammonium hydroxide as ammonia and water source instead of bubbling ammonia through the alcohol and water mixture as it was reported for the original Stöber recipe. Alcohol and ammonium hydroxide solutions were mixed for 20 minutes and then TEOS was quickly poured into the reactor to initiate the reaction.

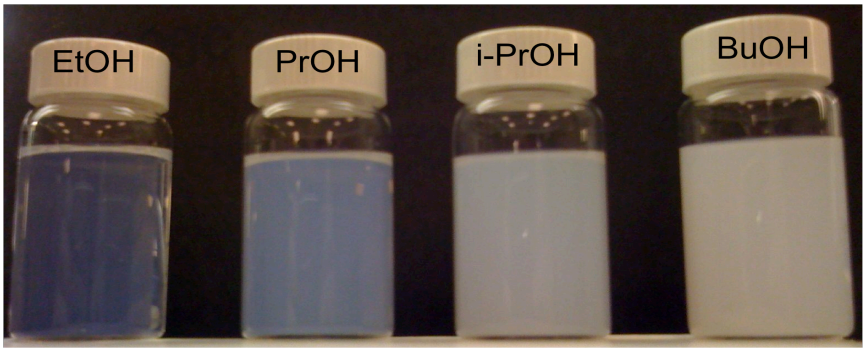


Figure 4-1: Silica sols prepared in ethanol, n-propanol, iso-propanol and n-butanol after one month.

Colloidal sol samples prepared to investigate effect of solvent alcohol were named according to the alcohol used during the synthesis such as MeOH, EtOH, PrOH, i-PrOH and BuOH (Table 4-1: Initial Stöber reactant compositions in different solvent media.). All reactions were conducted under stoichiometric conditions where no flocculation was observed and all sols, except MeOH, could retain their stability for months as shown in Figure 4-1.

Table 4-1: Initial Stöber reactant compositions in different solvent media.

Sample	**$[NH_3]_{aq}$ (M)**	**[TEOS] (M)**	**Solvent**
MeOH	0.4	0.7	Methanol
EtOH	0.4	0.7	Ethanol
PrOH	0.4	0.7	*n*-Propanol
i-PrOH	0.4	0.7	*iso*-Propanol
BuOH	0.4	0.7	*n*-Butanol

Silica particle formation was monitored by measuring changes in particle size, solution conductivity and TEOS and soluble silica concentrations. Preparation conditions of samples are presented in Table 4-2. All experiments were conducted in ethanol at room temperature.

Table 4-2: Initial Stöber reactant compositions in ethanol media.

Sample	**[TEOS] (M)**	**$[H_2O]$ (M)**	**$[NH_3]_{aq}$ (M)**	**$TEOS/H_2O/NH_3$**
S1	0.80	1.35	0.48	1/1.7/0.6
S2	0.16	1.35	0.48	1/8.5/3
S3	0.32	1.35	0.48	1/4.2/1.5
S4	0.32	2.09	0.48	1/6.5/1.5
S5	0.32	2.74	0.48	1/8.5/1.5
S6	0.32	1.02	0.36	1/3.2/1.1
S7	0.32	6.77	2.39	1/21/7.5
S8	0.32	1.35	0.36	1/4.2/1.1
S9	0.32	1.35	0.1	1/4.2/0.3

The changes in the concentrations of TEOS and intermediates during the course of the reactions were monitored by using liquid state ^{29}Si-NMR. Prior to each analysis, TEOS was added to ammonium hydroxide/alcohol solution under vigorous stirring to minimize localized reaction zones during the mixing of the reactants. After mixing for 2 min, the mixture was immediately transferred into a 5 mm (O.D.) quartz NMR sample

tube, and analyzed. The resulting spectra were internally referenced to a tetramethylsilane (TMS) standard. Chromium (III) acetyl acetonate, $Cr(acac)_3$, 0.016 M was added as the spin relaxation agent. Numerous studies have shown that $Cr(acac)_3$ had no effect on the studied reactions [33, 140, 141]. ^{29}Si NMR experiments were performed in duplicate on a Varian Inova 500 MHz Spectrometer at a spectral frequency of 99.258 MHz. The kinetics of the Stöber reaction was monitored using ^{29}Si-NMR spectroscopy by running the 384 number scans at 30-minute intervals up to 20 hours. The spectra were acquired using a spectral width of 18 940 Hz, 64k data points, 384 scans, and a pulse delay of 3s using 60° pulse angle with an acquisition time of 1.7s. In a separate experiment, first 30 minute of the synthesis reaction was monitored by 5-minute intervals. The concentration of TEOS was determined by comparing the subsequent NMR scans to the initial Q_0^0. Prior to each set of experimental solutions, the integrated area of the initial Q_0^0 peak of TEOS, observed without the presence of catalyst and water, was taken as being 100%. During the experiments, gelation did not occur; recycle delay was kept constant throughout the measurements.

Dynamic light scattering analyses (DLS) were conducted to determine the intensity weighted mean particle size and the width of the particle size distribution (polydispersity index, PdI) by using ZetaSizer Nano (Malvern, UK). Before each DLS analysis, dilution versus concentration screening was performed to find the appropriate dilution at which the particle size is independent of concentration. Thus, multiple scattering and particle-particle interactions could be minimized. Three individual measurements were per each sample were performed and then averaged. The average particle diameter was given along with the width of the distribution (Average diameter ± width of the size distribution). The temperature was maintained constant at 25 ± 0.1 °C. Particle size analysis of the silica nanoparticles on dip-coated mica substrates was also performed using Atomic Force Microscopy (AFM) Veeco Nanoscope IIIa Multimode SPM Tapping Mode, silicon probes, which have 42 N/m spring constant (Olympus, OMCL-AC160TS). By use of a KSV Sigma 700 Tensiometer (KSV Instruments Ltd.), silica particles were coated by dipping a freshly cleaved mica substrate into silica sols, with a velocity of 1 mm/min and then pulled from the solution under a constant velocity of 5 mm/min. The coated mica samples were dried and maintained in a closed box. AFM images were processed by using WSxM software package.

4.4. RESULTS AND DISCUSSION

4.4.1. NMR Experiments

There are many methods to monitor silicon alkoxide/water/alcohol systems such as UV, IR spectroscopy, ^{1}H, ^{17}O and ^{29}Si NMR. NMR plays an important role in the characterization of the complex series of chemical reactions since local environments of several nuclei can be probed in solution as well as in solid samples. Liquid ^{29}Si NMR specifically provides a useful tool to screen the consumption of TEOS, and formation of hydrolyzed and condensed species during the reaction. In addition to identification of each Si-containing species, kinetic data could be extracted as it allows quantification of each TEOS derivative.

During the presentation of NMR data, each silicon site (Q_j^i) were labeled conventionally, where Q denotes the potentially four (quad)-functionality for polymerization, and *i* and *j* denote the number of siloxane bridges and silanol bonds on the given silicon, respectively. Thus, the number of ethoxy groups on the silicon is (*4-i-j*) and fully hydrolyzed monomer corresponds to Q_4^0. Figure 4-2 shows step-wise hydrolysis of TEOS with each hydrolyzed species labeled with this notation.

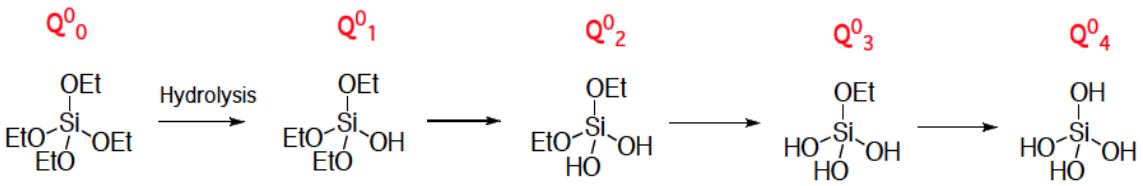
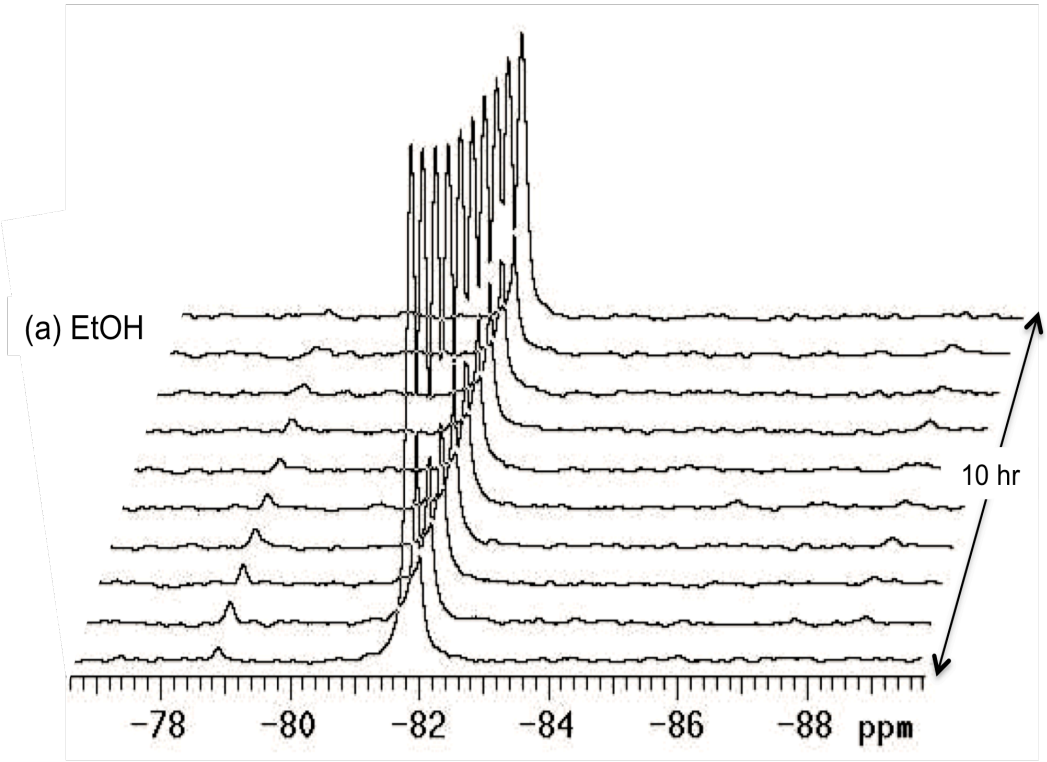
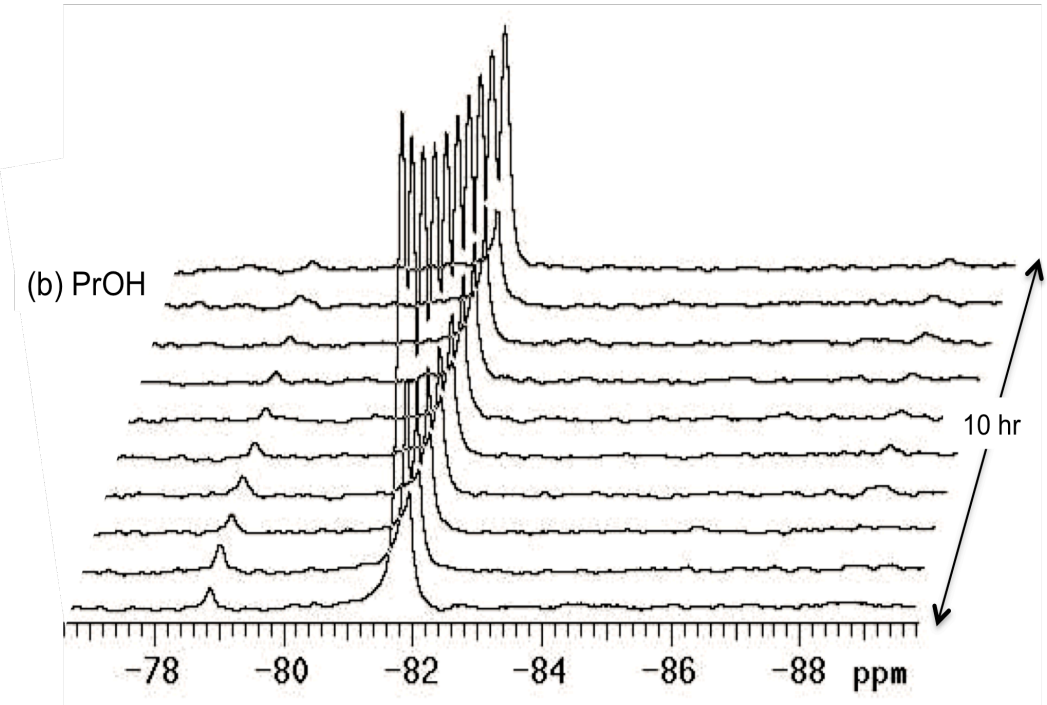
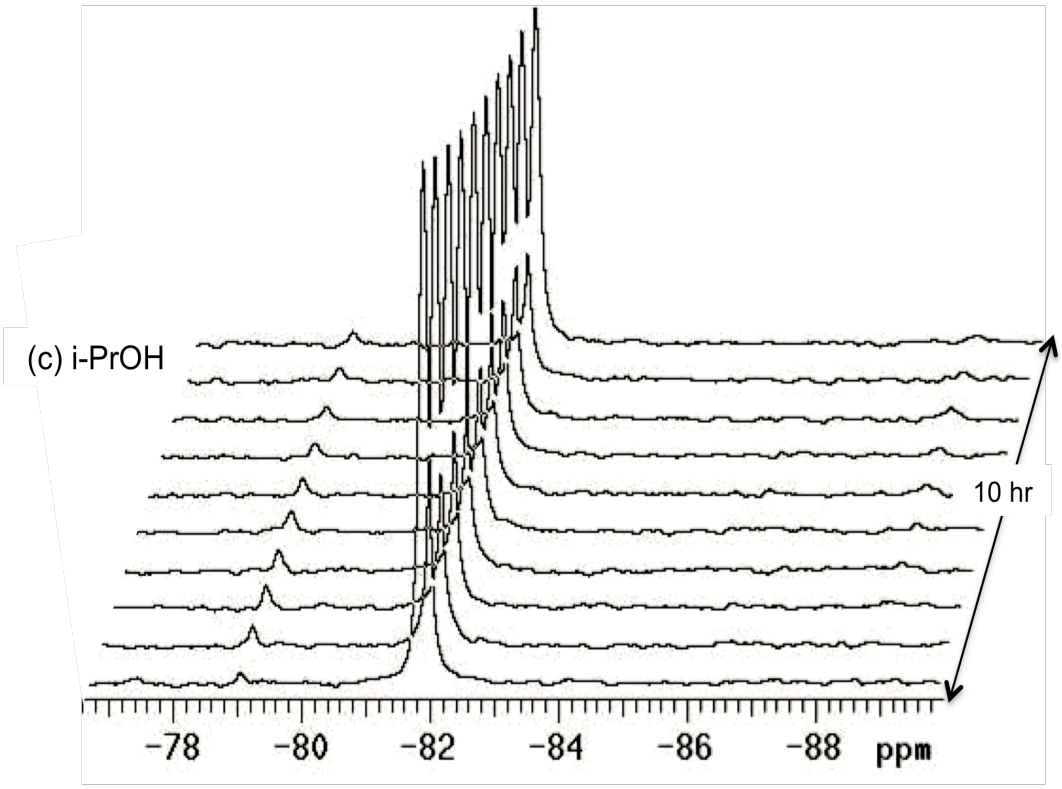


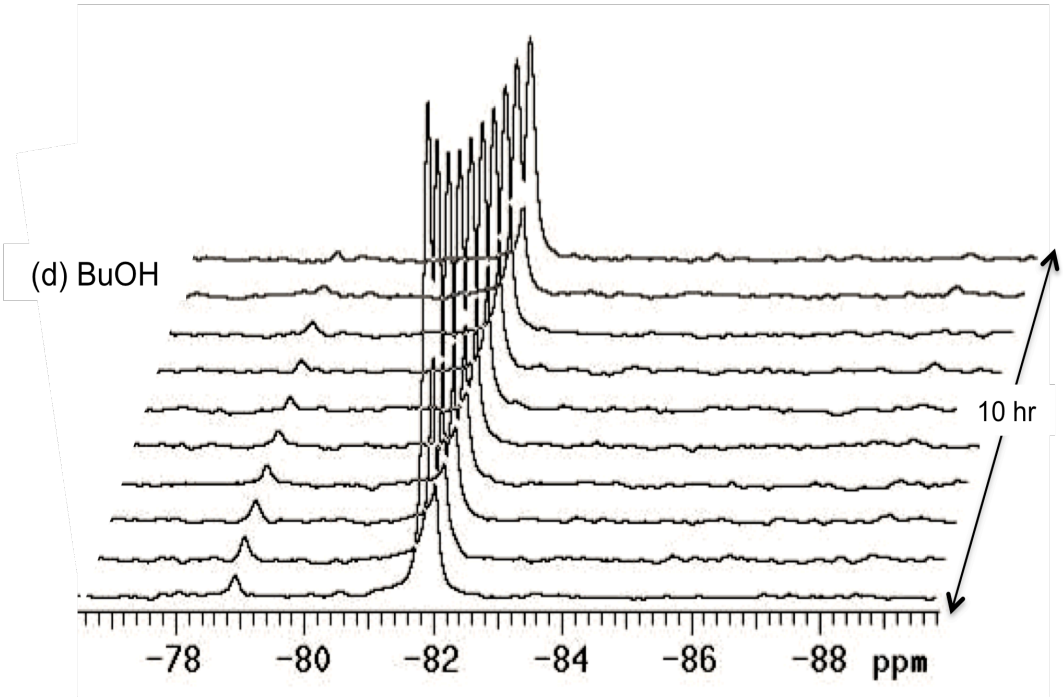
Figure 4-2: Hydrolysis of TEOS under basic conditions.

Time dependent concentrations of the liquid phase reactants and products generated during the modified Stöber reaction in five different alcohols (methyl, ethyl, n-propyl, iso-propyl, n-butyl alcohol) were determined by liquid state ^{29}Si-NMR analyses. The disappearance of monomer, TEOS, from its initial concentration level and the appearance of the intermediate species as a function of reaction time can clearly be seen in the NMR spectra provided in Figure 4-3.


(a) EtOH
10 hr
-78
-80
-82
-84
-86
-88
ppm


(b) PrOH
10 hr
-78
-80
-82
-84
-86
-88
ppm


(c) i-PrOH
10 hr
-78
-80
-82
-84
-86
-88
ppm


(d) BuOH
10 hr
-78
-80
-82
-84
-86
-88
ppm

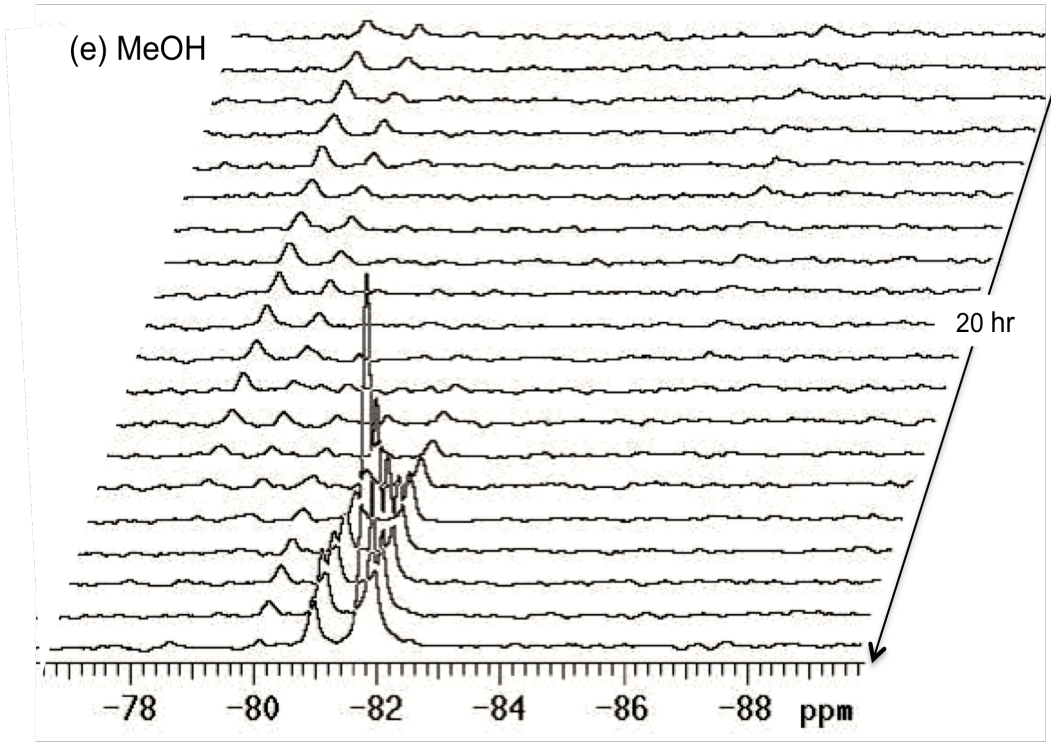


Figure 4-3: In-situ liquid ^{29}Si-NMR spectra of reaction mixture in (a) ethanol, (b) n-propanol, (c) iso-propanol, (d) n-butanol and (e) methanol.

NMR spectra for each set of experiments were used to reveal the effect of solvent on the hydrolysis of TEOS and generation of soluble species up to 10 hours with 30-minute intervals for EtOH, PrOH, i-PrOH and BuOH (Figure 4-3 a-d), and up to 20 hours for MeOH (Figure 4-3 e). The chemical shift of each soluble Si species and the corresponding molecular structure are listed in Table 4-3. The spectrum of TEOS supplied by Merck and internally referenced to TMS exhibited only one peak at -82.2 ppm (not shown here). Peak for unhydrolyzed TEOS with no bridging oxygen (Q_0^0), which was the primary peak for all alcohol systems, slightly shifted to -81.9 ppm with respect to dilution in all alcoholic solutions applied. In addition to primary TEOS peak, two resonance signals appeared at -78.9 ppm and -88.8 ppm, which correspond to Q_1^0 and Q_0^1, respectively (Figure 4-3 a to d). These intermediate products were previously identified by Brinker and Scherer in ethanol systems [17]. However, these two shifts were detected at -80.9 ppm and -85.8 ppm for methanol (Figure 4-3 e). In addition to this, it was possible to observe the doubly hydrolyzed monomer of TEOS (Q_2^0) at -80.1 ppm in methanol. Additional species observed at -79.3 ppm and -78.5 ppm were

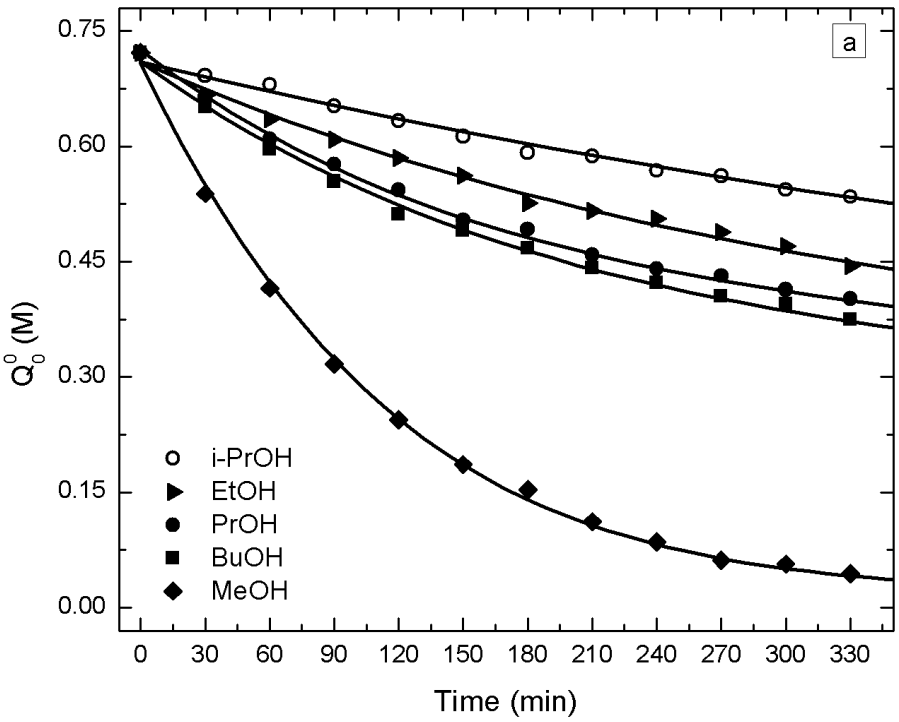
assigned as triply hydrolyzed (Q_3^0) and completely hydrolyzed monomer (Q_4^0) of TEOS, which formed lately during the reaction in methanol. The difference between the shifts of each consecutive hydrolyzed species in methanol was equal at 0.8-0.9 ppm for each –OH that is substituted for $–OCH_2CH_3$, whereas this difference was 3 ppm for all the other alcohols used for the same reaction.

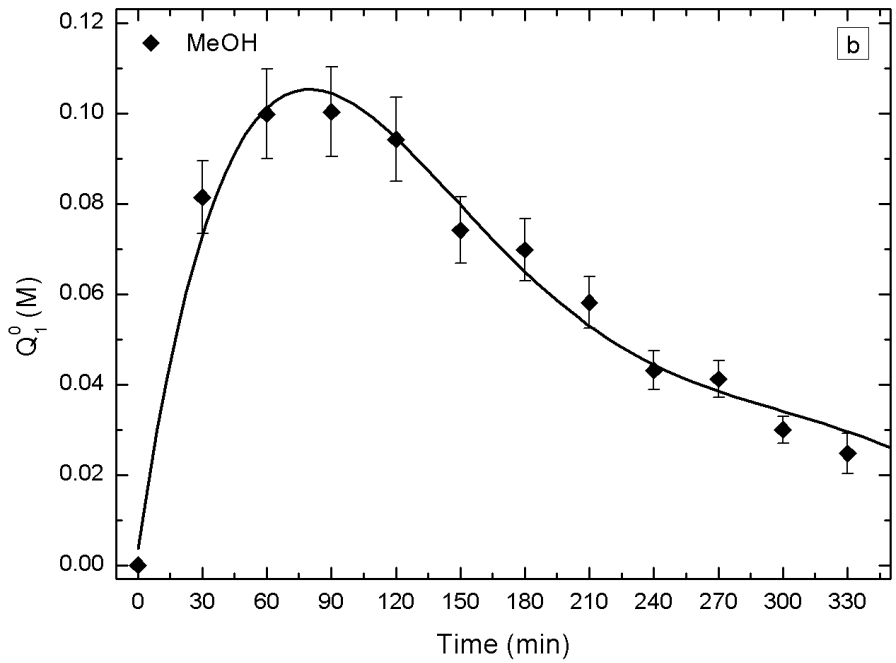
Table 4-3: Liquid ^{29}Si-NMR chemical shift (δ).

	Structures	**δ (ppm)**	
		MeOH	**EtOH, PrOH, i-ProH, BuOH**
Q_0^0	$Si^*(OC_2H_5)_4$	-81.9	-81.9
Q_1^0	$Si^*(OC_2H_5)_3OH$	-80.9	-78.9
Q_2^0	$Si^*(OC_2H_5)_2(OH)_2$	-80.1	-
Q_3^0	$Si^*(OC_2H_5)(OH)_3$	-79.3	-
Q_4^0	$Si^*(OH)_4$	-78.5	-
Q_0^1	$(OC_2H_5)_3Si^*OSi(OC_2H_5)_3$	-85.8	-88.8

NMR spectra displayed in Figure 4-3 indicate that the hydrolysis of TEOS (Q_0^0) predominantly resulted in the generation of Q_1^0, the singly hydrolyzed monomer, which is the common intermediate species for all solvent systems. However, solvent used for Stöber synthesis affected the hydrolysis rate and time dependent consumption and type of the intermediate species (detectable by NMR) in the reaction medium.

Figure 4-4 presents the time dependent concentrations of Q_0^0 and Q_1^0 obtained by *in-situ* liquid ^{29}Si-NMR analyses of each studied reaction mixture. Figure 2-a shows the monotonic decay of TEOS from its initial level (0.7 M) in different solvents. The relative rates of TEOS consumption in the solvents used decreases at the following order: MeOH>BuOH>PrOH>EtOH>i-PrOH. Despite the unexpected rate in methanol, initial hydrolysis rate of TEOS increases with molecular weight of the primary alcohols. On the other hand, slowest reaction rate observed for i-PrOH also elucidates that steric properties of the solvent alcohol influences the initial hydrolysis rate of the organoalkoxysilane.


a
0.75
0.60
0.45
0.30
0.15
0.00
Q_0^0 (M)
i-PrOH
EtOH
PrOH
BuOH
MeOH
0
30
60
90
120
150
180
210
240
270
300
330
Time (min)


b
MeOH
0.12
0.10
0.08
0.06
0.04
0.02
0.00
Q_1^0 (M)
0
30
60
90
120
150
180
210
240
270
300
330
Time (min)

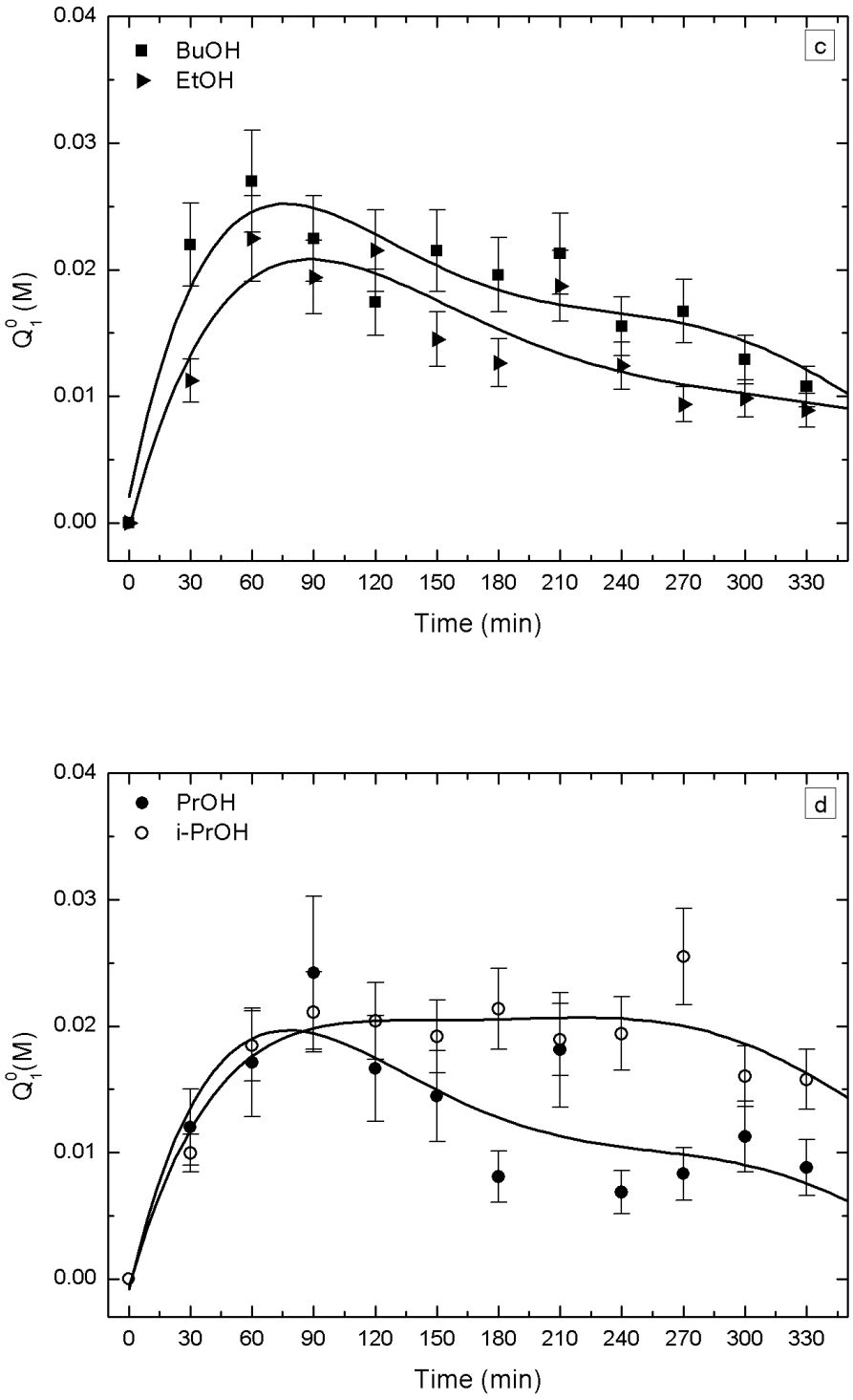


Figure 4-4: (a) Time-dependent TEOS consumption in different solvents and generation of singly hydrolyzed species in (b) methanol, (c) ethanol and n-butanol, (d) n-propanol and iso-propanol.

During the initial hydrolysis of TEOS, singly hydrolyzed monomer, Q_1^0, first exhibits a maximum and then reaches to a steady-state value (Figure 4-4 b). The fast rate observed for initial hydrolysis in MeOH also resulted in build-up of hydrolyzed monomer in the reaction, which is 4-5 times higher than that of the hydrolyzed species in other solvents. Interestingly, Q_1^0 concentration reached the maximum level in all solvents at the same time (at the end of the first hour). In literature, it was proposed that Q_1^0 concentration must only exceed 0.01 M to produce the first nanostructures [27, 29]. It was also confirmed by our findings that the concentration of the singly hydrolyzed species elevates during the so-called induction time for nucleation, however, maximum Q_1^0 concentration is not required for the onset of nucleation. This was also shown by our dynamic light scattering experiments since it was possible to analyze the size of the particles within 30 minutes of the reaction in repetitive analysis.

By each subsequent hydrolysis (and condensation), negatively charged transition state (Figure 4-5) becomes more stable with the increased electron-withdrawing capabilities of -OH (and -OSi) compared to -OR. Since the increased stability of the transition state increased the reaction rate, each subsequent step occurred more quickly as hydrolysis and condensation proceeded [17]. This is why only the monomers and the dimer could be detected under basic conditions as evidenced by ^{29}Si-NMR analyses and indicates that inductive effects play an important role on the hydrolysis rate irrespective of the solvent type. Excluding the case for methanol, only the first hydrolyzed monomer could be monitored since there is an apparent build up of this monomer, which also shows that hydrolysis of this monomer is the rate determining step for the hydrolysis reactions.

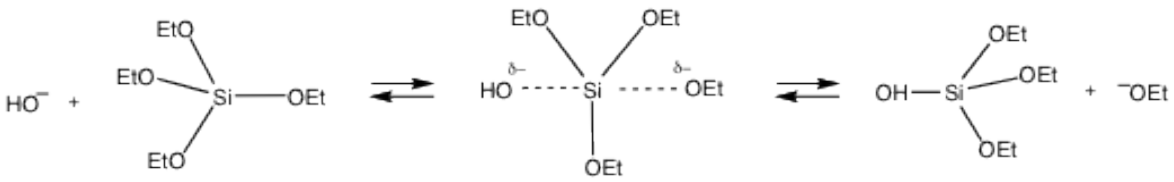


Figure 4-5: Proposed hydrolysis mechanism for TEOS under basic conditions [19].

In case of methanol, although the reaction was the fastest, second hydrolyzed species (Q_2^0) was also evident. In addition to the second hydrolyzed species, third (Q_3^0) and fully hydrolyzed (Q_4^0) species could only be monitored after the gelation started (after the system was arrested). High concentration of hydrolyzed monomers, and subsequent polymeric-like initial mass fractals in addition to high concentration of more compact clusters in the reaction probably caused a reaction-limited monomer-cluster percolation. This was attributed to more stabilized and solvated state of the hydrolyzed monomer besides the stable penta-coordinated transition state during the hydrolysis in methanol.

The influence of relative amounts of reagents (TEOS, ammonia and water) on hydrolysis kinetics, particle size and polydispersity of the particles in ethanol was also systematically investigated. Table 4-2 summarizes the amounts of reagents conducted. Figure 4-6 shows the typical time dependent ^{29}Si NMR spectrum of sample S7 during the hydrolysis of the precursor, TEOS. Common peaks detected and that could be monitored for all samples with a broad range of initial compositions are also the predominant TEOS peak and a hydrolysis product peak. TEOS (Q_0^0) peak appeared at -81.3 ppm and the singly hydrolyzed monomer (Q_1^0) at -78.5 ppm. However, based on the initial concentration of the reactants, it was possible to identify some of the condensation products such as Q_0^1 dimer $(EtO)_3 Si * OSi(EtO)_3$, which was detected at -89 ppm.

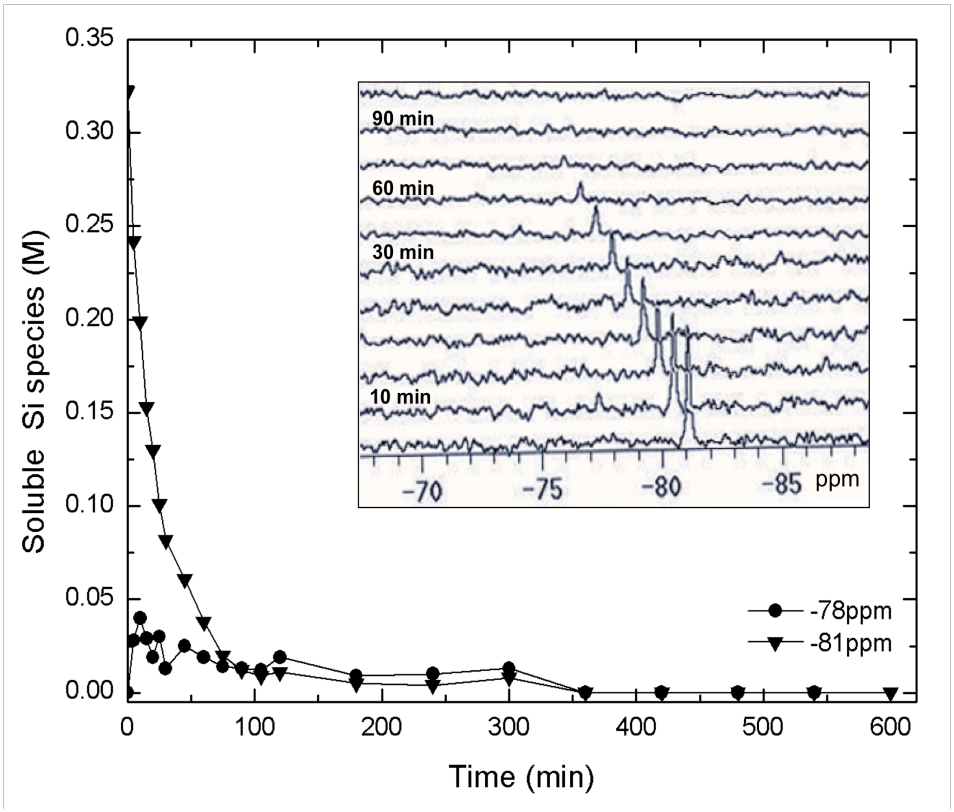


Figure 4-6: The typical ^{29}Si-NMR spectra of the reaction solution S7 with respect to time (inset) and the time dependent concentrations of soluble Si species (main).

In all systems studied (S1-S9), by the initial decay of TEOS, the singly hydrolyzed monomer exhibits a maximum within 2 hours. When the decay of TEOS is fast, at high water and ammonia concentrations, the initial maximum of the species appears within first 10 minutes of the reaction (Figure 4-6 main). For those systems, the singly hydrolyzed monomer could be detected for shorter periods of time (Figure 4-6 inset). On the other hand, for the broad initial ammonia and water concentration range applied, it was observed that irrespective of the initial ammonia, water or precursor concentration used, singly hydrolyzed monomer concentration follows the same trend and forms a plateu. The effect of TEOS concentration on the hydrolysis kinetics is obtained by comparing samples S1, S2 and S3. The effect of ammonia content on the hydrolysis kinetics is obtained by comparing samples S3, S8 and S9. The effect of water content on the hydrolysis kinetics is obtained by comparing samples S3. S4 and S5. The combined effect of water and ammonia by the variation of aqueous ammonia on hydrolysis kinetics is obtained by comparing samples S6, S7 and S8. Some of the typical time-dependent concentration profiles are shown in Figure 4-7. Concentration profiles form the base for further calculation of the hydrolysis rate constants.

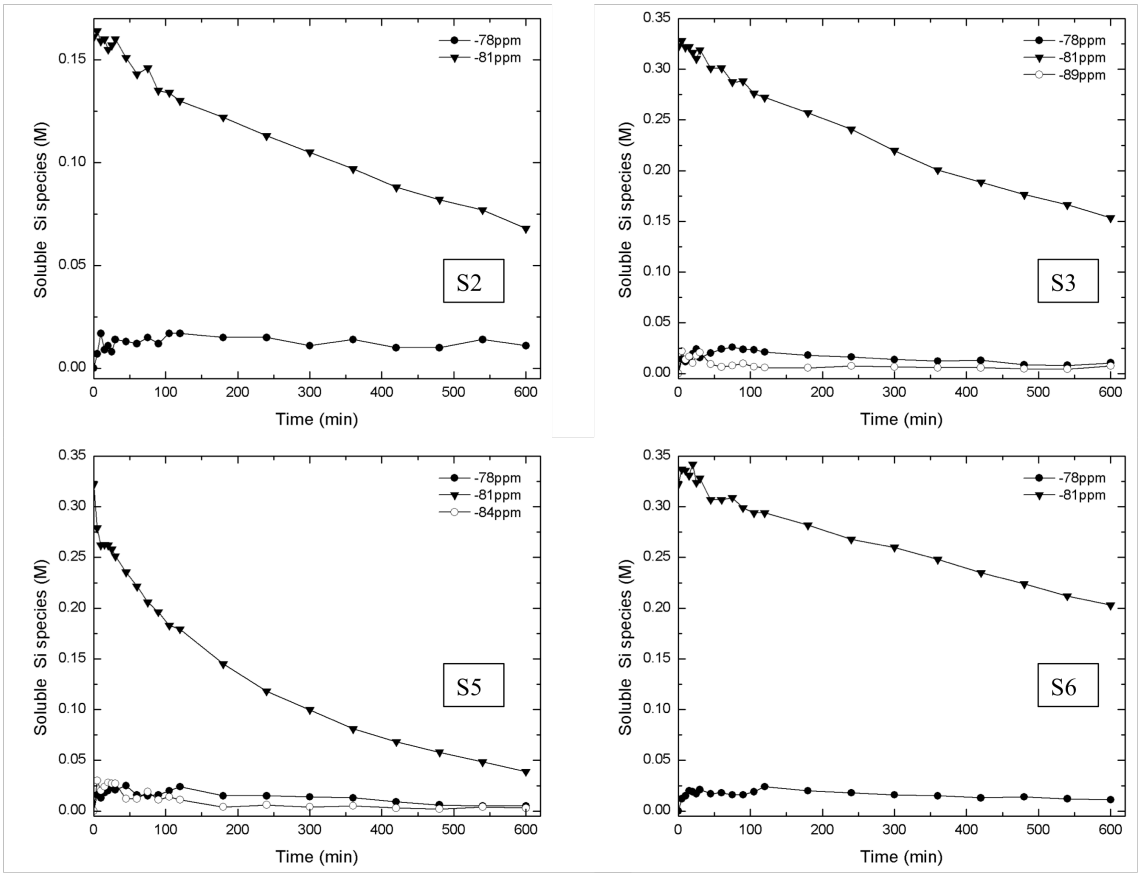


Figure 4-7: The time dependent concentrations of soluble Si species for the solutions with molar ratio of TEOS/H_2O/NH_3 at S2: 1/8.5/3, S3: 1/4.2/1.5, S5: 1/8.5/1.5, S6: 1/3.2/1.1.

4.4.2. Dynamic Light Scattering Experiments

DLS presents a powerful tool to determine the particle size and size distribution in silica aquasols and organosols [142]. The technique measures the time-dependent fluctuations in the intensity of scattered light that due diffusion of particles undergoing Brownian motion, which is then related to the hydrodynamic size of particles. During the presentation of results mean intensity vs. size (diameter, nm) was preferred since intensity is the basic distribution obtained from DLS measurement. On the other hand, by intensity profiling, the presence of larger moieties could be better presented even they exist in lower amounts since the intensity of scattering of a particle is proportional to the sixth power of its diameter.

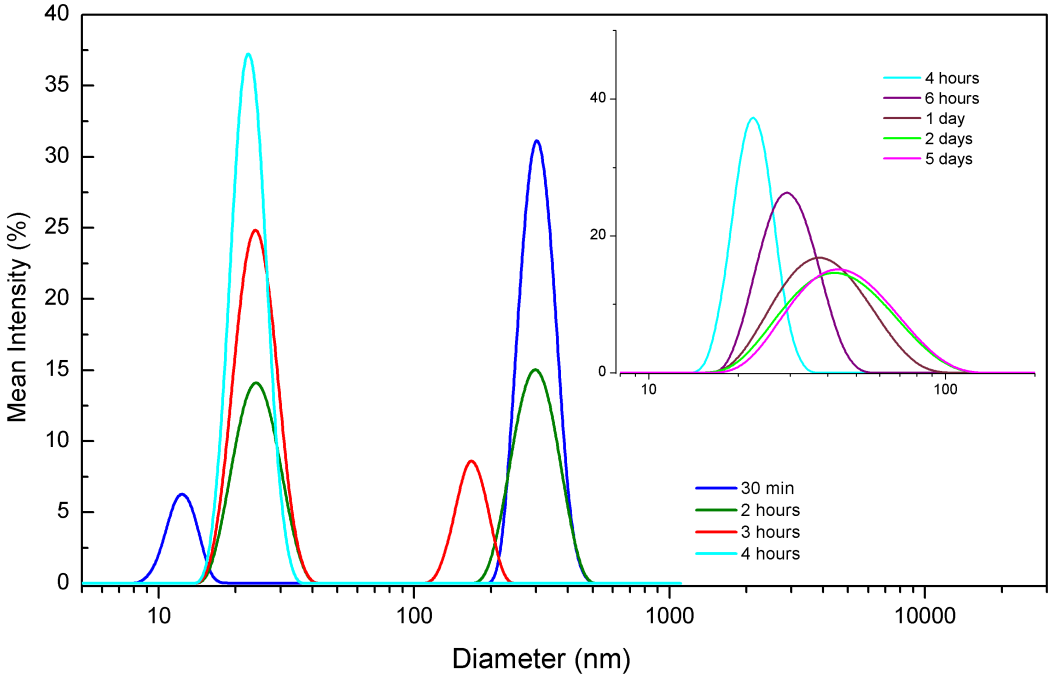


Figure 4-8: Change in the hydrodynamic radii of silica nanoparticles for S3 measured by DLS up to 10 days.

The dependence of particle size on the reaction time was obtained by sampling the system at regular time intervals and analyzing the samples by DLS. Prior to the description of the results we first note that Zetasizer (Malvern, UK) used for DLS analysis ensures the detectable particle size within the range of 0.3 nm - 6 μm. The time dependent measurements during the formation and growth of the particles were collected for 10 days till no significant change in the size distribution profile of colloidal silica sol was distinguished. Among three consecutive runs of each sample there was no significant changes in the size and size distribution of the particles, which shows that time for data collection (~5 min/run) was short compared to the time scale for changes in the structures of the silica particles. This was maintained by slowing down the growth kinetics by using low concentrations of ammonia and water after several preliminary studies that are not shown here.

A typical particle size profile for the silica sol formation is shown in Figure 4-8, where it is possible to observe some unstable oscillations and multi-modal distributions at the beginning of the Stöber reaction. After the oscillations, the particle size reaches a meta-stable regime, where the particle size attains a monodisperse character that is

followed by the steady-state regime, where the particle size remains practically constant with time. The smallest particles detected within 30 min were in the size range of 10 – 15 nm in diameter, which are argued to be primary colloidal particles.

There are two major opposing statements proposed for the nucleation and growth of silica nanoparticles. Matsoukas and Gulari [26] stated that nucleation is the result of the reaction between two reactive hydrolyzed monomers; thereby the "particle grows only by monomer addition". The balance between monomer addition and nucleation determines the polydispersity and the final particle size. On the other hand, Bogush and coworkers explains the growth as controlled aggregation of subparticles a few nanometer in size [27, 28]. Particle formation results from the aggregation of small subparticles (or primary particles) that are slowly produced during the entire reaction period. This aggregation is controlled in the sense that once the aggregates or "particles" have reached a certain size, and hence a certain colloidal stability because of their surface charge, the growth continues only by aggregation with the small subparticles and not by collisions with other (larger) particles. Lately, Bailey and coworkers demonstrated by the cryo-TEM technique that the formation of primary particles were described as the formation of polymer structures that collapsed at a certain critical size to small primary particles, anymore as a homogeneous precipitation as proposed by Bogush and coworkers [33]. Unstable oscillations and multi-modal distributions observed up to 4 hours were attributed to the formation of gel-like polymeric structures. Simultaneous collapse of some structures reaching an average critical size around 20 nm is also seen within this period. On the other hand, slight variations in the average critical size can be attributed to reversible condensation reactions until the colloidal stability was established. The reversibility of the condensation reactions was reported by Harris and coworkers [143] and it was evidenced by equilibrium concentrations of soluble silica that remained in the supernatant after the growth of the spheres. Particle growth continued rather slowly up to 2 days, and finally colloidal stability was obtained at a broader size distribution. DLS measurements on another system showed that particles with hydrodynamic diameter of 156 nm (measured after 24 hours of reaction) could retain their size (158 nm) after 10 days. It was also reported by Van Helden et al. that the silica particle size was stabilized after 10 hours, and the opalescence of the alcosol was preserved for a few months [21].

Time dependent change in the mean particle size based on DLS intensity profiles for different solvents (methanol, ethanol, n-propanol, iso-propanol, n-butanol) are given in Figure 4-9. In these plots, multimodal distribution is neglected and particle growth with an onset of average critical size is presented. The smallest particle size, which showed an average particle size of 6.5±1.5 nm, was obtained in methanol, and interestingly, there was no significant change in the mean hydrodynamic diameter of the particles in methanol until the gelation started.

The first particles to appear in all cases were fairly large within 30 min. The initial average hydrodynamic diameters of the particles detected by DLS were 6.5±1.5 nm, 9.6±1.6 nm, 24±10 nm and 46±13 nm for MeOH, EtOH, PrOH and BuOH sols, respectively. Similar initial sizes were obtained for PrOH and i-PrOH, however silica particles in i-PrOH stabilized at a bigger size in a longer period of time. Temporal increase in size for all samples is attributed to the addition of hydrolyzed or partially hydrolyzed TEOS molecules to the existing particles, which is consistent with earlier studies [35, 144]. Similarly, Boukari et al. reported that the stability length scale of initial silica particles as a result of time dependent small-angle X-ray scattering measurements were ≈8 to 10 nm in methanol and ≈16 to 20 nm in ethanol at a different concentration of TEOS (0.5 M), ammonia (0.1 M) and water (1.1 M) [35]. Our findings in agreement with the results of Boukari et al. show that initial particle size (or the size of the particles detectable by a certain technique) depends particularly on the solvent and this was mainly attributed to the interactions between the solvent and the partially hydrolyzed species derived from TEOS.

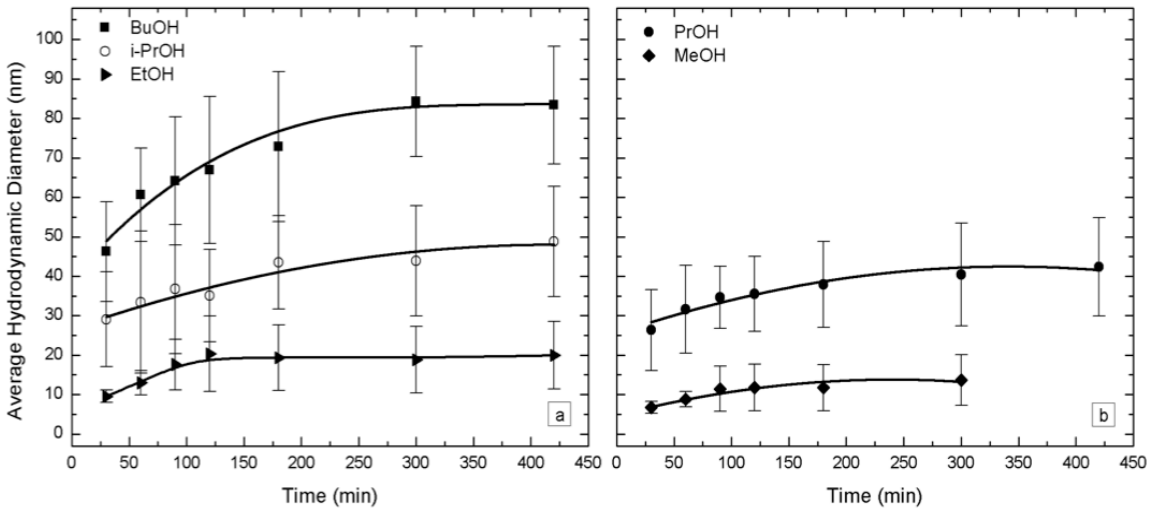


Figure 4-9: Average hydrodynamic diameter of silica particles as a function of time during synthesis in different solvents, analyzed by DLS. The solvents include methanol, ethanol, n-propanol, iso-propanol and n-butanol. The error bars indicate the width of the size distribution of the particles (full width at half maximum).

Tapping Mode AFM height images of silica nanoparticles at the end of the fifth hour are presented in Figure 4-10. It was clearly demonstrated by AFM height images that approximately spherical particles were obtained irrespective of the solvent type. Silica particles were highly aggregated upon dip-coating on mica substrates, which rendered size measurements more difficult since large aggregates cannot be used for this purpose. This condition was more pronounced for smaller particles due to higher level of aggregation. On the other hand, this provided higher possibility of producing densely packed films as seen by the continuous mesh formed by the smaller particles obtained from MeOH sample. However, average diameter of the particles was approximately 10-15% lower than the hydrodynamic diameter of the colloidal silica obtained by DLS, as expected.

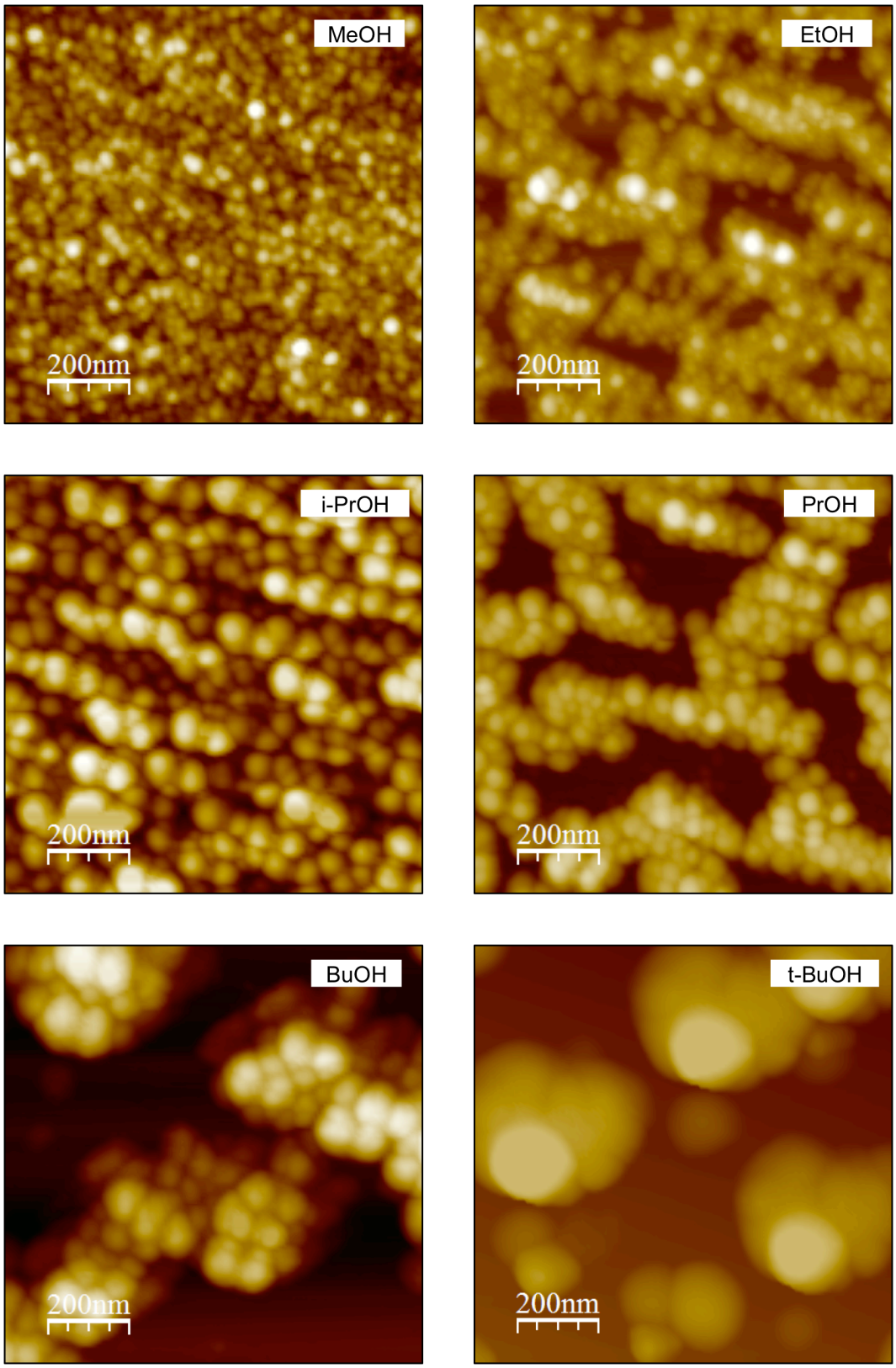


Figure 4-10: Tapping Mode AFM height images of silica nanoparticles synthesized in methanol, ethanol, n-propanol, iso-propanol, n-butanol and t-butanol (1x1μm).

4.4.3. TEOS Hydrolysis Rate versus Silica Particle Size

According to literature, five parameters play an important role in chemical reaction kinetics, and the size and size distribution of silica nanoparticles [15, 28, 128, 136]: (i) concentration of TEOS, (ii) concentration of ammonia, (iii) concentration of water, (iv) type of solvent, and (v) reaction temperature. In the present work, a systematic study was carried out to investigate the effects of initial reagent concentrations in ethanol and the effect of low molecular weight alcohol at room temperature and the results are discussed.

4.4.3.1. Effect of TEOS, Ammonia and Water Concentration

Silica particles on nanometer scale were prepared by Stöber method as described in the experimental section. Figure 4-11 illustrates the results of *in-situ* liquid state ^{29}Si-NMR analyses as the changes in time dependent TEOS monomer concentration with initial (a) TEOS, (b) ammonia and (c) water concentrations. The plots were obtained by using Eqn. (4.10), where ln[Q_0^0], or ln[TEOS], versus time should yield a straight line with pseudo-first-order rate constant of TEOS hydrolysis as slope and initial TEOS concentration as intercept. The linearity of ln[TEOS] versus time plots in Figure 4-11 confirms that our assumption provided in Eqn. (4.7) is valid and the hydrolysis reaction is of first-order with respect to precursor concentration. Pseudo-first-order rate constants of TEOS hydrolysis under different reaction conditins are given with the resulting mean hydrodynamic diameter of silica particles in Table 4-4.

Figure 4-11 (a), shown by samples S1, S2 and S3, represents the effect of initial TEOS concentration (0.16-0.8 M) on TEOS hydrolysis rate. There was no effect of initial TEOS concentration on both TEOS hydrolysis rate and particle size under experimental conditions at 0.48 M [NH_3] and 1.35 M [H_2O]. This agrees well with the results of Stöber [15], and disagrees with the results of Bogush et al. [38], who reported larger particles, and van Helden et al. [21], who found smaller particle due to increasing TEOS concentration.

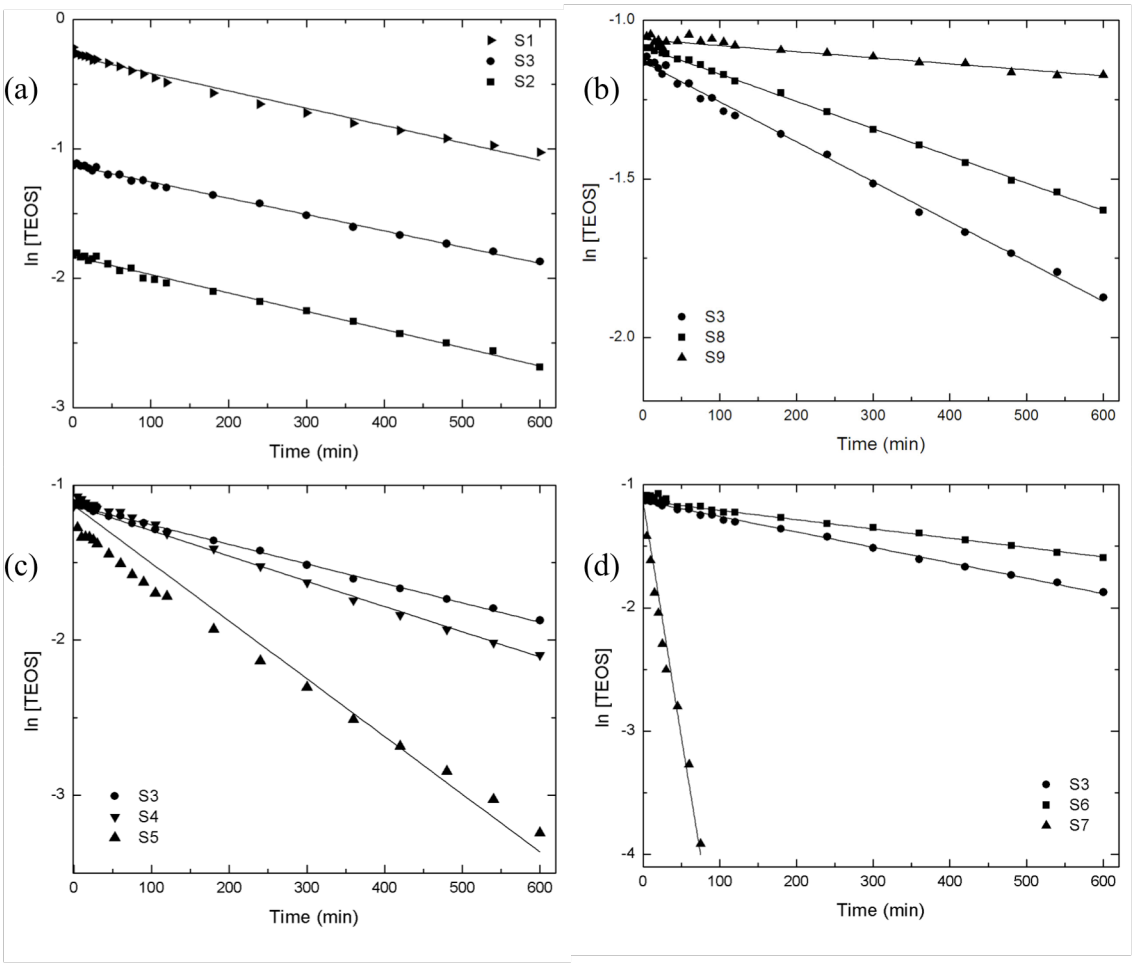


Figure 4-11: Time-dependent TEOS monomer concentration in ethanol media: (a) [TEOS]:0.8 (S1), 0.32 (S3), 0.16 (S2); [NH_3]:0.48; [H_2O]:1.35, (b) [TEOS]: 0.32; [NH_3]:0.48 (S3), 0.36 (S8), 0.10 (S9); [H_2O]:1.35 , (c) [NH_3]: 0.48; [TEOS]:0.32; [H_2O]:1.35 (S3), 2.09 (S4), 2.74 (S5). (d) [TEOS]: 0.32; [NH_3]:0.48, [H_2O]: 1.35 (S3); [NH_3]:0.36, [H_2O]: 1.02 (S6); [NH_3]:2.39, [H_2O]: 6.77 (S7). The slope of straight line is the pseudo first-order rate constant of TEOS hydrolysis.

Ammonia is used as the catalyst for hydrolysis and condensation reactions of TEOS in ethanol. As shown in Figure 4-11 (b) by samples S3, S8 and S9, TEOS hydrolysis rate increases with ammonia concentration (0.10-0.48M). Same trend is seen in silica particle size (Table 4-4). Faster kinetics and larger particle size was also seen due to increasing water concentration as presented in Figure 4-11 (c) by samples S3, S4 and S5 under experimental conditions at 0.48 M [NH_3] and 0.32 M [TEOS]. Water concentration did not have a substantial effect on particle size distribution (PdI), whereas polydispersity of particles decreased due to increasing ammonia concentration.

Table 4-4: Experimental conditions and results of *in-situ* liquid state ^{29}Si-NMR analyses (hydrolysis rate constant) and DLS measurements (hydrodynamic diameter of particles).

Sample	$[NH_3]$ (M)	$[H_2O]$ (M)	[TEOS] (M)	Rate Constant (l/mol.min)x10^{-3}	Particle Size[1] (nm)	PdI[2]
S1	0.48	1.35	0.80	1.34	28±0.0	0.10
S2	0.48	1.35	0.16	1.41	28±0.1	0.07
S3	0.48	1.35	0.32	1.25	27±0.1	0.08
S4	0.48	2.09	0.32	1.63	48±0.2	0.05
S5	0.48	2.74	0.32	3.72	67±1.0	0.03
S6	0.36	1.02	0.32	0.76	18±0.1	0.17
S7	2.39	6.77	0.32	38.3	962±28	0.16
S8	0.36	1.35	0.32	0.86	23±0.1	0.11
S9	0.10	1.35	0.32	0.19	13±0.4	0.24

[1] Intensity weighted mean hydrodynamic size of the ensemble collection of particles measured by DLS.
[2] Parameter calculated from a Cumulants analysis of the DLS measured intensity autocorrelation function

According to Matsoukas and Gulari, larger particles were obtained by increasing the concentration of ammonia and decreasing the concentration of water [26]. On the contrary, Park et al. obtained larger particle size in the higher water concentration. According to Park et al., a high nucleation rate occurs, thus a lot of sub-particles are produced at a short induction period when high water concentration is applied. This was explained by the higher tendency of silica sub-particles to agglomerate and to grow into a large particle due to stronger hydrogen bond of sub-particles when excess water is applied. The samples S3, S6 and S7 present the case, where both ammonia and water concentrations were increased by keeping their molar ratios constant at 0.32 M TEOS as shown by Figure 4-11 (d). It was demonstrated that the particle size could be tuned in the range from 18 nm to 962 nm. In addition, there was no reverse effect observed when ammonia concentration was increased to 2.39 M, leading to faster kinetics in the

presence of excess water. Both hydrolysis rate and particle size increased, while the size distribution was smallest at 0.48 M [NH_3], 1.35 M [H_2O], and 0.32 M [TEOS]. These results suggest that silica particles in desired size can be produced by simply adjusting the initial amount of ammonia and/or water (Figure 4-12).

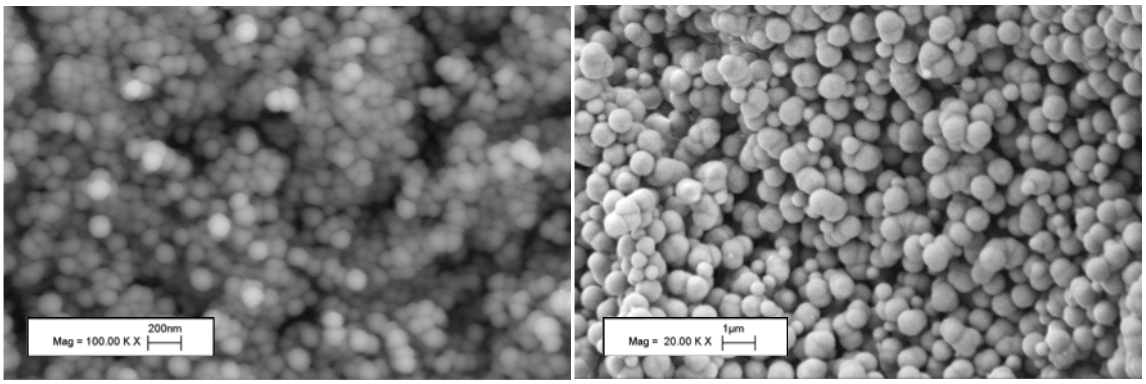


Figure 4-12: SEM images of silica particles synthesized by Stöber method. Average particle sizes are 120 nm and 600 nm.

Figure 4-13 presents the correlation between the TEOS hydrolysis rate and silica particle size under applied experimental conditions in ethanol media. To our knowledge, there is no report found in literature that presents the linear proportionality of TEOS hydrolysis rate with particle size. This supports the fact that faster hydrolysis kinetics promotes larger particle size. By faster hydrolysis, the induction time, during which the reaction generates growth units of the solid, is shorter. Therefore, accumulation rate of growth units to a critical supersaturation concentration is faster. At this point, the colloidal stability of the system and at what size the particles obtain the colloidal stability that prevents further aggregation are important phenomena, as stated by van Blaaderen et al. [144]. Particles formed at low concentrations of ammonia and water, and hence as a result of slower hydrolysis, may attain colloidal stability. However, larger particle size obtained by faster hydrolysis shows that primary particles agglomerate and grow to large particles due to higher concentrations of ammonia and water. There exist two opposing effects of increased amounts of ammonia and/or waterin terms on colloidal stability. In one hand, colloidal stability is favored due to the increased surface charge through the dissociation of silanol groups. On the other hand, the colloidal stability decreases with the increase in the concentration of ammonia and/or water since the increased concentration of NH_4^+ and OH^- decreases the double

layer thickness. Depending on the ionic strength during the growth and on the surface potential on silica, small siloxane moieties (either polymer-like or condensed subparticles) aggregate until colloidal stability is achieved [33]. If the particles are stable (at low concentration of ammonia), the aggregation stops relatively early and smaller particle size is obtained. At high ammonia concentration, the aggregation continues longer leading to the formation of bigger particles [144].

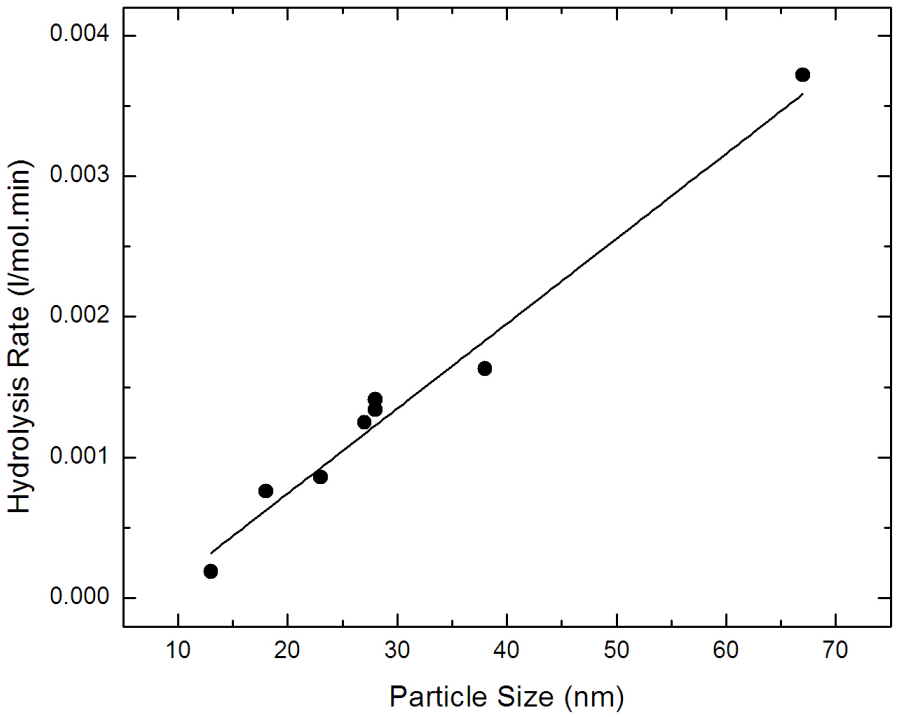


Figure 4-13: TEOS hydrolysis rate versus particles size of silica particles in ethanol media prepared under various experimental conditions.

4.4.3.2. Effect of Solvent

In-situ liquid state ^{29}Si-NMR analyses along with the measurements of hydrodynamic size of the silica particles with DLS indicated that solvent used in base-catalyzed sol-gel synthesis has significant effects on the growth kinetics and the ultimate size of the particles. As shown in Figure 4-14, the hydrolysis reaction is of first-order with respect to precursor concentration for all alcohols studied and pseudo-

first-order rate constant for hydrolysis can be obtained by the slope of the presented plots (Table 4-5).

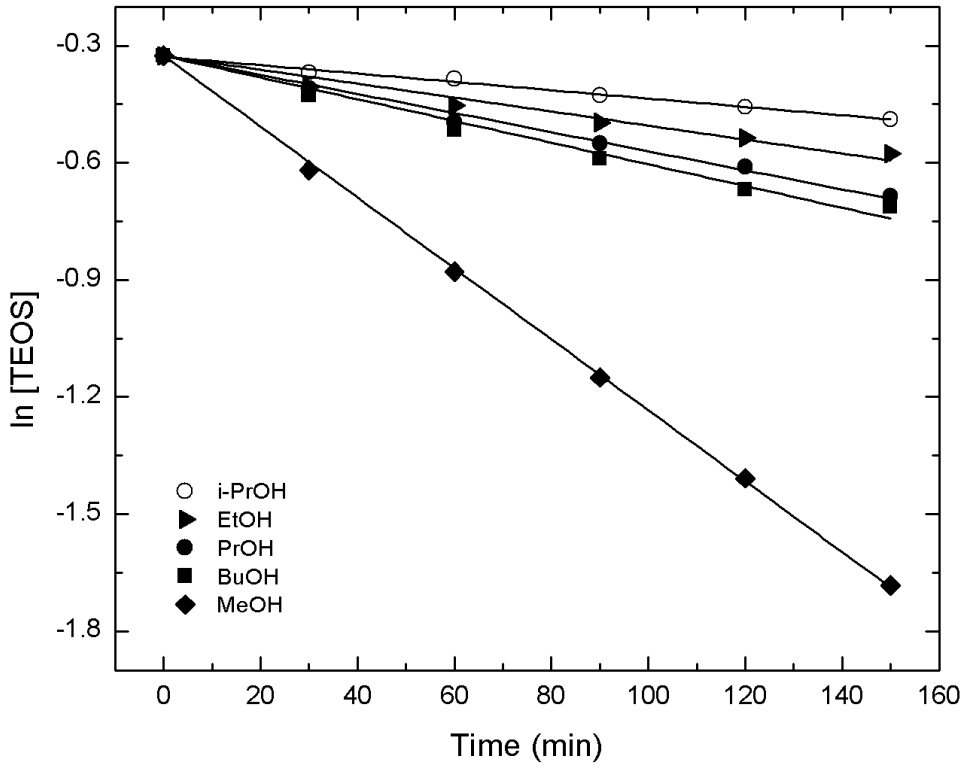


Figure 4-14: Effect of solvent alcohol chain length on hydrolysis rate of TEOS given by time dependent precursor consumption. The slope of straight line gives the pseudo first-order rate constant.

Solvating power of the solvents could be characterized by; (i) polarity, (ii) dipole moment and (iii) the availability of labile protons.

Solvent polarity is usually expressed by the dielectric constant, ε, which is a measure of the ability to insulate opposite charges from one another. Polar solvents are good insulators because their dipoles surround and associate with charged molecules. In sol-gel systems, pH>7 forms a boundary because both silica solubility and dissolution rates are maximized at or above pH 7, and because the silica particles are appreciably ionized above pH 7 [19].

Table 4-5: Effect of solvents on hydrolysis rate and particle diameter.

Sample	Dielectric Constant (ε), [145]	Hydrolysis Rate Constant[a] (l/mol.min)x10^{-3}	Mean Particle Diameter[b] (nm)	PdI[c]
MeOH	32.60	9.08	14±6.4	0.221
EtOH	24.60	1.79	19±8.5	0.201
PrOH	20.10	2.44	40±13	0.086
i-PrOH	18.30	1.09	44±14	0.075
BuOH	17.80	2.78	84±14	0.027
t-BuOH	12.50	-	149±35	0.054

[a]Pseudo hydrolysis rate constants calculated from the slope of the plots given in Figure 4.
[b]Intensity weighted mean hydrodynamic size of particles measured by DLS at the end of 5 hours.
[c]Polydispersity index calculated from cumulants analysis of the DLS measured intensity correlation function.

The average size and polydispersity of the particles given in Table 4-5 clearly indicates a direct correlation between the size of the particles and the dielectric constant of the solvent alcohol including the case for methanol. The results provided on Table 2 also clearly show that the ultimate size of the silica particles increases and the size distribution becomes narrower with increasing molecular weight and with decreasing dielectric constant of the alcohol. The variation between alcohol molecular weight and silica particle size corroborates the findings of others [30, 128, 146, 147].

Under basic conditions, first primary particles are formed and become stable as they attain a critical size. As shown in Table 4-5, solvents with higher dielectric constant decrease the critical size, and interestingly, time required for stabilization also decreases with the polarity of the solvent (Figure 4-9).

This correlation does not hold for the hydrolysis reaction rates in all solvents listed in Table 4-1. However, among primary alcohols, the hydrolysis rate is greater in a solvent with lower dielectric constant and higher molecular weight, excluding methanol (BuOH>PrOH>EtOH). This partial correlation shows that spatial charge distribution within the silicon alkoxide at different states of the reaction and specific properties of the solvent have substantial influence on reaction rates.

Possible explanation for the observed high hydrolysis rate in methanol may be transesterification. Hasegawa and Saka [133] and Peace et al. [148] reported that exchange rate increases when the steric hindrance of the alkoxy group decreases and

highest exchange rate was obtained for methanol. Lim et al. recently reported a substantial methoxy exchange of TEOS in methanol as a result of GC analyses in both acidic and basic conditions [134]. It is also known that the hydrolysis rate constant for tetramethyl orthosilicate (TMOS) is four times higher than for TEOS [149], similar to our hydrolysis rate in methanol and several times faster compared to other alcohols (Table 4-5). *In-situ* liquid ^{29}Si-NMR analyses showed 0.8-0.9 ppm differences in chemical shifts between consecutive hydrolysis products (Figure 4-2) for the sample "MeOH". Bernards et al. also reported a difference in chemical shift of about 0.85 ppm, which was measured for the methoxy-propoxy exchange independent of the type of group (alkoxy or -OH) attached to the silicon atom [130]. Therefore, chemical shifts for hydrolysis and alkoxy exchange products could overlap and may not be distinguishable. The differences in chemical shifts also agree with the observations of Green et al. [37] and Xu et al. [150] in methanol, although no direct evidence of transesterification was accessible.

All solvents used in this study have polar character with a high degree of available labile protons, which determines how strongly anions are solvated through hydrogen bonding. In polar systems, the free energy change in mixing is dominated by hydrogen-bonding forces [151]. Complete miscibility is expected to occur if the solubility parameters (δ) and degree of hydrogen bonding is similar between the components. Different contributions to the free energy of mixing, i.e., dispersive (δ_d), permanent dipole-dipole (δ_P) and hydrogen bonding (δ_h) interactions, is widely utilized, where;

$$\delta^2 = \delta_d^2 + \delta_p^2 + \delta_h^2 \qquad (4.11)$$

Table 4-6 lists the values of the components of the solubility parameter for water and the alcohols used as the solvent in this study. Hydrogen-bonding ability and miscibility increase as the alcohol molecular weight decreases. The activity coefficient of water in different alcohols estimated by Sadasivan et al. also presents the same trend [146].

Table 4-6: Solubility parameters of solvents at 25°C and contribution of various components [152].

Solvent	**δ**	**δ_d**	**δ_p**	**δ_h**
Water	47.8	15.6	16.0	42.3
Methanol	29.6	15.1	12.3	22.3
Ethanol	26.5	15.8	8.8	19.4
n-Propanol	24.5	16.0	6.8	17.4
i-Propanol	23.5	15.8	6.1	16.4
n-Butanol	23.1	16.0	5.7	15.8

δ: total Hildebrand parameter, **δ_d**: dispersion, **δ_p**: polar, **δ_h**:hydrogen bonding components

Under basic conditions it is well established that hydrolysis of TEOS occurs by an S_N2-Si mechanism, which involves penta-coordinated silicon intermediates or transition states (Figure 4-5). In a fast reaction, water dissociates into hydroxyl anions by the basic catalyst. As proposed by Iler [19], the hydroxide ion attacks the silicon atom and displaces the alkoxide anion with inversion of the silicon tetrahedron. In general, S_N2 mechanism is favored in the presence of polar aprotic solvents since they do not form hydrogen bonds, which could screen the nucleophile. Since protic solvent molecules form hydrogen bonding with the hydroxyl ions they lower the catalytic activity by suppressing the nucleophilicity. And hence catalytic activity is more retarded in case of ethanol and least retarded in case of n-butanol when we compare the primary alcohols with respect to their capacity and strength of hydrogen bonding (Table 4-5 and Table 4-6). However, if this was the dominant effect on the reaction mechanism, the reaction in methanol should have the slowest hydrolysis rate.

In addition to this retarding effect, hydrolysis could be facilitated through hydrogen bonding of the alkoxide anion with the solvent. Thus, stabilization of the transition state complex through hydrogen bonding could also play a major role to explain the four-fold increase in rate constant of methanol when compared to that of ethanol, which is in good agreement with the results of Green et al. [22]. However, despite the fact that further decrease is expected for n-propanol and n-butanol, initial hydrolysis rate was higher for these solvents. This could be attributed to a decrease in degree and strength of hydrogen bonding and to the variations in the local ordering of the hydroxide ions in TEOS-water-solvent reaction system. Although all solvents used in this study can act as donors and acceptors in hydrogen bonding, as the molecular

weight of the solvent increases, they exhibit lower dielectric constant and dipole moment values. Therefore, they are expected to hydrogen bond less strongly to hydroxide ions, which could be the reason of unexpectedly elevated reaction rates for n-propanol and n-butanol.

4.5. CONCLUSIONS

Stöber method was used to produce silica nanoparticles and the influence of reaction parameters on TEOS hydrolysis rate and resulting particle size were studied. A systematic investigation was presented to determine the effect of concentration of TEOS, ammonia and water in addition to the effect of type of alcohol used as the solvent. The hydrodynamic size of the particles was tuned in the range from 13 to 962 nm. It was demonstrated that the controlled synthesis of silica particle size can be achieved by systematically tuning the solution chemistry. It was demonstrated that initial TEOS concentration did not affect TEOS hydrolysis rate and the particle size. On the other hand, both the hydrolysis rate and the particle size strongly depend on the amount of ammonia and water. When ammonia and/or water concentration is increased, larger particles are obtained with respect to faster kinetics. Interestingly, TEOS hydrolysis rate was found to be linearly proportional to the particle size under applied experimental conditions.

Differences in particle sizes and initial hydrolysis rate of TEOS under basic conditions in different molecular weight alcohol solvents were investigated by liquid state ^{29}Si NMR, DLS, and AFM techniques. Solvent effects on initial hydrolysis kinetics, size and polydispersity of silica particles were discussed in terms of polarity and hydrogen-bonding characteristics of the solvents. Increased hydrolysis rate and larger particles were obtained for higher molecular weight primary alcohols. Secondary alcohol (iso-propanol) led to lower hydrolysis rates and larger particle size. Methanol exhibited an exceptional case with the highest hydrolysis rate and with the smallest particle size, which was mainly attributed to alkoxy exchange of TEOS in methanol. Under identical reaction conditions, both the particle size and the hydrolysis rate were found to be strongly dependent on the specific properties and spatial characteristics of the solvent. There is a clear correlation between the dielectric constant of the medium and the silica particle size obtained. Rates of the first order hydrolysis reactions are strongly dependent on the polarity, hydrogen-bonding capacity, chemical structure and nature of the alcohol used as the reaction solvent.

5. POLYURETHANEUREA-SILICA NANOCOMPOSITES: PREPARATION AND INVESTIGATION OF THE STRUCTURE-PROPERTY BEHAVIOR

5.1. INTRODUCTION

Polymeric nanocomposites have received widespread attention due to their enhanced physical, chemical and engineering properties and potential use in diverse fields of applications. Polymeric nanocomposites are mostly prepared by homogeneous dispersion of nanosized inorganic fillers within an organic polymeric matrix [43]. A wide range of polymeric nanocomposites has been prepared by using different polymer matrices (thermoplastic or thermoset) and inorganic fillers (organoclays, fumed silica, carbon nanofibers or nanotubes, graphene) [16, 95, 153-156]. The reinforcing effect of different classes of fillers depends mainly on; (i) particle structure, size and shape, (ii) loading concentration, (iii) strength of the matrix-filler interaction and (iv) distribution of the particles within the matrix. An important factor that influence the distribution of the fillers within the matrix is the preparation method of the nanocomposites, which could be melt-processing [157], solution blending [158] or in-situ polymerization [159].

Segmented thermoplastic polyurethanes, polyureas and poly(urethane-urea)s (TPU) constitute an important class of linear-segmented block copolymers with alternating hard and soft segments. In TPUs soft segments are usually medium to high molecular weight (M_n ~ 1000 - 3000 g/mol) α,ω-dihydroxy or α,ω-diamine terminated oligomers with glass transition (T_g) or softening temperatures well below room temperature (such as aliphatic polyethers and polyesters, polyisobutylene, polydimethylsiloxane). Hard segments are generally formed by the reaction of the diisocyanate with a low molecular weight diol (urethane) or diamine (urea), through the so-called chain extension reactions [160, 161]. Due to the thermodynamic incompatibility between the soft and the hard segments TPUs display phase separated morphologies or nanostructures [58, 59, 160]. Strong hydrogen bonding between the urethane or urea type hard segments lead to the formation of a physically crosslinked

network, which strongly contributes to the interesting combination of properties of TPUs. Due to strong hydrogen bonded hard segments dispersed in a continuous soft matrix, TPUs are regarded as 'self-reinforcing' materials.

Polyester soft segment based TPUs find applications in wire insulation, automobile fascia, footwear (lifts, ski boots, football cleats), wheels (industrial, skateboard), and adhesives [161]. In general, polyesters produce much tougher TPUs with a better range of physical properties when compared with their polyether based homologs. Major advantages offered by polyether based TPUs are superior low temperature flexibility and improved hydrolytic stability [58, 162]. Lately, there is a growing interest to broaden the range of applications for polyether based TPUs beyond the current limits by the addition of nanosized fillers. Recently, several studies have shown that mechanical and thermal properties of TPUs can be improved through the preparation of nanocomposites. However, most of these studies are conducted on polyester based TPUs, where organo-modified silicates [96, 157, 163], carbon nanotubes [164-166], carbon nanofibers [167, 168] and fumed silica nanoparticles [53, 101, 104, 169] were used as fillers.

In TPU based nanocomposites there is only a limited number of studies that address the use of colloidal silica especially for the polyether-based materials. In these studies, silica sol was either blended with polyol (prior to the reaction with diisocyanate) [89, 170-172] or added to monomers at the stage of polyester preparation by polycondensation [173] to avoid agglomeration of the particles. On the other hand, there is no report in the literature dealing with the use of silica sol "as synthesized and aged" in basic media for the preparation of polyether-based TPU/silica nanocomposites, specifically through solution blending of the copolymer and the silica sol.

The central theme of this study is to systematically investigate the reinforcing effect of silica nanoparticles in polyether-based TPU/silica nanocomposites. For this purpose, colloidal silica with average particle size in 29 – 215 nm range was prepared by modified Stöber method [15]. Poly(tetramethylene oxide) based segmented urethaneurea copolymer with a hard segment content of 20% by weight and poly(ethylene oxide) based segmented urethaneurea copolymer with a hard segment content of 30% by weight were synthesized and provided by Polymer Science and Technology Laboratories in Koc University. Nanocomposites with silica loadings of 1 to 40% by weight and with silica sizes from 29 to 214 nm were prepared by mixing the copolymer solution and the colloidal silica, prepared in a common organic solvent. The

effects of silica concentration and particle size on physical, thermal and mechanical properties of the resultant polyurethane-urea nanocomposites were investigated.

5.2. EXPERIMENTAL

5.2.1. Materials

Poly(tetramethylene oxide)glycol (PTMO-2K) with $<M_n>$ = 2,040 g/mol and diamine chain extender 2-methyl-1,5-diaminopentane (MDAP) were kindly provided by DuPont. The diisocyanate, bis(4-isocyanatocyclohexyl)methane (HMDI) was kindly supplied by Bayer and had a purity better than 99.5%. Dibutyltin dilaurate (DBTDL) was obtained from Witco and is used as a catalyst by diluting to 1 weight % in tetrahydrofuran. Reagent grade 2-propanol (IPA) and tetrahydrofuran (THF), aqueous ammonia solution (NH_4OH, 25% wt.) and tetraethylortosilicate (TEOS, >99%) were obtained from Merck. All chemicals were used as received.

5.2.2. Synthesis Polyurethaneurea Copolymer

Polyurethaneurea segmented copolymers with 20% by weight hard segment content were synthesized by using the two-step polymerization procedure, called the "prepolymer method". All reactions were carried out in three-neck, round bottom, Pyrex reaction flasks equipped with a mechanical overhead stirrer, a thermometer and an addition funnel. Temperature control was provided by a heating mantle. For the preparation of isocyanate terminated prepolymer, calculated amounts of PTMO-2K and HMDI were introduced into the reaction flask, heated to 80 ˚C and stirred in bulk. 150 ppm of DBTDL (1 weight % solution in THF) was used as catalyst. Prepolymer formation reaction was monitored by Fourier Transform Infrared spectroscopy (FTIR). Prepolymer reactions were completed in about 1 hour. The heat was then turned off and the prepolymer was dissolved in THF to make a solution with a solids content of about 80% by weight. The solution was then cooled down to room temperature and further diluted with IPA to make a 60% solution. Chain extension reaction was performed at room temperature by the dropwise addition of MDAP solution in IPA (20% solids) onto the prepolymer solution. As the polymer molecular weight and the viscosity of the solution increased, the system was diluted with THF/IPA mixture (7/3 by volume) to a final solids content of about 20% by weight. Completion of the reaction was determined

by FTIR spectroscopy by monitoring the disappearance of the strong isocyanate peak at 2260 cm^{-1}. The polyurethaneurea solution obtained was cast in a Teflon mold. The mold was kept at room temperature for 24 hours and then placed in a vacuum oven at 60˚C for 24 hours for complete evaporation of the solvent.

Gel permeation chromatography (GPC) measurements were performed on a Viscotek VE 2001 series instrument equipped with four columns (2xT3000, T2000 and TGuard) and Viscotek VE 3580 refractive index detector. DMF was used as the mobile phase at 50 °C with a flow rate of 1 mL/min. Polymer samples were prepared at a concentration of 1-2 mg/mL in DMF. Molecular weights were determined from calibration curves plotted from narrow molecular weight polystyrene standards.

5.2.3. Preparation and Characterization of Silica Sol

Silica sols were prepared in basic medium by using sol-gel method [15]. In conventional basic sol-gel systems, ethanol is used as the parent alcohol when TEOS is employed as the precursor. However, in this study, we used isopropanol (IPA) as the solvent to enhance the compatibility and mixing conditions of the silica sol and the polyurethaneurea copolymer, which is soluble in a THF/IPA solvent mixture.

Sol-gel reactions were carried out in 100 mL glass reactors with low to moderate mixing speeds at room temperature (25±2°C). Initially, IPA and aqueous ammonia were mixed and ultrasonicated for 20 minutes, and then TEOS was quickly poured into the reactor to initiate the reaction. Silica sols of various particle size were prepared at molar ratios of [TEOS]/ $[NH_3]_{aq}$ = 0.8, 1.7 and 2.8 and denoted as S1, S2 and S3, respectively. Prior to blending with copolymer solution, silica sols were aged for 4 days. TEOS concentration was monitored by *in-situ* liquid ^{29}Si-NMR analysis in isopropanol and it was seen that its consumption reaches a plateu after 4 days (Figure 5.1).

Hydrodynamic diameter and size distribution of silica nanoparticles in 2-propanol and zeta potential of silica sols were analyzed with Dynamic Light Scattering (DLS) Zetasizer Nano (Malvern, UK). Particle size analysis of the silica nanoparticles on dip-coated mica substrates was also performed with Atomic Force Microscopy (AFM) Veeco Nanoscape IIIa Multimode SPM Tapping Mode, silicon probes, which have 42 N/m spring constant (Olympus, OMCL-AC160TS). Transmission electron microscopy (TEM) analysis was performed using a Philips-FEI Tecnai G2 F20 S-Twin at 200 kV accelerating voltage in order to investigate the distribution of silica

nanoparticles in copolymer. A drop silica sol was deposited on carbon coated Lacey formvar films supported in 300 mesh copper grids (Ted Pella). The grid then was allowed to air-dry for 5 minutes and oven-dry at 50°C for 15 minutes.

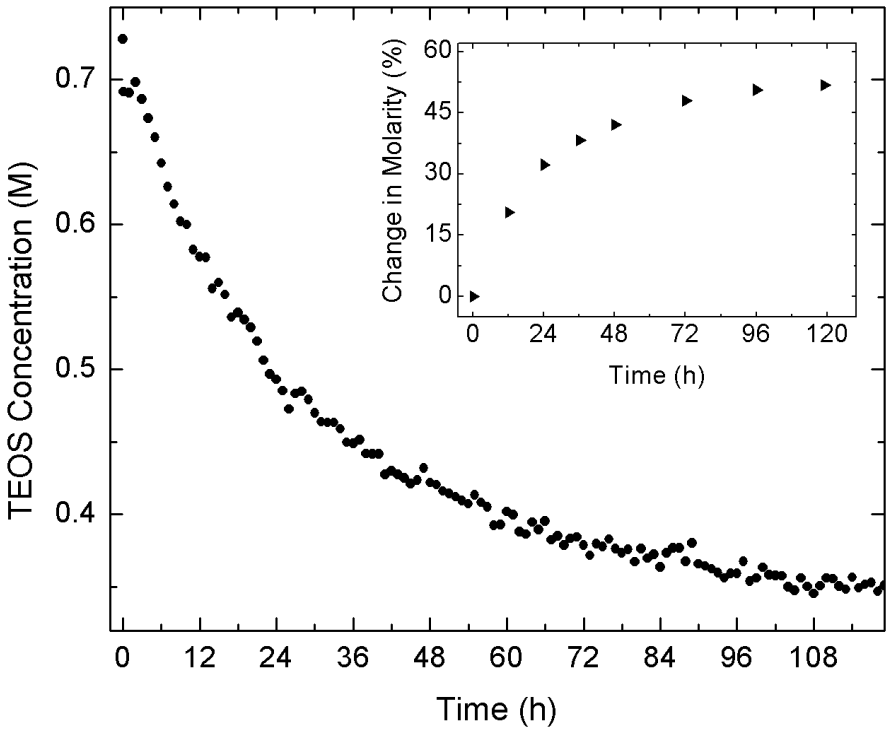


Figure 5-1: Time dependent TEOS consumption (main) and change in molarity (inset) in isopropanol for S2.

5.2.4. Preparation of Nanocomposites

Silica/TPU nanocomposites were prepared by dissolving PTMO-based or PEO-based TPU in IPA (10% solids by weight) and then adding the silica sols. The mixture was stirred on a magnetic stirrer until a homogeneous distribution is ensured. To obtain thin films (0.3-0.5 mm) the solutions were cast into Teflon molds and the solvent was evaporated first at room temperature and then in a vacuum oven at 50 °C until complete drying.

5.2.5. Characterization of Nanocomposites

FTIR spectra were recorded on a Thermo Scientific Nicolet Impact 400D Spectrometer. Solutions were cast on KBr discs and films were obtained after evaporating the solvent with an air gun. 32 scans were taken for each spectrum with a resolution of 2 cm^{-1}. Omnic 6.0 Software is used to monitor/analyze the spectra. ATR-IR spectra were recorded on a thermo scientific Smart iTR Instrument with Diamond ATR crystal and with an incident angle of 42° Omnic Software is used to monitor the spectra. 16 scans were taken for each spectrum with a resolution of 4 cm^{-1}.

Field-emission Scanning Electron Microscopy (FE-SEM) (SUPRA 35VP, LEO, Germany) was used to investigate the morphologies of composite films. The films were fractured in liquid nitrogen and the fracture surfaces (cross-section) were coated with a thin layer of carbon prior to SEM examinations. TPU/silica blend deposited and dried on carbon coated Lacey formvar films was also imaged by TEM.

Thermal behavior of nanocomposites were analyzed by DSC 204 Phoenix Differential Scanning Calorimetry (Netzsch, Germany) between -160 and 80 ˚C, under N_2 atmosphere and at a heating and cooling rate of 10 ˚C/min. Thermogravimetric analyses were carried out using STA 449C simultaneous thermal analyzer (Netzsch, Germany) under nitrogen atmosphere with a heating rate of 10 ˚C/min, from ambient temperature to 900 ˚C.

Stress-strain tests were performed on an Instron model 4411 tester. Dog-bone specimens (ASTM D 1708) were punched out of the films. Tensile tests were performed with a crosshead speed of 25.0 mm/min (L_o= 24.0 mm). Tests were conducted at room temperature and for each polymer at least three specimens were tested. Hysitron TI 950 TriboIndenter nanomechanical test instrument was used to perform quasi-static indents on the samples. Displacement-controlled quasi-static tests were performed on the samples using a diamond Berkovich probe.

5.3. RESULTS AND DISCUSSION

Segmented TPUs are complex multi-phase materials due to their intrinsic structural heterogeneity arising from the differences in the solubility parameters of the hard (HS) and the soft (SS) segments and nature and strength of the inter and intramolecular interactions between HS and SS. In general the morphology of TPUs containing 20-25% by weight HS consists of spherical HS domains distributed in the elastomeric SS matrix. The aim of this study is the preparation and characterization of silica nanoparticle filled polyurethane-urea copolymers. To achieve this, silica nanoparticles with average particle sizes in 30-215 nm range were synthesized and utilized. PTMO based polyurethane-urea copolymer with a HS content of 20% by weight was prepared by using a cycloaliphatic diisocyanate (HMDI) and a short diamine (2-methyl-1,5-diaminopentane) chain extender and a two-step polymerization reaction called the prepolymer method. PTMO with an average molecular weight $<M_n>$=2040 g/mol was used as the soft segment. GPC analyses showed that the resultant polymer had number and weight average molecular weights of $<M_n>$=65,000 g/mol and $<M_w>$=116,000 g/mol with a PDI of 1.78. Primary focus of this study was to investigate the nature and extent of interactions between silica nanoparticles employed as fillers with the soft and/or hard segments of the polyether based thermoplastic polyurethane-urea copolymer. In addition, the effect of the size and the amount of the silica incorporation on thermal, mechanical and morphological properties of TPU/silica nanocomposites were also investigated.

5.3.1. Preparation and Properties of the Colloidal Silica

Colloidal silica with three different particle sizes were prepared by the reaction of TEOS and dilute aqueous ammonium hydroxide in isopropanol at 25 °C, using a modified Stöber method [15]. Table 5-1 shows the reaction stoichiometry employed and the size and size distribution of silica sols obtained and their stability provided by zeta potential measurements. DLS was used to determine the average size and the size distribution of silica particles. Average hydrodynamic diameters of three sets of silica particles were 29, 74 and 215 nm with respect to variations in the aqueous ammonia concentration. Particle size distribution in silica sols decreased with particle size and exhibited an almost monodisperse distribution for S2 and S3. Zeta potential values of

silica sols were lower than critical stability limit of -30 mV with larger particles showing greater zeta potential values than smaller particles.

Table 5-1: Properties of the colloidal silica (and sols) incorporated in TPU/silica nanocomposites.

Sample	$[TEOS]/[NH_3]_{aq}$	D^a_{DLS} (nm)	D^b_{AFM} (nm)	PdI^c_{DLS}	ζ^d_{DLS} (mV)
S1	2.8	29±0.7	19±3.5	0.3±0.02	-67±8.8
S2	1.7	74±0.2	68±13	0.1±0.03	-74±7.1
S3	0.8	215±3.3	200±25	0.04±0.03	-87±2.3

[a] Hydrodynamic radius measured by dynamic light scattering (DLS).
[b] Average particle diameter detected by atomic force microscopy Tapping mode.
[c] Polydispersity index calculated from a Cumulants analysis of the DLS measured intensity autocorrelation function. PdI is an indication of variance in the sample and given in the range [0,1].
[d] Zeta potential of colloidal sol measured by DLS Zetasizer Nano.

AFM Tapping mode and TEM images of the silica nanoparticles are provided in Figure 5-2 and Figure 5-3, respectively. The mean particle diameter of silica nanoparticles determined by AFM size profiles on mica substrates was 19, 68 and 200 nm. Significantly smaller particle size determined by AFM pointed out profound particle shrinking due to dehydration even at room conditions. The mean particle diameter of silica nanoparticles determined by TEM was 15, 50 and 180 nm. The difference between AFM and TEM measurements is also significant, meaning that dry particles still undergo dehydration as the samples are taken out of the room environment and transferred to vacuum.

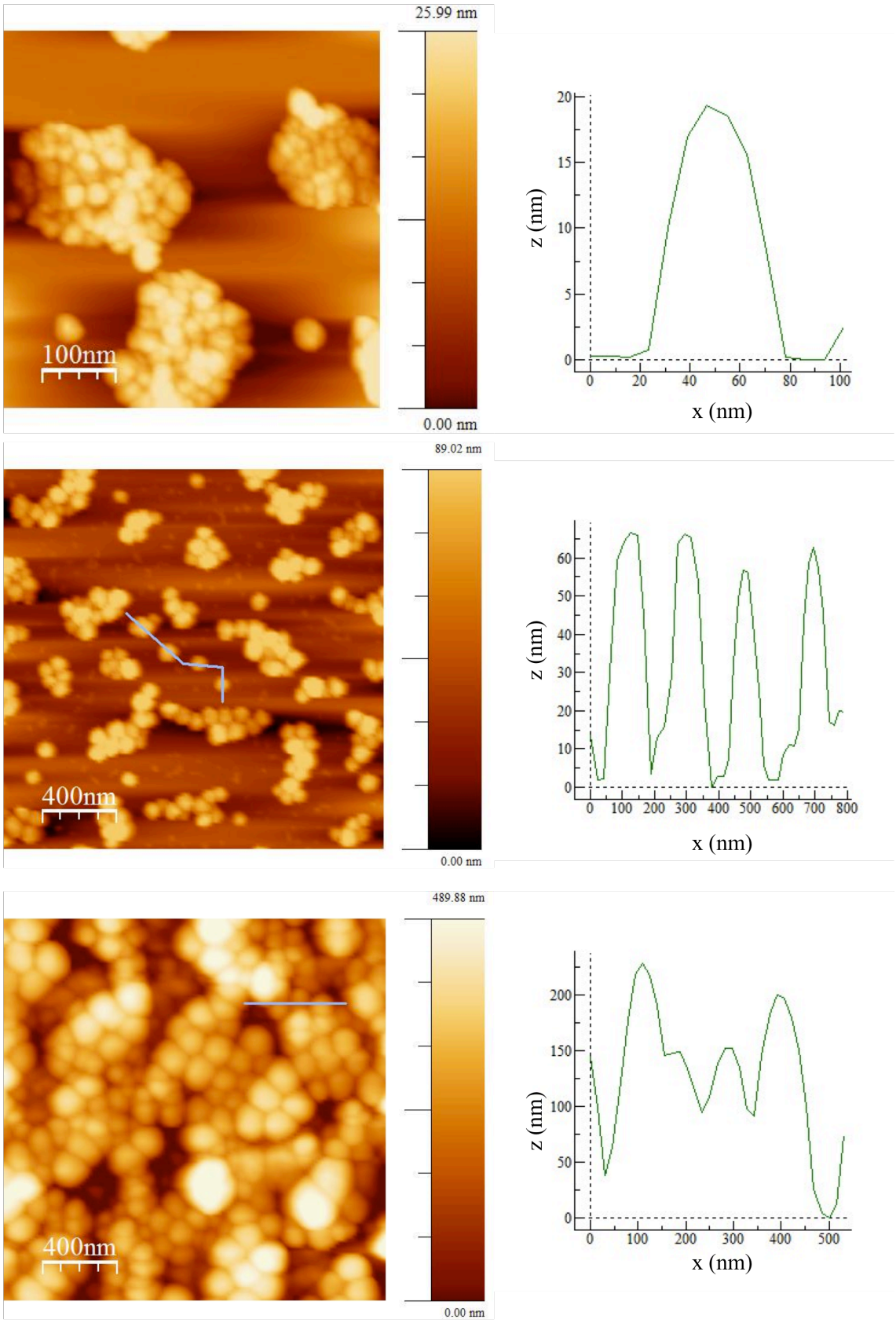
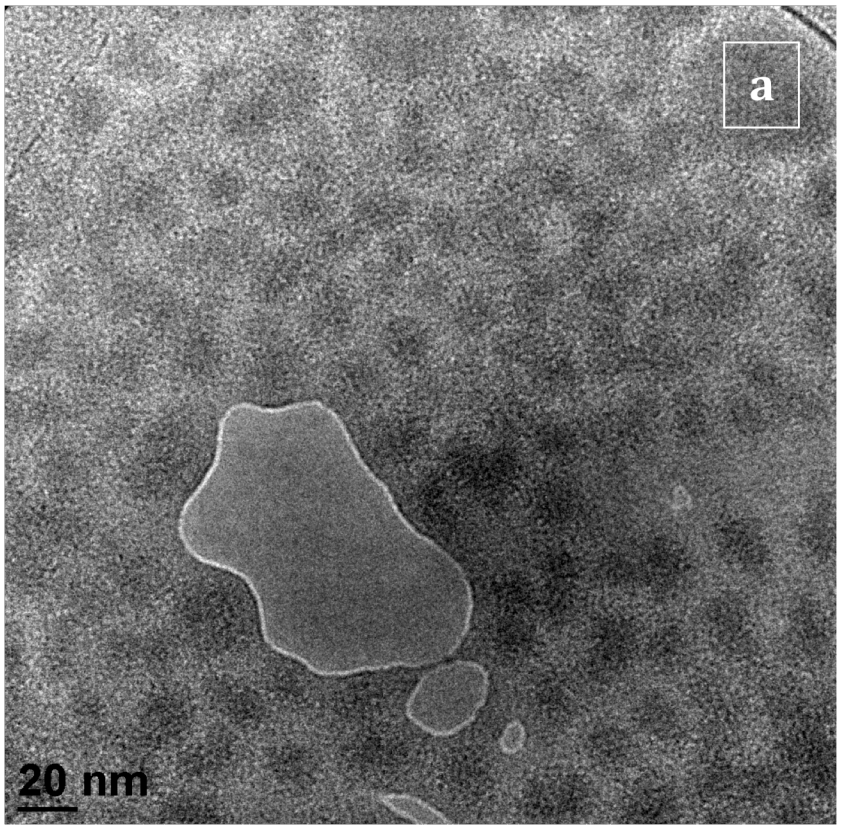
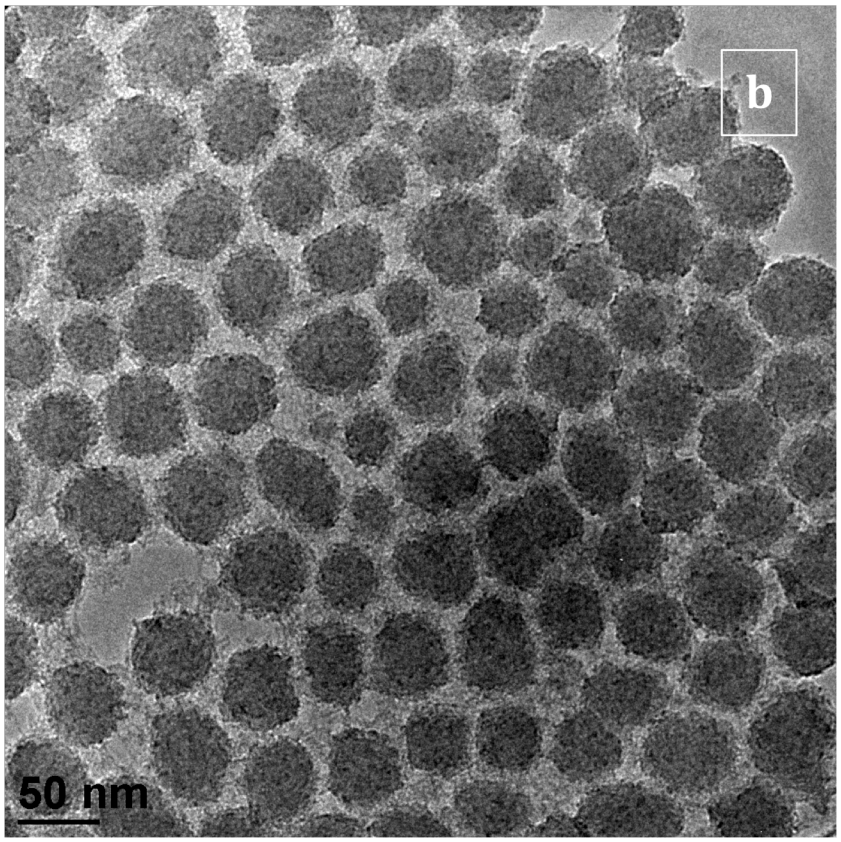


Figure 5-2: Tapping Mode AFM height images and profiles of (a) S1 (0.5x0.5 µm), (b) S2 and (c) S3 (2x2 µm).


a
20 nm


b
50 nm

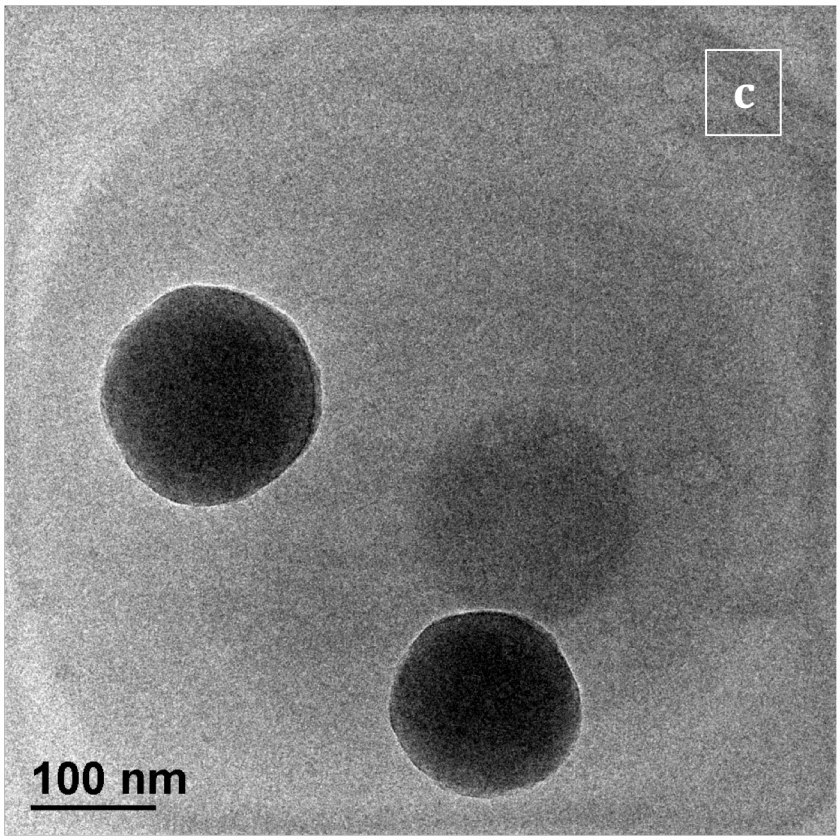


Figure 5-3: TEM images of (a) S1, (b) S2 and (c) S3.

Figure 5-4 provides the FTIR spectra of the silica powders, which were dried after aging the silica sols for 4 days. The IR spectra of synthesized silica nanoparticles respectively show asymmetric stretching bands of Si-O-Si and Si-OH groups at 1040 and 960 cm^{-1} respectively. Furthermore, broad stretching bands in 3300-3500 cm^{-1} range is due to the surface hydroxyl (O-H) groups hydrogen bonded with water molecules on the silica surface. Asymmetric stretching bands of $-CH_3$ and $-CH_2$ at 2976 cm^{-1} and 2930 cm^{-1} respectively, indicate the presence of unhydrolyzed ethoxy groups ($-OCH_2CH_3$) on the silica surface. Apparently, ethoxy replacement by hydroxyl groups is more complete under higher ammonia concentration, which leads to greater extent in silanol condensation and bigger particles. On the other hand, under lower ammonia concentration, since the ethoxy groups decrease the connectivity of polysilicic acid chains, silica network densification is also prevented as seen in Figure 5-2 (a).

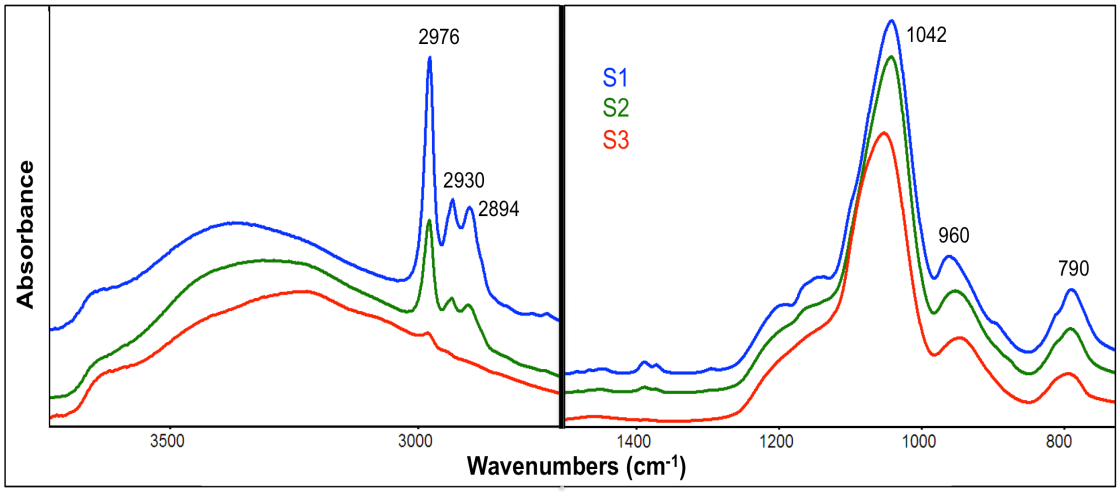


Figure 5-4: FTIR-ATR spectra of dried colloidal silica designated as S1, S2 and S3.

5.3.2. Composition and the Morphology of the Nanocomposites

Table 5-2 gives the compositions of the PTMO-based TPU/silica nanocomposites prepared in this study. In the coding TPU-20 indicates a polyurethaneurea with polymethylene oxide based soft segment and a hard segment content of 20% by weight, followed by the description of the silica used (S1, S2 or S3) and the silica content (1-40) in weight percent.

Table 5-2: Compositions of TPU/colloidal silica composites.

Sample	Silica Size (DLS/nm)	Silica Content (Weight %)
TPU-PTMO-20	-	-
TPU-PTMO-20-S2-1	29	20
TPU-PTMO-20-S2-5	74	20
TPU-PTMO-20-S2-10	215	20
TPU-PTMO-20-S2-20	74	1
TPU-PTMO-20-S2-40	74	5
TPU-PTMO-20-S1-20	74	10
TPU-PTMO-20-S3-20	74	40

Morphology of polyurethaneureas has been extensively investigated by AFM, TEM and SAXS studies. These studies indicated that depending on their compositions, hard segments in PTMO-based polyurethane-ureas are randomly oriented cylindrical domains 5-10 nm in width (and up to ca. 100 nm in length) and/or spherical domains in the order of 10-15 nm in diameter with interdomain spacing of 10-20 nm [174-176]. Hence, mean particle sizes of ca. 20-200 nm were particularly chosen to demonstrate the effect of particle sizes comparable to and bigger than the size of hard domains in the continuous polymeric matrix.

One of the key features that determines the enhancement in the performance and properties of the nanocomposites is the quality of the dispersion of the nano-sized particles in the polymeric matrix. Dispersion of the nanoparticles (intrinsically) depends on matrix-filler compatibility and surface energy of the particles as well as (extrinsically) the mixing method and conditions of the two phases. Silica particles could be specifically problematic due to presence of hydroxyl groups that lead to the formation of various sizes of agglomerates. Several studies indicate the aggregation and agglomeration of silica particles in polyurethane matrices regardless of filler size and silanol content [44, 52, 53, 177]. Mean agglomerate size could reach up to 1 μm with respect to clustering of agglomerates at increased silica amounts. Common solutions to agglomeration have been surface modification of silica particles [87, 89] and/or in-situ polymerization techniques [52], which could be efficiently employed up to certain loading levels. In this study, to avoid any drawback related to dispersion of silica nanoparticles in the polymeric matrix, colloidal silica sol was prepared and directly blended with the polymer solution in a common solvent. Solution blending technique was effective in avoiding the agglomeration of the silica nanoparticles and homogeneous blends were obtained prior to casting as demonstrated by the TEM image provided in Figure 5-5. One drop of polymer/silica blend (TPU-PTMO-20-S2-20) dried on a TEM grid clearly shows the random distribution of silica particles in the polymeric matrix.

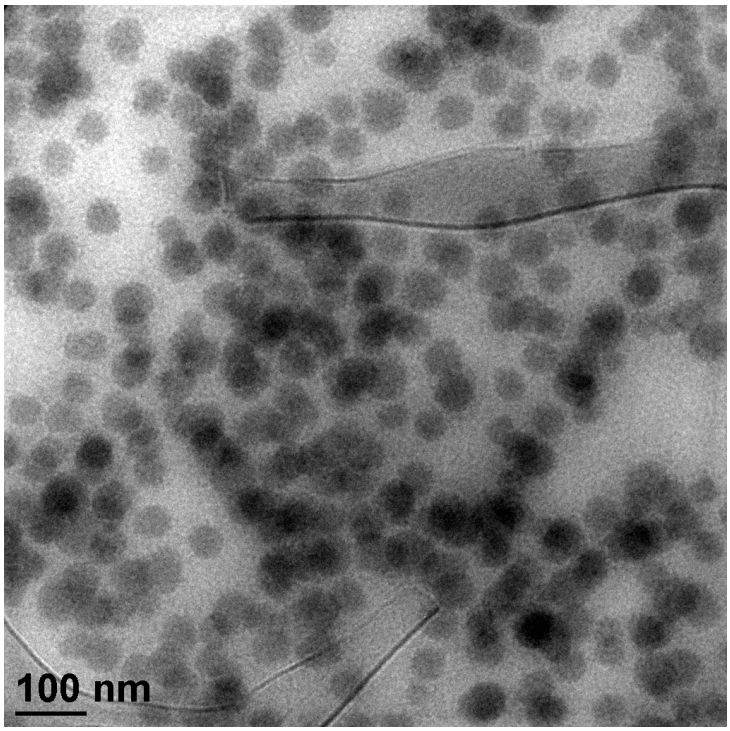


Figure 5-5: TEM image of TPU-PTMO-20-S2-20 blend dried on carbon coated Lacey formvar film supported in 300 mesh copper TEM grids.

Morphology of TPU/silica nanocomposite films was also studied by electron microscopy. SEM images of 20 wt% silica (S1-S3) containing PTMO based TPU are reproduced in Figure 5-6. Figure 5-6 (a) shows the smooth cross-section of neat TPU. SEM images of silica filled TPU samples given by Figure 5-6 (b-d) clearly show that no matter which particle size was employed, silica particles had a random but fairly homogeneous distribution throughout the polymeric matrix. The diffuse boundary between the polymer and the particles also indicated a strong interfacial interaction between two phases. TPU/silica nanocomposites with silica size lower than 100 nm resulted in even cross-section surfaces. However, widespread void formation in the polymer layer next to the filler surface was observed at cross-sections of the nanocomposites comprised of 200 nm silica particles (Figure 5-6 d and f). Similarly, extensive void formation was also revealed at cross-section SEM images of 40 wt% silica loading (Figure 5-6 e). It is interesting to note that silica particles retained their spherical shape and mean diameter after solution blending with the polyurethaneurea.

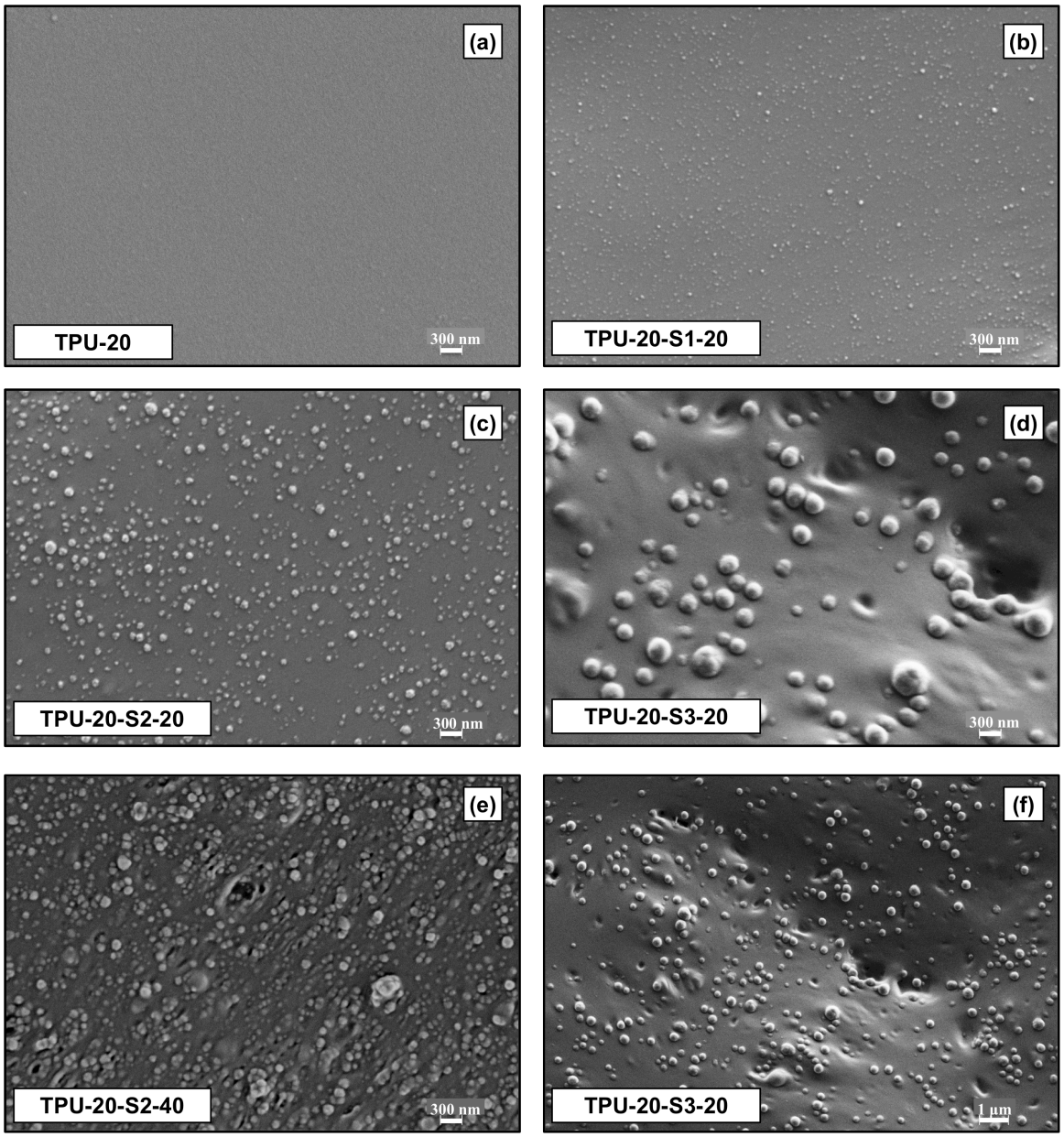


Figure 5-6: SEM micrographs of TPU/silica nanocomposite cross-sections. 50 kX magnification: (a) TPU-PTMO-20 neat polymer, (b) TPU-PTMO-20-S1-20 (c) TPU-PTMO-20-S2-20 , (d) TPU-PTMO-20-S3-20, (e) TPU-PTMO-20-S2-40 and 20kX magnification: (f) TPU-PTMO-20-S3-20.

5.3.3. FTIR Studies on Nanocomposites

In order to understand the nature and extent of intermolecular interactions between silica and polyurethane-urea matrix, extensive FTIR investigations were performed on the nanocomposites. FTIR spectroscopy is a simple and useful tool in

determining the presence and the extent of possible interactions between silica and polyurethane-urea copolymer since changes in the hydrogen bonding character of polyurethane-urea matrix by the incorporation of silica nanoparticles can be easily detected by comparing the spectra of unfilled and silica filled samples. In this study our main focus was to identify the specific interactions between; (i) the hard segments and silica, and (ii) ether linkages present in the soft segment and silica. For this purpose, we examined specific regions in the IR spectroscopy, where strong absorptions were observed by urethane and urea groups (specifically N-H and C=O absorption bands), and ether (C-O-C) backbones. Peak shifts and shape changes especially at the hydroxyl and amine (3600 – 3000 cm^{-1}), carbonyl (1800 – 1500 cm^{-1}) and ether (1200 – 1000 cm^{-1}) regions, for the hard and soft segments respectively, are indications of an interaction between the silica and the matrix.

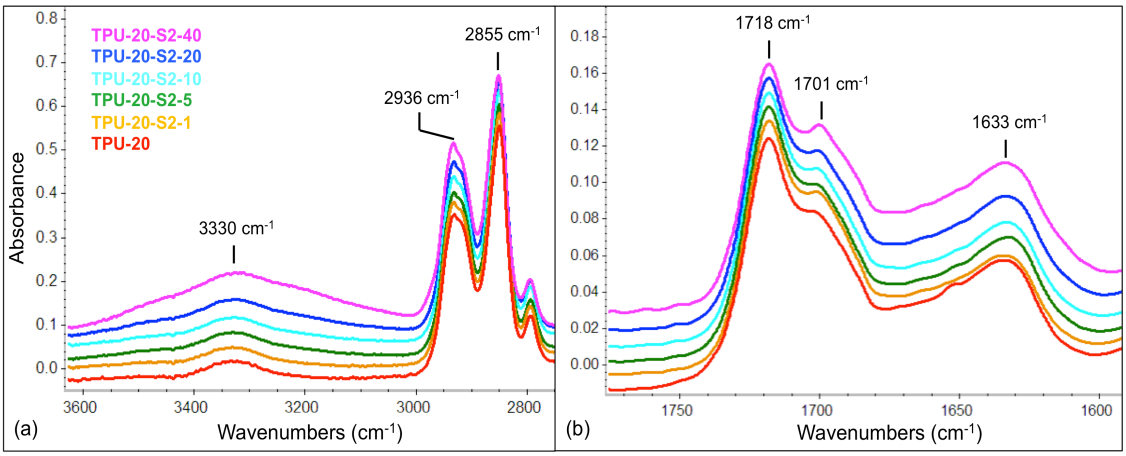


Figure 5-7: FTIR investigation of (a) N-H and (b) carbonyl regions of virgin TPU-20 and silica nanocomposites as a function of the amount of silica filler.

Figure 5-7 (a) and (b) provide 3600-3000 cm^{-1} (N-H) and 1800-1600 cm^{-1} (C=O) regions of the FTIR spectra for base TPU-20 copolymer and silica nanocomposites containing 74 nm S2 silica as a function of the amount of filler. As can be seen in Figure 5-7 (a), TPU-PTMO-20 (bottom spectrum) shows a symmetrical N-H absorption band in 3200-3400 cm^{-1} range. No dramatic change in the peak shape or position is observed for nanocomposites containing up to 20% by weight of silica. On the other hand substantial broadening of the peak which covers the 3600-3000 cm^{-1} range is observed for 40% silica containing nanocomposite. This indicates a disruption in the interaction between N-H groups by the incorporation of large amounts of silica.

On the other hand no major reorganization or change in the peak position or shape is observed in the carbonyl region (Figure 5-7 (b)) of the FTIR spectra when TPU-20 and its nanocomposites are compared.

FT-IR spectra in the ether region are presented in Figure 5-8. Stretching vibrations of C-O-C group of neat PTMO-2K was observed at 1112 cm^{-1} (not displayed here). Therefore, the band observed at 1104 cm^{-1} in IR spectra of neat TPU-20 was attributed to the hydrogen bonding interaction between N-H and C-O-C groups. It should also be noted that similar band shift, which could be due to hydrogen bonding association of ether groups, was also observed in model studies of PTMO-2K/silica blends. Unlike the N-H and C=O regions, when the ether region of the FTIR spectra is investigated, major changes in the peak positions and shapes are observed. As shown in Figure 5-8, the peaks at ether region of the spectrum both broadened and shifted to lower wavenumbers as a function of the amount silica incorporation. Broadening of the peaks is attributed to the overlapping of Si-O-Si stretching of silica filler and C-O-C peaks of the polymeric matrix. The shift in the peak positions to the left, which also intensifies with increasing amount of silica filler in the matrix, is an indication of freshly formed hydrogen bonding between the hydroxyl groups on the silica surface and the oxygen atoms in the ether linkages of the PTMO backbone, due to increases in the surface contact area and number of hydroxyl groups. FTIR results indicate that silica nanoparticles interact mainly with the soft segment matrix, however, they do not significantly affect the hydrogen bonded hard domain structure.

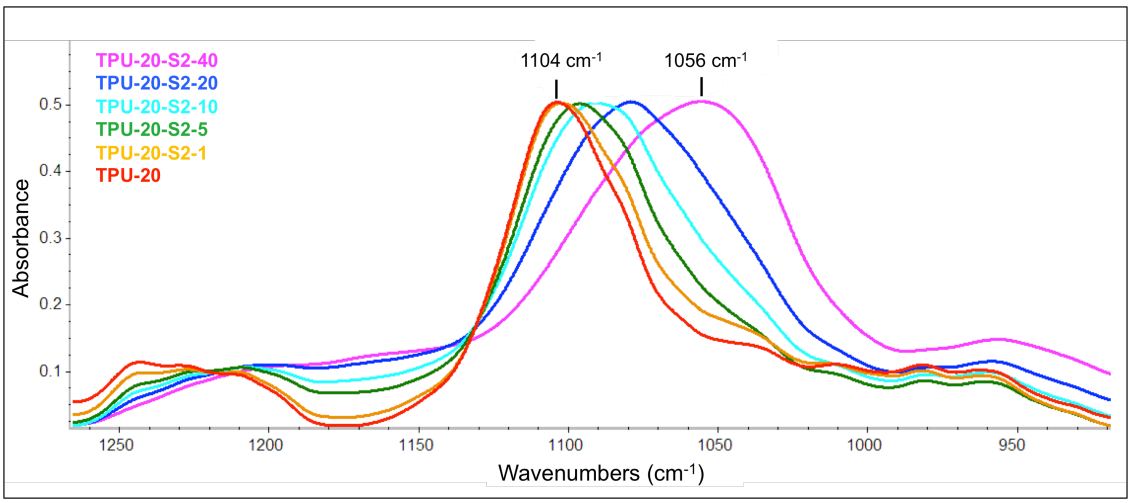


Figure 5-8: Comparative FTIR spectra of the ether region for TPU-PTMO-20 and its nanocomposites with S2.

FTIR spectroscopy was also utilized to investigate the effect of silica particle size on the interaction with ether groups in TPU-20 at constant silica loading of 20% by weight. Change in the size of the silica filler did not indicate any remarkable change in the FTIR spectra in the N-H and C=O regions of the nanocomposites. On the other hand as shown in Figure 5-9, ether peaks displayed broadening and shifted to shorter wavenumbers (from 1104 cm^{-1} to 1079 cm^{-1}) as the silica particle size increased from 29 to 215 nm at constant loading of 20% by weight.

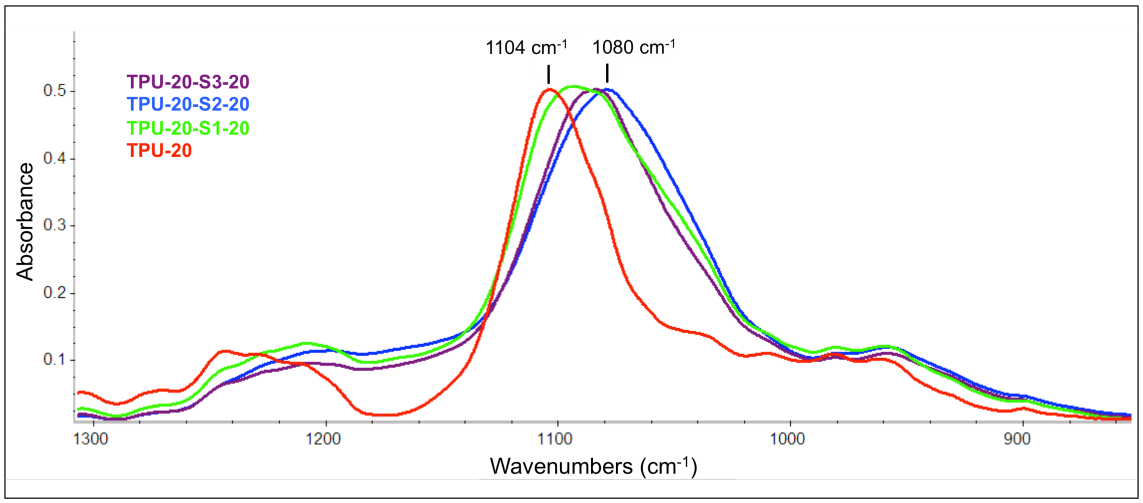


Figure 5-9: Comparative FTIR spectra of the ether region for TPU-PTMO-20 and its nanocomposites with 20% by weight S1, S2 and S3.

5.3.4. Thermal Analyses by DSC and TGA

Thermal analyses of the nanocomposite films were performed by DSC and TGA measurements. Following the results of the FTIR studies, which indicated strong interaction between silica nanoparticles and the PTMO soft segment, model DSC studies were conducted on PTMO oligomer and its blend with 20% by weight of 74 nm silica (S2) in order to better understand this phenomena. DSC thermograms for these samples are reproduced in Figure 5-10. PTMO oligomer displayed a well defined T_g at -80 °C and a sharp melting peak with maximum at 26 °C, which are in good agreement with the previously reported values [178]. Addition of 20% by weight S2 silica did not influence the position of the PTMO melting peak. However, heat of fusion decreased approximately by 20%, which may be expected.

Similar studies were also performed on TPU-PTMO-20 and its nanocomposite with 20% by weight S2. As reproduced in Figure 5-10, DSC thermogram of TPU-20 displayed a well defined T_g for the soft segment matrix at -78.5 °C but did not show any crystallization or melting peaks. TPU-20-S2-20 nanocomposite also showed a PTMO soft matrix T_g at -75.0 °C, but no melting transitions.

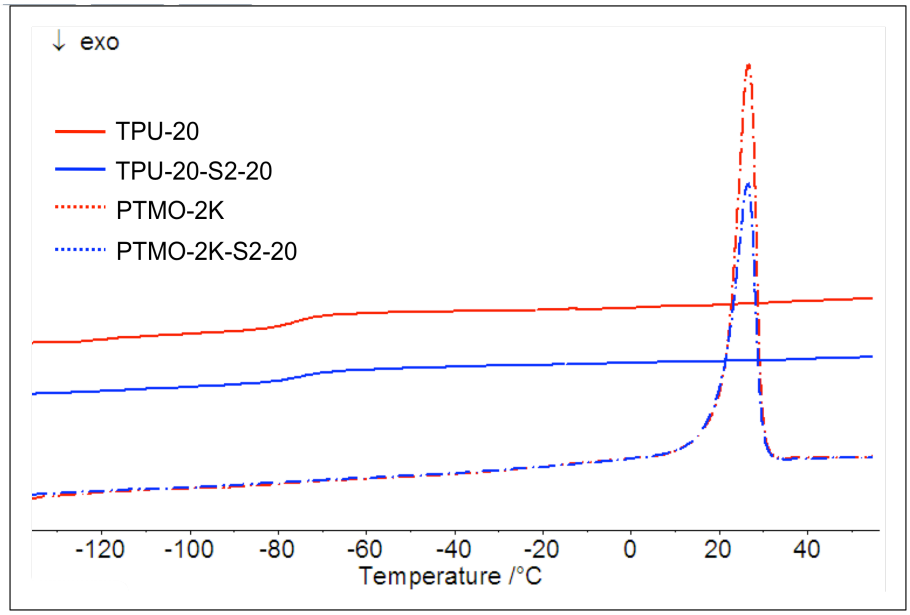


Figure 5-10: DSC curves of PTMO, PTMO-S2-20, TPU-PTMO-20 and TPU-PTMO-20-S2-20.

DSC analyses of a large number of nanocomposites were performed and the results are listed in Table 5-3. No significant change in the soft segment T_g was observed regardless of the silica size or the amount of incorporation. This phenomenon, which was also observed by several researchers [87, 89, 170, 179], indicates no change in the soft segment mobility in the presence of silica particles dispersed in the polymeric matrix.

Based on the interaction between the soft segments and silica nanoparticles that was evidenced by FTIR and homogeneous random distribution of the particles by SEM analyses, a decrease in the segmental mobility was expected. It is well-known that in polyether urethanes and ureas, (N−H) groups form hydrogen bonds with both the carbonyl (C=O) of the hard segments and the oxygen (−O−) in the polyether soft segments [160]. We agree with Sadeghi et al. that by silica addition into the polymeric matrix, hydrogen bonding between N-H groups and ether groups might be replaced by

hydrogen bonding between silica particles and ether groups in the soft segment of TPU, and thereby no major change was recorded in the total segmental mobility [179]. The disruption in the N-H absorption band and the significant band shifts in the ether region of the TPU in the presence of silica particles support this phenomenon. In addition, the T_g of the soft segments becomes broader and the heat capacity changes at glass transition (ΔC_p at T_g) show a steady decrease with increasing amount of silica. The decrease in heat capacity differences with increased filler content was expected since the filler does not contribute to the glass transition and hence the need of potential energy to create the volume for the segmental mobility decreases. However, the broadening of soft segment glass transition was attributed to the restricted mobility of the soft segment chains [180].

Table 5-3: Thermal properties of the TPUs/silica nanocomposites.

Sample	**Filler**		**Residual Mass (wt%) at 650°C**	**T_g (°C)**	**ΔC_p at T_g (J/gK)**
	Size (nm)	ca. wt %			
TPU-PTMO-20	-	-	0.18	-75.8	0.387
TPU-PTMO-20-S2-1	74	1	0.71	-75.0	0.384
TPU-PTMO-20-S2-5	74	5	4.81	-74.3	0.377
TPU-PTMO-20-S2-10	74	10	11.2	-76.1	0.369
TPU-PTMO-20-S2-20	74	20	21.4	-75.1	0.293
TPU-PTMO-20-S2-40	74	40	40.9	-74.6	0.144
TPU-PTMO-20-S1-20	29	20	17.0	-74.2	0.274
TPU-PTMO-20-S3-20	215	20	19.8	-75.4	0.335

TGA analyses were proposed to ascertain the thermal stability of polyether based TPU/silica nanocomposites. Figure 5-11 displays thermogravimetric curves of prepared nanocomposites between 140-700°C, which represents the region for more than 95% weight loss, under nitrogen atmosphere. The decomposition of polyether based neat TPU-20 starts at approximately 330°C and single slope for weight loss is observed for the breakage of urethane-urea bonds, and subsequent thermal decomposition of the polyether polyol [181]. On the other hand, by silica addition a second slope appears up to 400°C due to dehydroxylation of silanol groups and the degradation of the residual TEOS [182]. As clearly seen in Figure 5-11, the slope of

weight loss decreases by increasing the silica amount. The dashed lines indicating 50% weight loss clearly show that thermal resistance at high temperature is considerably enhanced in the presence of silica particles, and this was attributed to the thermal insulation effect of silica, as observed by Kim et al. [183, 184]. Residual masses of the nanocomposites after complete degradation at 650 °C are also listed in Table 5-3. These results compares well with the theoretical silica weight percentage of TPU/silica nanocomposites.

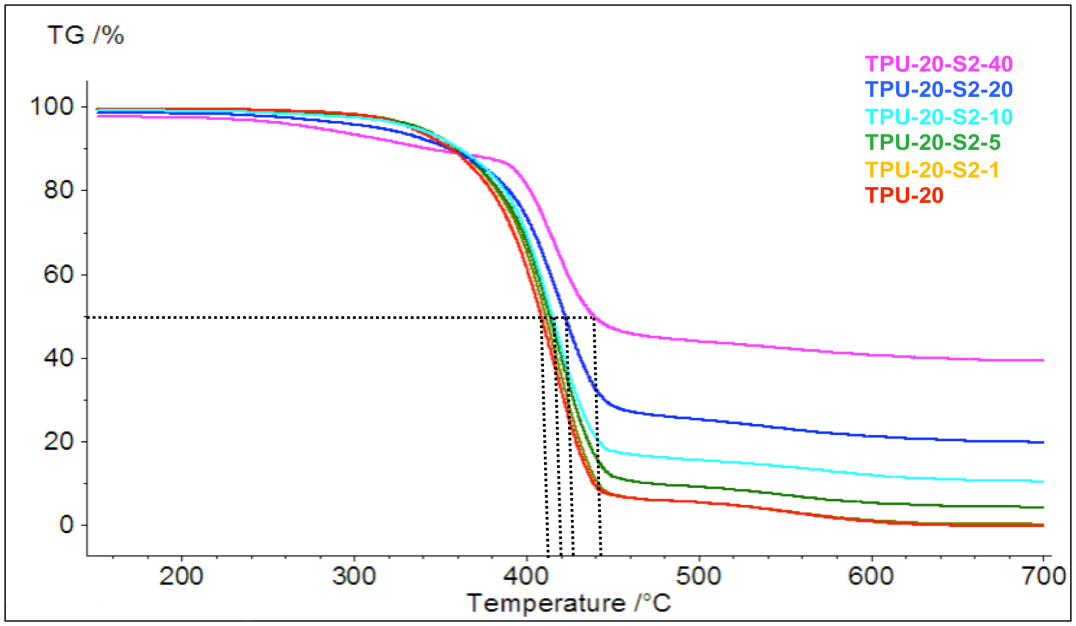


Figure 5-11: TG curves of TPU/silica nanocomposites as a function of silica content. Dashed lines indicate the increase in thermal degradation temperature for 50%weight loss in the presence of silica particles.

5.3.5. Stress-Strain Behavior

Segmented polyurethaneureas generally display excellent elastomeric properties with high tensile strengths and elongation at break values. To understand the effect of nanosilica incorporation on tensile properties, detailed stress-strain analysis of the nanocomposites were performed. Representative stress-strain curves for TPU-PTMO-20 and its nanocomposites containing different amounts of 74 nm S2 silica are provided in Figure 5-12. Detailed results regarding the analysis of the stress-strain studies are provided on Table 5-4.

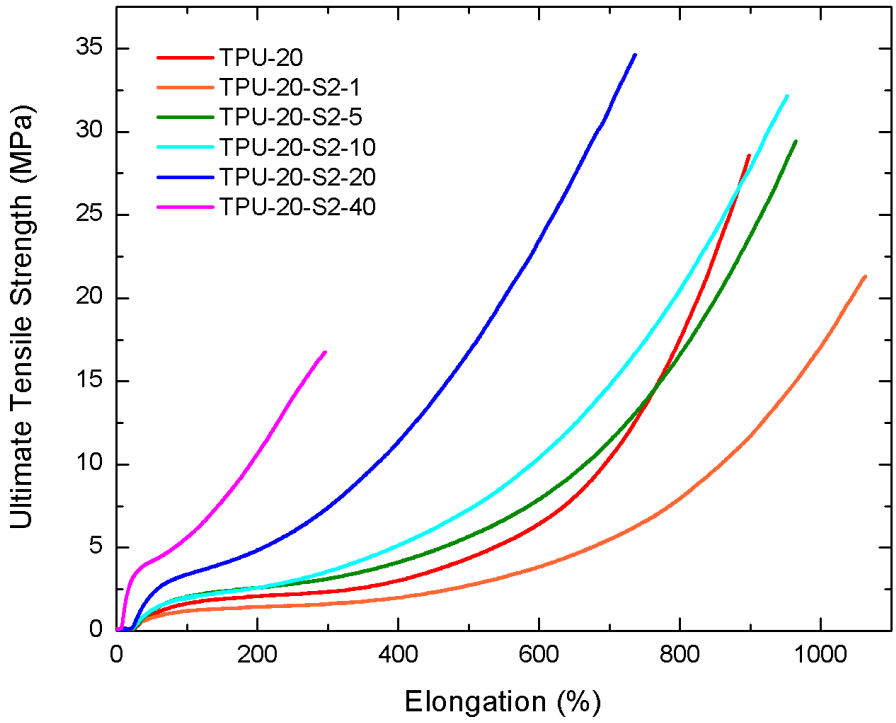


Figure 5-12: Stress-strain curves of TPU-PTMO-20 and its nanocomposites containing 1 to 40wt% of S2 colloidal silica.

As shown in Figure 5-12 and on Table 5-4, TPU-PTMO-20 displays fairly nice elastomeric properties with a Young's modulus of 4.3 MPa, ultimate tensile strength of 27.8 MPa and elongation at break of 1000%. As expected, incorporation of silica resulted in an increase in the moduli of the nanocomposites as a function of the amount of the filler (except for TPU-PTMO-20-S2-1) from 4.3 MPA for TPU-PTMO-20 to 37.0 MPa for TPU-PTMO-20-S2-40. A slight increase in the tensile strengths and a slight decrease in the elongation at break values of the nanocomposites as a function of silica content, up to 20% silica, was also observed. Interestingly, the sample containing only 1% by weight of nanosilica S2, TPU-PTMO-20-S2-1 displayed a lower modulus, lower ultimate tensile strength and a higher elongation at break value when compared with TPU-PTMO-20, which could be attributed to the plasticizing effect of the colloidal silica. Similar behavior was also observed by Bistricic et al. [185] and Lee et al. [177] for samples containing low amounts of nanosilica. Very surprisingly, TPU-PTMO-20-S2-40 displayed a dramatic reduction in ultimate tensile strength and elongation at break values when compared with TPU-PTMO-20. This is most probably due to incomplete mixing of the filler and the matrix and formation of silica agglomerates and

the voids formed between these agglomerates and the polymer layer as shown in SEM images provided in Figure 5-6 (e). These voids most probably lead to local stress concentrations and result in premature failure.

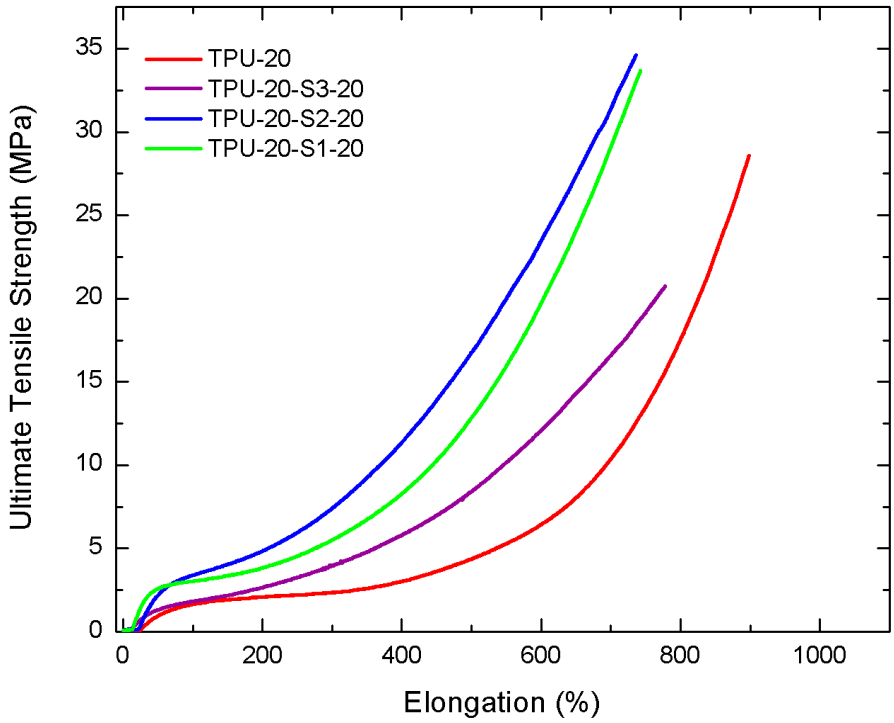


Figure 5-13: Stress-strain curves of TPU-PTMO-20 and nanocomposites containing 20 weight% S1, S2 and S3 colloidal silica.

To understand the influence of silica particle size on tensile properties, stress-strain behavior of nanocomposites containing 20 wt% S1, S2 and S3 silica were also investigated. Representative stress-strain curves for TPU-PTMO-20 and the nanocomposites are provided on Figure 5-13. Results are also summarized on Table 5-4. As expected, nanocomposites display higher Young's modulus values when compared with the TPU-PTMO-20. More importantly they also show fairly good improvements in the ultimate tensile strengths, such as 35.4 MPa and 33.1 MPa for TPU-PTMO-20-S1-20 and TPU-PTMO-20-S2-20 respectively, when compared with 27.8 MPa for TPU-PTMO-20. These results indicate that nanocomposites prepared from smaller particles with larger surface area per unit mass may be more attractive as reinforcing fillers in nanocomposites.

Table 5-4: Tensile properties of TPU-20 and silica nanocomposites

Sample	Filler		Tensile Properties*		
	wt %	Size (nm)	M (MPa)	TS (MPa)	E (%)
TPU-PTMO-20	-	-	4.3±1.3	27.8±3.7	1000±30
TPU-PTMO-20-S2-1	1	75	3.8±1.0	27.7±9.9	1070±20
TPU-PTMO-20-S2-5	5	75	6.7±1.6	28.2±2.4	970±40
TPU-PTMO-20-S2-10	10	75	6.7±1.4	30.9±2.9	950±90
TPU-PTMO-20-S2-20	20	75	10.8±0.2	33.1±3.9	800±20
TPU-PTMO-20-S2-40	40	75	37.0±3.0	23.6±5.4	430±30
TPU-PTMO-20-S1-20	20	29	10.7±0.9	35.4±2.9	850±50
TPU-PTMO-20-S3-20	20	215	8.6±4.1	19.6±3.1	830±40

*M: Young's Modulus TS: Ultimate tensile strength at break E: Elongation at break

Nanomechanical tests were also performed by using quasi-static indents on TPU/silica nanocomposite films to understand the relationship between the hardness and fracture toughness with respect to filler size. Table 5-5 summarizes the mechanical responses in terms of average values of the reduced modulus (E_r) and hardness (H) for each sample, where both micro-hardness and contact stiffness (given by reduced modulus) increased as the silica particle size decreased in nanocomposites containing 20 weight% silica loading.

Table 5-5: Nanomechanical properties of nanocomposites containing 20 weight% silica

Sample	h_c (nm)	E_r (MPa)	H (MPa)	Plasticity (Ductility) Index
TPU-20	920±22	13.0±0.6	1.6±0.06	8.1
TPU-20-S1-20	960±5	23.3±0.4	2.5±0.02	9.3
TPU-20-S2-20	971±4	19.3±0.3	2.0±0.02	9.6
TPU-20-S3-20	963±4	14.9±0.2	1.6±0.02	9.5

h_c – contact depth; E_r – reduced modulus; H – microhardness.

The ratio of E_r/H is usually referred to as the plasticity or ductility index of the material, which reflects the relative amount of plastic indentation work [186] and correlates well with the fracture toughness [187]. As can be seen in Table 5-5, by 20

weight% silica loading, plasticity and hence the fracture toughness of the TPU/silica nanocomposites could be enhanced regardless of the particle size.

Another interesting observation was the difference in the structure or the topography of the ruptured surfaces after tensile tests, when unfilled and silica filled TPU-PTMO-20 were compared. SEM micrographs of the ruptured surfaces for TPU-PTMO-20 and TPU-PTMO-20-S2-20 are shown in Figure 5-14. Figure 5-14 (a) shows a fairly clean surface for TPU-PTMO-20 after rupturing. On the other hand the Figure 5-14 (b) shows a more complex and tethered rupture for TPU-PTMO-20-S2-20, indicating a different fracture mode. Similar behavior was also observed in our previous studies on poly(silicone-urea)/silica composites, where increased rupture surface area with silica loadings above 20 weight% was reported [188]. In addition to these, strain induced fiber formation during rupture was clearly noticed with silica incorporation, indicating a clear interaction between polyurethane-urea copolymer and silica nanoparticles as seen in Figure 5-14 (b).

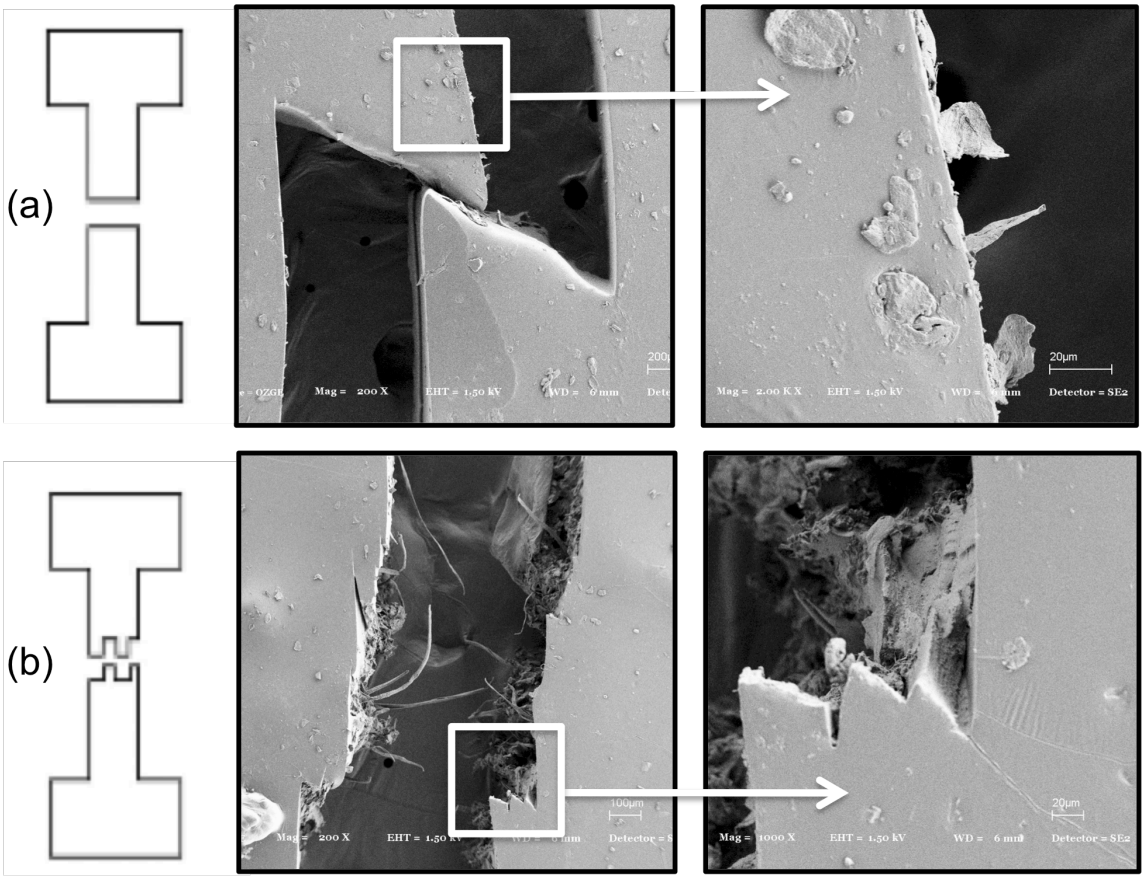


Figure 5-14: SEM images of tensile-fractured surfaces of (a) TPU-PTMO-20 and (b) TPU-PTMO-20-S2-20.

Additional supporting observation on the formation of fibrous structures was also obtained when surface cracks induced on TPU-PTMO-20-S2-20 was examined (Figure 5-15). This SEM micrograph also reveals the contribution of the polymer-particle interaction on the distribution of the particles in the polymeric matrix and the homogeneous distribution of the silica nanoparticles obtained by the solution blending used in this study for the preparation of the samples.

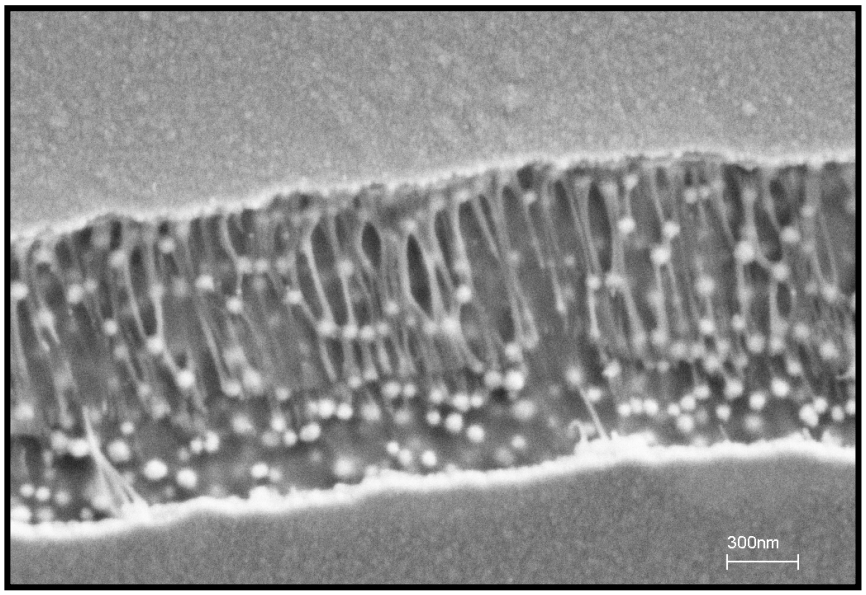


Figure 5-15: SEM micrograph of a surface fracture on TPU-PTMO-20-S2-20.

5.3.6. Influence of Soft Segment Chemistry on Nanocomposite Properties

In this final part of the study, the effect of soft segment chemistry is investigated by using poly(ethylene oxide), PEO, which has a lower molecular weight repeating unit compared to poly(tetramethylene oxide), PTMO as the soft segment component. Table 5-6 gives the compositions of the PEO based TPU/silica nanocomposites prepared in this study. In the coding, TPU-PEO-20 indicates a polyurethaneurea with PEO based soft segment and a hard segment content of 30% by weight, followed by the description of the silica used (S2) and the silica content (1-20) in weight percent.

Table 5-6: Compositions of TPU-PEO/colloidal silica composites.

Sample	Hydrodynamic Diameter (DLS/nm)	Silica Content (Weight %)
TPU-PEO-30	-	-
TPU-PEO-30-S2-1	74	1
TPU-PEO-30-S2-5	74	5
TPU-PEO-30-S2-10	74	10
TPU-PEO-30-S2-20	74	20
TPU-PEO-30-S2-40	74	40

In polyether urethanes and ureas, (−N−H) groups form hydrogen bonds with both the carbonyl (C=O) of the hard segments and the oxygen (−O−) in the polyether soft segments (Figure 5-16). The hydrogen bond energies calculated by quantum mechanical studies of urea-urea, urethane-urethane and urea-ether were reported to be 21.8, 18.4 and 19.2 kJ/mol, respectively [160]. The similarity between hydrogen bond energies of these interactions indicates a fairly strong competition between carbonyl and ether towards (−N−H). Therefore, at constant soft segment molecular weight PEO based TPU results in higher phase mixing compared to PTMO based TPU due to higher ether-urethaneurea interactions. When 20 weight% hard segment ratio was applied for PEO based copolymers, mechanically non-durable films were obtained due to phase-mixing. Therefore, hard segment content was increased to 30 weight% to be able to attain films that have mechanically identical properties with the films prepared by using PTMO

based soft segment and a hard segment content of 20% by weight. The results of the tensile tests will be discussed later in this chapter.

Table 5-7: Tensile properties of TPU polymers with various soft segment components with molecular weight of 2000 g/mol and hard segment ratio.

Sample	Soft Segment	Hard Segment Ratio (weight%)	M (MPa)	TS (MPa)	E (%)
TPU-20	PTMO	20	4.3±1.3	27.8±3.7	1000±30
TPU-PEO-20	PEO	20	NA	NA	NA
TPU-PEO-30	PEO	30	4.7±1.2	26.2±2.1	1150±30
TPU-PEO-40	PEO	40	24.3±7.2	34.4±5.7	725±40

The morphology and particle distribution in 20 and 40 wt% TPU/silica nanocomposite films was imaged by SEM at 100kX magnification. The images of silica filled nanocomposite samples given by Figure 5-17 (a and b) clearly show that silica particles had a randomly even distribution in the polymeric matrix. In addition, no evident agglomeration was detected during cross section (Figure 5-17 a) and surface imaging (Figure 5-17 b) of the nanocomposites. Figure 5-17 (b) also exhibits a rare surface crack, which enables us to see the distribution of silica particles upon drying. In addition to even distribution of the particles, no void formation (good particle-polymer interaction) around the particles was observed.

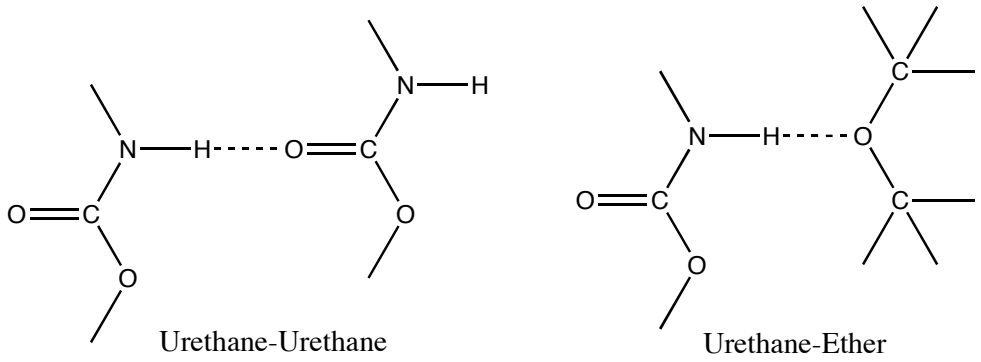


Figure 5-16: Representation of hydrogen bonding in polyether based TPUs.

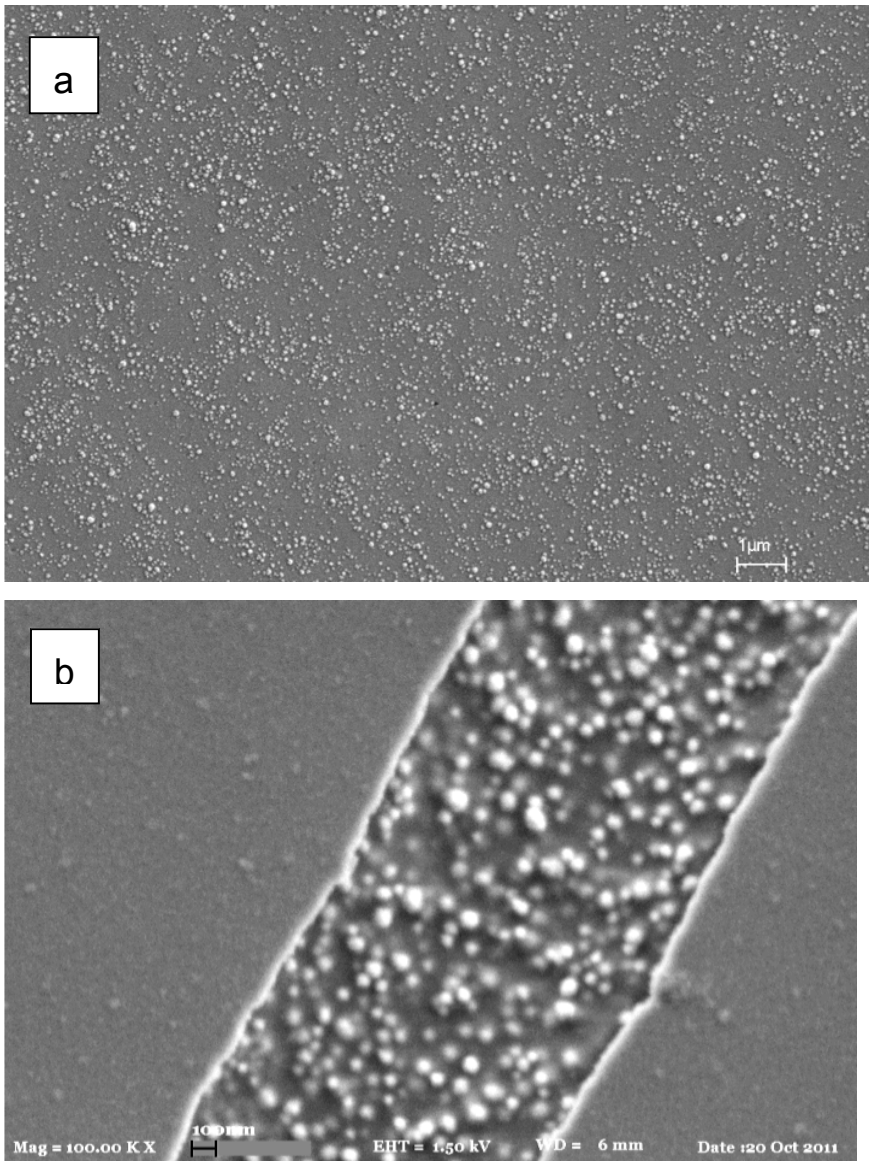


Figure 5-17: SEM micrographs of TPU-PEO-30-S2-20 at 100 kX magnification: (a) cross-section and (b) surface.

FT-IR studies of neat copolymer and nanocomposites with 1, 5, 10, and 20 wt% silica filler amount were performed. ATR-IR spectra for carbonyl region (1800-1600 cm^{-1}) and ether region (1200 – 1000 cm^{-1}) of neat copolymer (TPU-PEO-30) and representative nanocomposites are shown in Figure 5-18 and Figure 5-19, respectively. No significant change was detected in the N-H (3600-3000 cm^{-1}) region of the matrices after filler incorporation (not shown here). Neat TPU-PEO-30 shows single hydrogen-bonded urethane carbonyl stretch at 1715 cm^{-1} and ordered H-bonded urea carbonyl peak at 1630 cm^{-1} [160, 189]. No significant change, yet just a slight shoulder around 1700 cm^{-1}, was observed in urethane carbonyl region of the nanocomposites compared

to the neat polymer (Figure 5-18). On the other hand, the ordered H-bonded urea carbonyl peak at 1630 cm^{-1} slightly shifts to higher wavenumbers and a shoulder appears around 1655 cm^{-1}. The shifts for ordered (1630-1645 cm^{-1}) and disordered (1660-1670 cm^{-1}) hydrogen-bonded urea groups for polyether based urea copolymers were reported by Yilgor et al [160]. Intensity of the peak showing the disordered H-bonded carbonyl urea (1655 cm^{-1}) increases with filler amount and a broad shoulder is seen in the spectrum of 20 weight% silica filled nanocomposite. These changes in urea carbonyl peak positions and intensities indicate that silica filler addition had a disruptive effect on H-bonding behavior of urea groups present in hard domains of the PEO based polyurethaneurea copolymer, while the urethane carbonyl groups were not affected by the presence of silica.

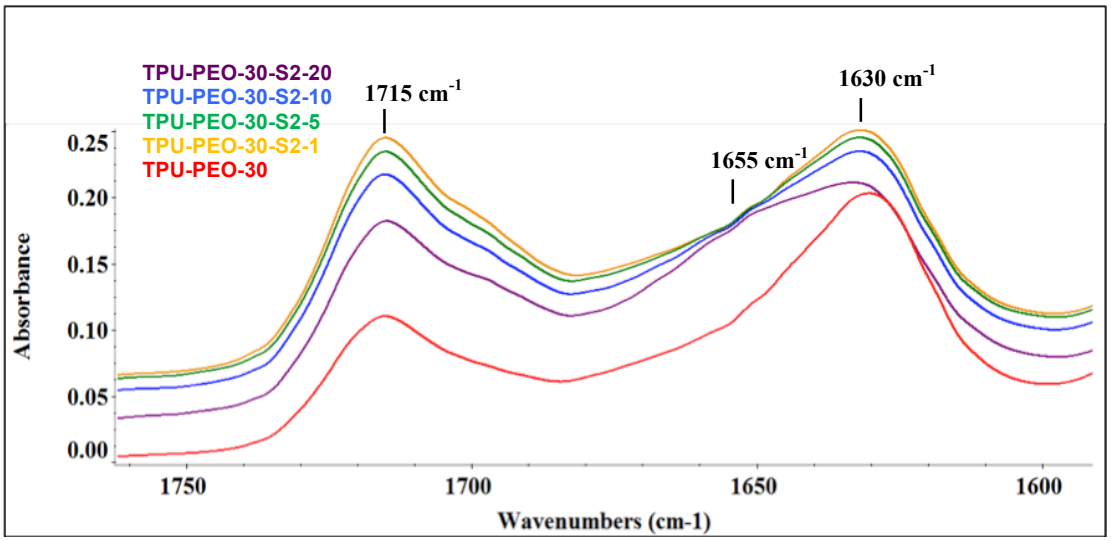


Figure 5-18: ATR-IR investigation of carbonyl region of the neat copolymer (TPU-PEO-30) and corresponding nanocomposites with filler loadings of 1-20wt%.

Similar to our observations for PTMO based systems, FT-IR spectra of the PEO based nanocomposites exhibit substantial changes in the ether region where C-O-C stretching peak (1700 cm^{-1}) is present: peaks are both broadened and shifted to the lower wavenumbers (Figure 5-19). Broadening is attributed to overlapping of Si-O-Si stretching of silica filler and C-O-C of the polymeric matrix, while the shift of the peak positions to the right is attributed to the formation of new hydrogen bonds between the hydroxyl groups on the silica surface and the ether linkages in the PEO backbone. The shift to lower wavenumbers intensifies with increasing filler content due to increase in

filler surface area and hence the hydroxyl groups interacting with the polymeric matrix. FTIR results indicate that silica nanoparticles strongly interact with soft segment matrix through hydrogen bonding.

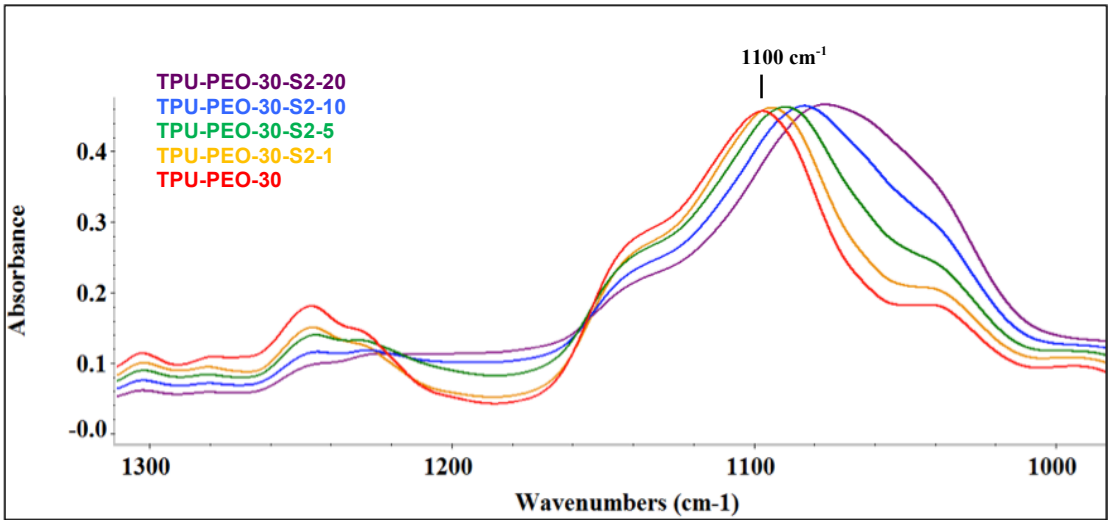


Figure 5-19: ATR-IR investigation of ether region of the neat copolymer (TPU-PEO-30) and corresponding nanocomposites with filler loadings of 1-20wt%.

The effect of filler content on the thermal properties was investigated by DSC analyses as shown in Figure 5-20. The samples were heated from -160 to 80°C with a heating rate of 10°C/min, and to avoid any effect of so-called 'thermal history', second heating profiles were used for DSC traces. As seen in Figure 5-20, TPU-PEO-30 neat copolymer exhibits a single endothermic peak at 53°C and melting temperature stays almost same for all nanocomposite systems. The heat of fusion obtained is directly proportional to the weight percentage of crystalline portion of TPU-PEO-30, which majorly stems from the soft segment PEO. DSC traces of the nanocomposites indicate that the amount of crystallinity of PEO in the TPU/silica nanocomposites was reduced with the increase in silica content. The decrease of the heat of fusion in nanocomposites indicating lower values of crystallinity is attributed to the interaction between soft segment ether groups and silica nanoparticles. The reduction of weight percentage of crystalline PEO is attributed to the constrained mobility of macromolecular chains in the polymeric matrix with silica incorporation. The movement, and hence the crystallizability, of the macromolecular chains, was limited due to strong interaction with the silica surface. Two mechanisms were reported in literature to explain the

reduction in crystallinity of polymer chains caused by nano-sphere incorporation [190, 191]. First mechanism underlines the spatial confinement of chains in the small volumes between nano-particles, which results in reduction in chain mobility and ability to attach a growing crystal. Second mechanism points out the effective pinning of chains on particle surfaces. Therefore, fixed contact points form, and molecular motion is restricted. Although spatial confinement is plausible at high enough volume fractions of fillers in well-dispersed systems, pinning at interfaces may also be effective in crystallinity reduction as supported by hydrogen bonding interactions between soft segment of the copolymer and surface silanols on the silica surface, and the sharp decrease in heat of fusion even at low filler concentration.

To understand the influence of nanosilica incorporation on tensile properties, stress-strain analysis of the nanocomposites were performed. Representative stress-strain curves for TPU-PEO-20 and its nanocomposites containing different amounts of 74 nm S2 silica are provided in Figure 5-21. Detailed results regarding the analysis of the stress-strain studies are provided on Table 5-8, where *M*, *TS* and *E* denote Young's modulus, ultimate tensile strength and elongation at break values, respectively.

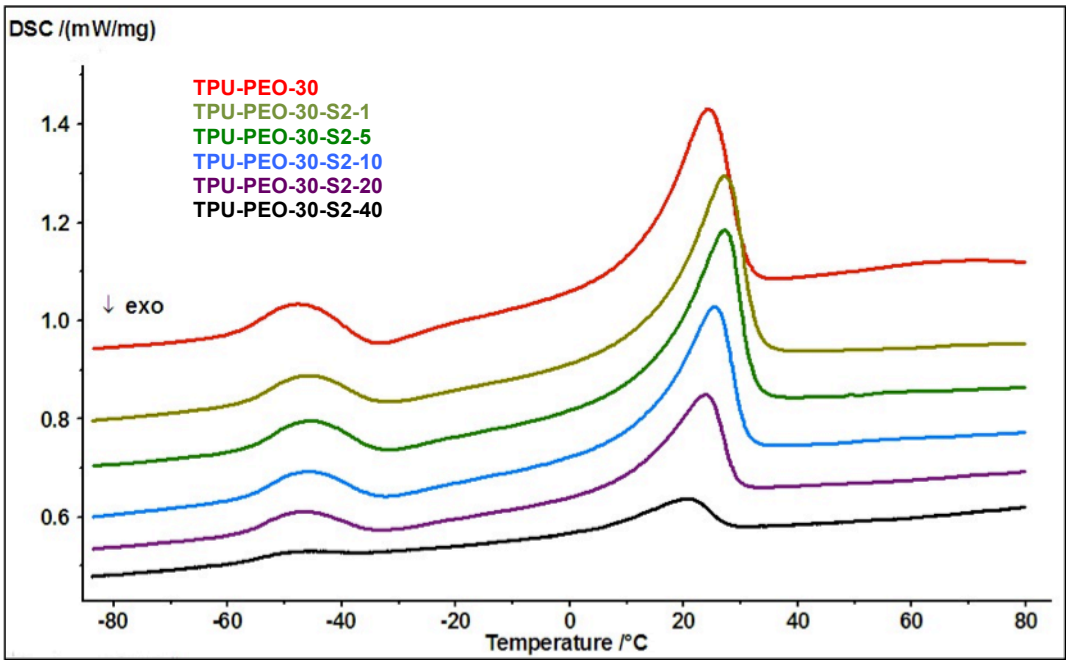


Figure 5-20: DSC traces of neat copolymer (TPU-PEO-30) and corresponding nanocomposites with filler loadings of 1-20wt%.

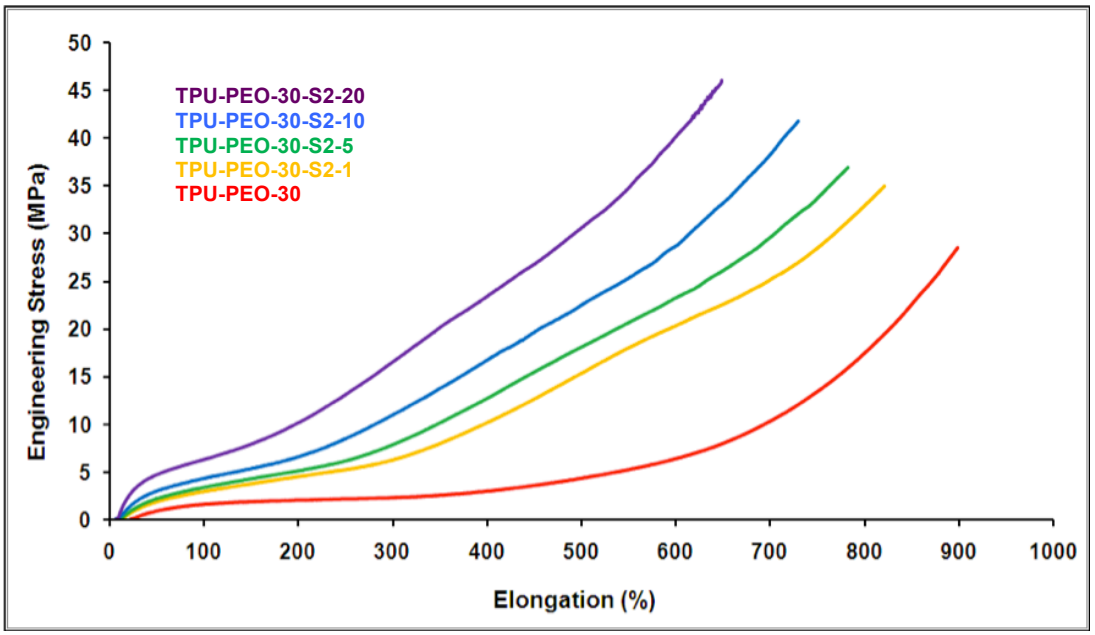


Figure 5-21: Stress-strain curves of the neat copolymer (TPU-PEO-30) and corresponding nanocomposites with filler loadings of 1-20wt%.

Table 5-8: Mechanical test results of neat polymer and corresponding nanocomposites.

Sample	M (MPa)	TS (MPa)	E (%)
TPU-PEO-30	4.7±1.2	26.2±2.1	1150±30
TPU-PEO-30-S2-1	6.6±0.1	32.5±3.4	790±40
TPU-PEO-30-S2-5	7.0±0.8	34.1±2.4	760±30
TPU-PEO-30-S2-10	11.2±0.6	40.5±3.7	710±20
TPU-PEO-30-S2-20	26.7±4.0	45.1±2.1	640±10

*M: Young's Modulus TS: Ultimate tensile strength at break E: Elongation at break

As seen in Figure 5-21 and Table 5-8, TPU-PEO-20 neat copolymer displays elastomeric properties with a modulus of about 4.7 MPa, ultimate tensile strength of about 26 MPa and elongation at break slightly over 1000%, which are similar to the mechanical properties of PTMO based TPU-20. Tensile tests show that both modulus and tensile strength significantly increased with filler amount, however even 1 weight% silica addition caused 30% decrease in percent elongation at break, which increases up to 45% at 20 wt% silica loading. It is well known that in segmented polyurethanes the modulus is directly related to the type and amount of hard segment in the copolymer [192]. On the other hand, tensile strength and elongation at break reflect the combined effects of hard and soft segments or more precisely the overall morphology of the

copolymer. As shown by FT-IR spectra (Figure 5-18) silica particles seem to disturb the H-bonding behavior of the urea groups in hard segments, which act as well-distributed fillers in the polymeric matrix. The enhancement in both modulus and tensile strength of the nanocomposites indicates that overall morphology of the polymer was not disrupted while the presence of filler had a reinforcing effect due to the prominent interaction of the silica nanoparticles with the PEO based soft domains through hydrogen bonding. The decrease in elongation at break is thus attributed to the decreased mobility of PEO chains with respect to their strong interaction with silica surface.

Table 5-9: Comparison of mechanical properties of PTMO and PEO based TPU/silica nanocomposites based on percent increase/decrease in Young's modulus (M), ultimate tensile strength (TS) and elongation at break (E). Percent changes were given in comparison with the corresponding properties of the neat polymers.

Sample	**Young's Modulus (%Δ)**	**Tensile Strength (%Δ)**	**Elongation at Break (%Δ)**
TPU-PTMO-20-S2-1	-11.6	-0.4	+6.0
TPU-PEO-30-S2-1	+40.4	+24.0	-31.3
TPU-PTMO-20-S2-5	+55.8	+1.4	-3.5
TPU-PEO-30-S2-5	+48.9	+30.1	-33.9
TPU-PTMO-20-S2-10	+55.8	+11.2	-5.0
TPU-PEO-30-S2-10	+138	+54.6	-38.3
TPU-PTMO-20-S2-20	+151	+19.1	-21.0
TPU-PEO-30-S2-20	+468	+72.1	-44.3

Table 5-9 compares the changes in tensile behavior of PTMO and PEO based TPU nanocomposites. The increase in both modulus and tensile strength is substantially larger for PEO based nanocomposites when compared with those of PTMO based nanocomposites. On the other hand, the loss in elongation at break at 1-20 weight% filler incorporation is 0-21% and 31-45% for PTMO based and PEO based TPU/silica nanocomposites, respectively. This was attributed to the differences in hard segment content and soft segment chemistry of the copolymers. It was previously shown that polymer-silica interaction was majorly due to interaction between the soft segment ether

groups and the surface silanols of silica nanoparticles for PTMO based systems. On the other hand, as the hard segment content was increased for PEO based systems, it was presented that silica nanoparticles also interact with the urea carbonyl groups of the hard segments in addition to the prominent interaction between silica surface silanols and the ether groups of the soft segment. The nanoparticles interaction with soft and hard segments of the copolymer at the same time may increase the interconnectivity between the segments leading to a stiffer structure.

Another tentative explanation can be based on the area density of oxygen atoms in the dominant ether segments that are in contact with the silica nanoparticle surface containing SiOH groups. An ethylene oxide monomer is ~4 Å long, a tetramethylene oxide monomer is about ~7 Å long, and both are about 4 Å wide and contain one oxygen atom prone to hydrogen bonds. Therefore, the area density of strongly bonded ether oxygens for an extended ether chain on the silica nanoparticles surface is ~6.0 and 3.5 per nm^2 for PEO and PTMO, respectively. The silica surface contains typically 4.6 SiOH groups per nm^2 [6], and thus the number density of attractive hydrogen bonds per interfacial area between the polyether segments and the silica surface can be substantially higher for PEO compared to PTMO based TPU, supporting higher elastic moduli and tensile strength.

5.4. CONCLUSIONS

In the second part of this dissertation, polymer-filler interactions in polyether based thermoplastic polyurethane (TPU)/silica nanocomposites were studied. For this purpose, the effect of (i) filler size, (ii) filler loading and (iii) soft segment chemistry on the morphology as well as on the thermal and mechanical properties of the nanocomposite systems was studied. The nanocomposites were effectively prepared by solution blending in iso-propyl alcohol. The TPU copolymer consisted of polyurethane prepolymer with alternating soft polyether segments and hard isocyanate segments, further linked by diamine chain extenders into polyurethane-urea. Three different silica nanoparticles with average diameters of 29, 74 and 215 nm were prepared in our laboratories and used as fillers in amounts varying between 1 and 40 weight%. To investigate the influence of soft segment chemistry, poly(tetramethylene oxide), PTMO, and poly(ethylene oxide), PEO, were used as soft segment components in two different copolymers along with bis(4-isocyanatocyclohexyl)methane as diisocyanate and 2-methyl-1,5-diaminopentane as chain extender. Samples were characterized by FTIR spectroscopy, scanning electron microscopy (SEM), thermal analysis, tensile tests and nanoindentation to understand the influence of the nanoparticle size, content and soft segment chemistry on the ultimate properties of the resultant nanocomposites.

Solution blending using a common solvent avoided the agglomeration of silica nanoparticles and produced homogeneous nanocomposites of both copolymers as evidenced by SEM results. FTIR studies showed stronger interaction between silica particles and the polyether matrices, as compared to the urethaneurea hard segments. However, soft segment T_g remained the same regardless of soft segment chemistry, the silica size or the amount of incorporation. Even distribution of silica nanoparticles in the polyurethane-urea matrices enhanced the mechanical properties of the nanocomposites, which primarily dependent on the size of the silica nanoparticles and amount of loading. Increased filler content up to about 20% by weight lead to materials with higher elastic moduli and tensile strength values, while further increase resulted in loss of the elastomeric properties of PTMO-based systems. Incorporation of silica nanoparticles with smaller particle sizes provided better enhancement in the modulus and tensile strength of the nanocomposites formed, while retaining their elastomeric properties. In addition to enhance tensile properties, fracture toughness of the nanocomposites were

improved, regardless of the silica particle size. Moreover, thermal stability of nanocomposites was improved due to thermal insulation effect of silica.

Similar trend was observed in the tensile properties of PEO-based systems, however higher level of improvement was obtained both for elastic moduli and tensile strength with silica loading. This was attributed to the differences in hard segment content and soft segment chemistry of the copolymers. In addition to the major interaction between silica surface and ether sites of the soft segment, silica incorporation also affected the ordering in the hard segment. On the other hand, due to the substantial interaction between ether sites of the soft segment and silanol groups on the silica surface, crystallizability of the PEO soft segment decreased with the silica content.

In summary, we have introduced a simple method to prepare nanocomposites of polyether based TPU/silica nanocomposites with a range of mechanical properties and homogeneous distribution of silica particles using solution blending of a copolymer solution and silica sols “as synthesized and aged” in common solvents at room temperature.

REFERENCES

1. *Basic Characteristics of AEROSIL fumed silica*, in *Technical Bulletin Fine Particles N11*. 1997, Evonik Degussa AG: Hanau.
2. Bergna, H.E. and Roberts, W.O., *Colloidal silica: fundamentals and applications*. Surfactant science series, 2006, Boca Raton, FL: CRC Taylor & Francis.
3. Vansant, E.F., Van Der Voort, P., and Vrancken, K.C., *Characterization and chemical modification of the silica surface*. Studies in surface science and catalysis, 1995, Amsterdam: New York.
4. Unger, K.K., *Porous silica, its properties and use as support in column liquid chromatography*. Journal of chromatography library, 1979, Amsterdam: New York.
5. Pauling, L., *The nature of the chemical bond and the structure of molecules and crystals : an introduction to modern structural chemistry*. 3d ed. The George Fisher Baker non-resident lectureship in chemistry at Cornell University, 1960, Ithaca, N.Y.: Cornell University Press.
6. Zhuravlev, L.T., *Concentration of hydroxyl-groups on the surface of amorphous silicas.* Langmuir, 1987, 3(3): p. 316-318.
7. Kim, H.C. and Dubois, G., *Dekker Encyclopedia of Nanoscience and Nanotechnology*, 2005, New York: Taylor & Francis.
8. Jana, S.C. and Jain, S., *Dispersion of nanofillers in high performance polymers using reactive solvents as processing aids.* Polymer, 2001, 42(16): p. 6897-6905.
9. Michel, W., *Fumed silicas reinforce elastomers*, in *Gummi Fasern Kautschuk*. 2007.
10. Vansant, E.F., Van Der Voort, P., and Vrancken, K.C., *Characterization and Chemical Modification of the Silica Surface*, 1995, New York: Elsevier Science.
11. Fendler, J.H., *Atomic and molecular clusters in membrane mimetic chemistry.* Chemical Reviews, 1987, 87(5): p. 877-899.
12. Bagwe, R.P., Hilliard, L.R., and Tan, W., *Surface modification of Ssilica nanoparticles to reduce aggregation and nonspecific binding.* Langmuir, 2006, 22(9): p. 4357-4362.
13. Bagwe, R.P., Yang, C., Hilliard, L.R., and Tan, W., *Optimization of dye-doped silica nanoparticles prepared using a reverse microemulsion method.* Langmuir, 2004, 20(19): p. 8336-8342.
14. Durgun, G., Ocakoglu, K., and Ozcelik, S., *Systematic tuning the hydrodynamic diameter of uniformed fluorescent silica nanoparticles.* The Journal of Physical Chemistry C, 115(33): p. 16322-16332.
15. Stöber, W., Fink, A., and Bohn, E., *Controlled growth of monodisperse silica spheres in the micron size range.* Journal of Colloid and Interface Science, 1968, 26(1): p. 62-69.

16. Zou, H., Wu, S., and Shen, J., *Polymer/Silica Nanocomposites: Preparation, Characterization, Properties, and Applications.* Chemical Reviews, 2008, 108(9): p. 3893-3957.

17. Brinker, C.J. and Sherer, G.W., *Sol-gel science: the physics and chemistry of sol-gel processing*, 1990, San Diego: Academic Press.

18. van Blaaderen, A. and Vrij, A., eds. *Synthesis and characterization of colloidal model particles made from organoalkoxysilanes*. Colloidal silica: fundamentals and applications, ed. H.E. Bergna and W.O. Roberts. 2006, CRC Press: Taylor & Francis Group: Florida. 65.

19. Iler, R.K., *The Chemistry of Silica*, 1979, New York: Wiley.

20. Kolbe, G., *Das komplexchemische Verhalten der Kieselsäure*. 1956: Jena.

21. Van Helden, A.K., Jansen, J.W., and Vrij, A., *Preparation and characterization of spherical monodisperse silica dispersions in nonaqueous solvents.* Journal of Colloid and Interface Science, 1981, 81(2): p. 354-368.

22. Green, D.L., Harris, M.T., Jayasundara, S., Lin, J.S., Hu, M.Z., and Lam, Y.F., *Early stage silica formation in methanol and ethanol*, in *Ceramic Nanomaterials and Nanotechnology*, M.Z. Hu and M.R. DeGuire, Editors. 2003. p. 33-58.

23. LaMer, V.K. and Dinegar, R.H., *Theory, production and mechanism of formation of monodispersed hydrosols.* Journal of the American Chemical Society, 1950, 72(11): p. 4847-4854.

24. Matsoukas, T. and Gulari, E., *Self-sharpening distributions revisited polydispersity in growth by monomer addition.* Journal of Colloid and Interface Science, 1991, 145(2): p. 557-562.

25. Matsoukas, T. and Gulari, E., *Monomer-addition growth with a slow initiation step - A growth-model for silica particles from alkoxides.* Journal of Colloid and Interface Science, 1989, 132(1): p. 13-21.

26. Matsoukas, T. and Gulari, E., *Dynamics of growth of silica particles from ammonia-catalyzed hydrolysis of tetra-ethyl-orthosilicate.* Journal of Colloid and Interface Science, 1988, 124(1): p. 252-261.

27. Bogush, G.H. and Zukoski, C.F., *Studies of the kinetics of the precipitation of uniform silica particles through the hydrolysis and condensation of silicon alkoxides.* Journal of Colloid and Interface Science, 1991, 142(1): p. 1-18.

28. Bogush, G.H. and Zukoski, C.F., *Uniform silica particle-precipitation - an aggregative growth-model.* Journal of Colloid and Interface Science, 1991, 142(1): p. 19-34.

29. Lee, K., Look, J.L., Harris, M.T., and McCormick, A.V., *Assessing extreme models of the Stober synthesis using transients under a range of initial composition.* Journal of Colloid and Interface Science, 1997, 194(1): p. 78-88.

30. Harris, M.T., Brunson, R.R., and Byers, C.H., *The base-catalyzed hydrolysis and condensation reactions of dilute and concentrated TEOS solutions.* Journal of Non-Crystalline Solids, 1990, 121(1-3): p. 397-403.

31. van Blaaderen, A. and Kentgens, A.P.M., *Particle morphology and chemical microstructure of colloidal silica spheres made from alkoxysilanes.* Journal of Non-Crystalline Solids, 1992, 149(3): p. 161-178.

32. Lee, K., Sathyagal, A.N., and McCormick, A.V., *A closer look at an aggregation model of the Stober process.* Colloids and Surfaces A: Physicochemical and Engineering Aspects, 1998, 144(1,Äì3): p. 115-125.

33. Bailey, J.K. and Mecartney, M.L., *Formation of colloidal silica particles from alkoxides.* Colloids and Surfaces, 1992, 63(1-2): p. 151-161.

34. Boukari, H., Long, G.G., and Harris, M.T., *Polydispersity during the formation and growth of the Stober silica particles from small-angle X-ray scattering measurements.* Journal of Colloid and Interface Science, 2000, 229(1): p. 129-139.

35. Boukari, H., Lin, J.S., and Harris, M.T., *Probing the dynamics of the silica nanostructure formation and growth by SAXS.* Chemistry of Materials, 1997, 9(11): p. 2376-2384.

36. Boukari, H., Lin, J.S., and Harris, M.T., *Small-angle X-ray scattering study of the formation of colloidal silica particles from alkoxides: Primary particles or not?* Journal of Colloid and Interface Science, 1997, 194(2): p. 311-318.

37. Green, D.L., Jayasundara, S., Lam, Y.F., and Harris, M.T., *Chemical reaction kinetics leading to the first Stober silica nanoparticles - NMR and SAXS investigation.* Journal of Non-Crystalline Solids, 2003, 315(1-2): p. 166-179.

38. Bogush, G.H., Tracy, M.A., and Zukoski, C.F., *Preparation of monodisperse silica particles: Control of size and mass fraction.* Journal of Non-Crystalline Solids, 1988, 104 p. 95-106.

39. Rao, K.S., El-Hami, K., Kodaki, T., Matsushige, K., and Makino, K., *A novel method for synthesis of silica nanoparticles.* Journal of Colloid and Interface Science, 2005, 289(1): p. 125-131.

40. Yokoi, T., Sakamoto, Y., Terasaki, O., Kubota, Y., Okubo, T., and Tatsumi, T., *Periodic arrangement of silica nanospheres assisted by amino acids.* Journal of the American Chemical Society, 2006, 128(42): p. 13664-13665.

41. Hartlen, K.D., Athanasopoulos, A.P.T., and Kitaev, V., *Facile preparation of highly monodisperse small silica spheres (15 to >200 nm) suitable for colloidal templating and formation of ordered arrays.* Langmuir, 2008, 24(5): p. 1714-1720.

42. Batazs, A.C., Emrick, T., and Russell, T.P., *Nanoparticle polymer composites: Where two small worlds meet.* Science, 2006, 314(5802): p. 1107-1110.

43. Schaefer, D.W. and Justice, R.S., *How nano are nanocomposites?* Macromolecules, 2007, 40(24): p. 8501-8517.

44. Zhou, S., Wu, L., Sun, J., and Shen, W., *The change of the properties of acrylic-based polyurethane via addition of nano-silica.* Progress in Organic Coatings, 2002, 45(1): p. 33-42.

45. Wu, C.L., Zhang, M.Q., Rong, M.Z., and Friedrich, K., *Tensile performance improvement of low nanoparticles filled-polypropylene composites.* Composites Science and Technology, 2002, 62(10-11): p. 1327-1340.

46. Ajay K. Manna, P.P.D., D. K. Tripathy,, *Dynamic mechanical properties and hysteresis loss of epoxidized natural rubber chemically bonded to the silica surface.* Journal of Applied Polymer Science, 2002, 84(12): p. 2171-2177.

47. Kickelbick, G., *Concepts for the incorporation of inorganic building blocks into organic polymers on a nanoscale.* Progress in Polymer Science, 2003, 28(1): p. 83-114.

48. Kim, D., Lee, J.S., Barry, C.M., and Mead, J.L., *Effect of fill factor and validation of characterizing the degree of mixing in polymer nanocomposites.* Polymer Engineering and Science, 2007, 47(12): p. 2049-2056.

49. Naka, Y., Komori, Y., and Yoshitake, H., *One-pot synthesis of organo-functionalized monodisperse silica particles in W/O microemulsion and the effect of functional groups on addition into polystyrene.* Colloids & Surfaces A: Phys. Eng. Asp., 2010, 361(1-3): p. 162-168.

50. Palza, H., Vergara, R., and Zapata, P., *Composites of polypropylene melt blended with synthesized silica nanoparticles.* Composites Science & Technology, 2011, 71(4): p. 535-540.

51. Gonzalez-Irun Rodriguez, J., Carreira, P., Garcia-Diez, A., Hui, D., Artiaga, R., and Liz-Marzan, L., *Nanofiller effect on the glass transition of a polyurethane.* Journal of Thermal Analysis & Calorimetry, 2007, 87(1): p. 45-47.

52. Chen, Y., Zhou, S., Yang, H., Gu, G., and Wu, L., *Preparation and characterization of nanocomposite polyurethane.* J Colloid Interface Sci, 2004, 279(2): p. 370-8.

53. Vega-Baudrit, J., Navarro-Bañón, V., Vázquez, P., and Martín-Martínez, J.M., *Addition of nanosilicas with different silanol content to thermoplastic polyurethane adhesives.* International Journal of Adhesion and Adhesives, 2006, 26(5): p. 378-387.

54. Jian, Z., Bao-Ku, Z., and You-Yi, X., *Characterization and dielectric property of polyimide-silica composite films prepared via sol-gel and thermal imidization process*, in *Journal of Materials Science*. 2005, Springer Science & Business Media B.V. p. 2623-2625.

55. Yu, Y.-Y. and Chen, W.-C., *Transparent organic,Äìinorganic hybrid thin films prepared from acrylic polymer and aqueous monodispersed colloidal silica.* Materials Chemistry & Physics, 2003, 82(2): p. 388.

56. Liu, Y.-L., Hsu, C.-Y., Wei, W.-L., and Jeng, R.-J., *Preparation and thermal properties of epoxy-silica nanocomposites from nanoscale colloidal silica.* Polymer, 2003, 44(18): p. 5159.

57. Kang, S., Hong, S.I., Choe, C.R., Park, M., Rim, S., and Kim, J., *Preparation and characterization of epoxy composites filled with functionalized nanosilica particles obtained via sol-gel process.* Polymer, 2001, 42(3): p. 879-887.

58. Szycher, M., *Handbook of Polyurethanes*, 1999, Washington D.C.: CRC Press.

59. Oertel, G., *Polyurethane Handbook*. 2nd ed, 1993, New York: Hanser.

60. *Rubber Technology*, ed. J.S. Dick, 2001, Munich: Hanser.

61. Bayer, O., Rinke, H., Siefken, W., Ortner, L., and Schild, H., in *I.G. Farben*. 1937: German Patent 728 981.

62. Christ, A.E. and Hanford, W.E., in *DuPont*. 1940.

63. *Thermoelastic Elastomers*. 2 ed, ed. G. Holden, 1996, New York: Hanser.

64. Schollenberger, C.S., Scott, H., and Moore, G.R., Rubber World, 1958, 137: p. 549.

65. Drobny, J.G., *Handbook of thermoplastic elastomers*. PDL/Plastics design library; Variation: PDL handbook series., 2007: Norwich, NY : William Andrew Pub.

66. Bhowmick, A.K. and Stephens, H.L., *Handbook of elastomers*. 2nd , rev. and expand ed. Plastics engineering, 2001, New York: M. Dekker. xii, 922 p.

67. *Current Topics in Elastomers Research*, ed. A.K. Bhowmick, 2008, New York: CRC Press Taylor & Francis.

68. *TPE demand to reach 3.1 mmt in 2009.* Rubber World, 2006, 233(5): p. 11-11.

69. Odian, G., *Principles of Polymerization*, 2004, New York: Wiley-Interscience.

70. *Block Copolymers in Nanoscience*, ed. M. Lazzari, G. Liu, and S. Lecommandoux, 2006, Weinheim: Wiley

71. Meier, D.J., *Theory of block copolymers. I. Domain formation in A-B block copolymers.* J. Poly. Sci.: Part C, 1969, 26: p. 81-98.

72. Lee, H.S., Wang, Y.K., and Hsu, S.L., *Spectroscopic analysis of phase separation behavior of model polyurethanes.* Macromolecules, 1987, 20(9): p. 2089-2095.

73. Sheth, J.P., Klinedinst, D.B., Wilkes, G.L., Iskender, Y., and Yilgor, I., *Role of chain symmetry and hydrogen bonding in segmented copolymers with monodisperse hard segments.* Polymer, 2005, 46(18): p. 7317-7322.

74. Clemitson, I., *Castable Polyurethane Elastomers*, 2008: CRC Press Taylor & Francis.

75. Yilgor, I., Wilkes, G.L., and McGrath, J.E., *Poly(urethane-siloxane) copolymers.1. Reaction-kinetics of model systems.* Abstracts of Papers of the American Chemical Society, 1982, 183(MAR): p. 91-POLY.

76. *Thermoplastic ether ester.* Rubber World, 2005, 231(4): p. 73-73.

77. Sheth, J.P., *Investigation of the influence of selected variables on the solid state structure-property behavior of segmented copolymers*, in *Chemical Engineering*. 2004, Virginia Polytechnic Institute and State University.

78. Bonart, R., Morbitzer, L., and Müller, E.H., J. Macromol. Sci., 1974, B9: p. 447.

79. Yilgor, I., Yilgor, E., Guler, I.G., Ward, T.C., and Wilkes, G.L., *FTIR investigation of the influence of diisocyanate symmetry on the morphology development in model segmented polyurethanes.* Polymer, 2006, 47(11): p. 4105-4114.

80. Abouzahr, S., Wilkes, G.L., and Ophir, Z., Polymer, 1982, 23: p. 1077-86.

81. Coleman, M.M. and Painter, P.C., *Hydrogen bonded polymer blends.* Progress in Polymer Science, 1995, 20(1): p. 1-59.

82. DiBottista, G., Gestermann, E., and BrÃ¤uer, W., *Next generation of soft TPUs.* Rubber World, 2004, 231(3): p. 36-38.

83. Yilgor, I. and Yilgor, E., *Structure-morphology-property behavior of segmented thermoplastic polyurethanes and polyureas prepared without chain extenders.* Polymer Reviews, 2007, 47(4): p. 487-510.

84. Bistričić, L., Baranović, G., Leskovac, M., and Bajsić, E.G., *Hydrogen bonding and mechanical properties of thin films of polyether-based polyurethane,Äìsilica nanocomposites.* European Polymer Journal, 46(10): p. 1975-1987.

85. Zhou, H., Chen, Y., Fan, H., Shi, H., Luo, Z., and Shi, B., *The polyurethane/SiO2 nano-hybrid membrane with temperature sensitivity for water vapor permeation.* Journal of Membrane Science, 2008, 318(1-2): p. 71-78.

86. Aso, O., Eguiazábal, J.I., and Nazábal, J., *The influence of surface modification on the structure and properties of a nanosilica filled thermoplastic elastomer.* Composites Science and Technology, 2007, 67(13): p. 2854-2863.

87. Chen, G., Zhou, S., Gu, G., and Wu, L., *Modification of colloidal silica on the mechanical properties of acrylic based polyurethane/silica composites.* Colloids and Surfaces A: Physicochemical and Engineering Aspects, 2007, 296(1-3): p. 29-36.

88. Kim, B.S., Park, S.H., and Kim, B.K., *Nanosilica-reinforced UV-cured polyurethane dispersion.* Colloid and Polymer Science, 2006, 284(9): p. 1067-1072.

89. Chen, G., Zhou, S., Gu, G., Yang, H., and Wu, L., *Effects of surface properties of colloidal silica particles on redispersibility and properties of acrylic-based polyurethane/silica composites.* Journal of Colloid and Interface Science, 2005, 281(2): p. 339-350.

90. Pattanayak, A. and Jana, S.C., *Thermoplastic polyurethane nanocomposites of reactive silicate clays: effects of soft segments on properties.* Polymer, 2005, 46(14): p. 5183-5193.

91. Cho, J.W. and Lee, S.H., *Influence of silica on shape memory effect and mechanical properties of polyurethane-silica hybrids.* European Polymer Journal, 2004, 40(7): p. 1343-1348.

92. Nunes, R.C.R., Fonseca, J.L.C., and Pereira, M.R., *Polymer-filler interactions and mechanical properties of a polyurethane elastomer.* Polymer Testing, 2000, 19(1): p. 93-103.

93. Nunes, R.C.R., Pereira, R.A., Fonseca, J.L.C., and Pereira, M.R., *X-ray studies on compositions of polyurethane and silica.* Polymer Testing, 2001, 20(6): p. 707-712.

94. Tien, Y.I. and Wei, K.H., *Hydrogen bonding and mechanical properties in segmented montmorillonite/polyurethane nanocomposites of different hard segment ratios.* Polymer, 2001, 42(7): p. 3213-3221.

95. Koerner, H., Liu, W., Alexander, M., Mirau, P., Dowty, H., and Vaia, R.A., *Deformation-morphology correlations in electrically conductive carbon nanotube--thermoplastic polyurethane nanocomposites.* Polymer, 2005, 46(12): p. 4405-4420.

96. Chen, T.K., Tien, Y.I., and Wei, K.H., *Synthesis and characterization of novel segmented polyurethane/clay nanocomposites.* Polymer, 2000, 41(4): p. 1345-1353.

97. Chavarria, F. and Paul, D.R., *Morphology and properties of thermoplastic polyurethane nanocomposites: Effect of organoclay structure.* Polymer, 2006, 47(22): p. 7760-7773.

98. Kohls, D.J. and Schaefer, D.W., *Mechanical properties of rubbers reinforced with porcelainite-derived precipitated silica. (cover story).* Rubber World, 2007, 236(1): p. 18-29.

99. Putman, M.C. and Putman, J.B., *The effect of silica dispersion on physical properties. (cover story).* Rubber World, 2006, 233(6): p. 39-44.

100. Thomas, S.S.R., *Rubber nanocomposites: preparation, properties, and applications*, 2010: Singapore ; Hoboken, NJ : John Wiley & Sons.

101. Torró-Palau, A.M., Fernández-García, J.C., César Orgilés-Barceló, A., and Martín-Martínez, J.M., *Characterization of polyurethanes containing different silicas.* International Journal of Adhesion and Adhesives, 2001, 21(1): p. 1-9.

102. Torró-Palau, A., Fernández-García, J.C., Orgilés-Barceló, A.C., Pastor-Blas, M.M., and Martín-Martínez, J., *Structural modification of sepiolite (natural magnesium silicate) by thermal treatment: effect on the properties of polyurethane adhesives.* International Journal of Adhesion and Adhesives, 1997, 17(2): p. 111-119.

103. Jaúregui-Beloqui, B., Fernández-García, J.C., César Orgilés-Barceló, A., Mar Mahiques-Bujanda, M., and Martín-Martínez, J.M., *Rheological properties of thermoplastic polyurethane adhesive solutions containing fumed silicas of different surface areas.* International Journal of Adhesion and Adhesives, 1999, 19(4): p. 321-328.

104. Vega-Baudrit, J., Sibaja-Ballestero, M., Vázquez, P., Torregrosa-Maciá, R., and Miguel Martín-Martínez, J., *Properties of thermoplastic polyurethane adhesives containing nanosilicas with different specific surface area and silanol content.* International Journal of Adhesion and Adhesives, 2007, 27(6): p. 469-479.

105. Daniels, M.W., Sefcik, J., Francis, L.F., and McCormick, A.V., *Reactions of a trifunctional silane coupling agent in the presence of colloidal silica sols in polar media.* Journal of Colloid and Interface Science, 1999, 219(2): p. 351-356.

106. Chang, K.C., Lin, H.F., Lin, C.Y., Kuo, T.H., Huang, H.H., Hsu, S.C., Yeh, J.M., Yang, J.C., and Yu, Y.H., *Effect of amino-modified silica nanoparticles on the corrosion protection properties of epoxy resin-silica hybrid materials.* J Nanosci Nanotechnol, 2008, 8(6): p. 3040-9.

107. Chang, K.-C., Lin, C.-Y., Lin, H.-F., Chiou, S.-C., Huang, W.-C., Yeh, J.-M., and Yang, J.-C., *Thermally and Mechanically Enhanced epoxy resin-silica hybrid materials containing primary amine-modified silica nanoparticles.* Journal of Applied Polymer Science, 2008, 108: p. 1629-1635.

108. Berne, B.J. and Pecora, R., *Dynamic Light Scattering*, 2000: Courier Dover Publications.

109. Mie, G., *Beiträge zur Optik trüber Medien, speziell kolloidaler Metallösungen.* Ann. Phys., 1908, 330: p. 377–445.

110. Malvern ®. *Nanosizer Zeta Manual*. 2012.

111. Pavia, D.L., *Introduction to spectroscopy*. 4th ed, 2009, Belmont, CA: Brooks/Cole, Cengage Learning. xv, 656, 48, 8, 15 p.

112. Jacobsen, N.E., *NMR Spectroscopy Explained: Simplified Theory, Applications and Examples for Organic Chemistry and Structural Biology*, 2007, New Jersey: John Wiley & Sons.

113. Nelson, J.H., *Nuclear magnetic resonance spectroscopy*, 2003, Upper Saddle River, NJ: Prentice Hall. xvi, 464 p.

114. Xu, Y., Wu, D., Sun, Y.H., Gao, H.C., Yuan, H.Z., and Deng, F., *A new study on the kinetics of Stober synthesis by in-situ liquid Si-29 NMR.* Journal of Sol-Gel Science and Technology, 2007, 42(1): p. 13-20.

115. Griffiths, P.R. and de Haseth, J.A., *Fourier Transform Infrared Spectrometry*. 2 ed. Chemical Analysis: A series of monographs on analytical chemistry and applications, ed. J.D. Winefordner, 2007, New Jersey: John Wiley & Sons.

116. Smith, B.C., *Fundamentals of Fourier Transform Infrared Spectroscopy*. 2 ed, 2011: CRC Press.

117. Goldstein, J., *Scanning electron microscopy and X-ray microanalysis : a text for biologists, materials scientists, and geologists*, 1981, New York: Plenum Press. xiii, 673 p.

118. Williams, D.B.C.C.B., *Transmission electron microscopy a textbook for materials science*. 2nd ed, 2009: New York : Springer.

119. Tomczak, N. and Goh, K.E.J., *Scanning probe microscopy*: Singapore ; Hackensack, NJ : World Scientific Pub. Co.

120. Höhne, G., Hemminger, W.F., and Flammersheim, H.-J., *Differential Scanning Calorimetry*, 2003, Heidelberg: Springer.

121. Sepe, M.P., *Thermal analysis of polymers*. Rapre Review Reports, 1997: Rapra Technology Ltd.

122. Davis, J.R., *Tensile testing*. 2nd ed, 2004: Materials Park, Ohio : ASM International.

123. Fischer-Cripps, A.C., *Nanoindentation*. 2rd ed. Mechanical engineering series, 2004, New York: Springer.

124. Andrade-Espinosa, G., Escobar-Barrios, V., and Rangel-Mendez, R., *Synthesis and characterization of silica xerogels obtained via fast sol-gel process.* Colloid and Polymer Science, 2010, 288(18): p. 1697-1704.

125. Perullini, M., Jobbagy, M., Bilmes, S.A., Torriani, I.L., and Candal, R., *Effect of synthesis conditions on the microstructure of TEOS derived silica hydrogels synthesized by the alcohol-free sol-gel route.* Journal of Sol-Gel Science and Technology, 2011, 59(1): p. 174-180.

126. Zhang, H.N., Zhao, Y., and Akins, D.L., *Synthesis and new structure shaping mechanism of silica particles formed at high pH.* Journal of Solid State Chemistry, 2012, 194: p. 277-281.

127. Zhao, B.B., Tian, C.H., Zhang, Y., Tang, T., and Wang, F.Y., *Size control of monodisperse nonporous silica particles by seed particle growth.* Particuology, 2011, 9(3): p. 314-317.

128. Tan, C.G., Bowen, B.D., and Epstein, N., *Production of monodisperse colloidal silica spheres: Effect of temperature.* Journal of Colloid and Interface Science, 1987, 118(1): p. 290-293.

129. Bernards, T.N.M., Janssen, M., and Vanbommel, M.J., *Influence of butanol on the hydrolysis condensation behavior of teos.* Journal of Non-Crystalline Solids, 1994, 168(3): p. 201-212.

130. Bernards, T.N.M., Vanbommel, M.J., and Boonstra, A.H., *Hydrolysis - condensation processes of the tetra-alkoxysilanes tpos, teos and tmos in some alcoholic solvents.* Journal of Non-Crystalline Solids, 1991, 134(1-2): p. 1-13.

131. Brinker, C.J., Keefer, K.D., Schaefer, D.W., Assink, R.A., Kay, B.D., and Ashley, C.S., *Sol-gel transition in simple silicates .2.* Journal of Non-Crystalline Solids, 1984, 63(1-2): p. 45-59.

132. Yamane, M., Inoue, S., and Yasumori, A., *Sol-gel transition in the hydrolysis of silicon methoxide.* Journal of Non-Crystalline Solids, 1984, 63(1-2): p. 13-21.

133. Hasegawa, I. and Sakka, S., *Trans-esterification reaction of tetreethoxysilane and butyl alcohols.* Bulletin of the Chemical Society of Japan, 1988, 61(11): p. 4087-4092.

134. Lim, J., Ha, S.W., and Lee, J.K., *Precise size-control of silica nanoparticles via alkoxy exchange equilibrium of tetraethyl orthosilicate (TEOS) in the mixed alcohol solution.* Bulletin of the Korean Chemical Society, 2012, 33(3): p. 1067-1070.

135. Sefcik, J. and McCormick, A.V., *Kinetic and thermodynamic issues in the early stages of sol-gel processes using silicon alkoxides.* Catalysis Today, 1997, 35(3): p. 205-223.

136. Aelion, R., Loebel, A., and Eirich, F., *Hydrolysis of ethyl silicate*.* Journal of the American Chemical Society, 1950, 72(12): p. 5705-5712.

137. Byers, C.H., Harris, M.T., and Williams, D.F., *Controlled microcrystalline growth studies by dynamic laser-light-scattering methods.* Industrial & Engineering Chemistry Research, 1987, 26(9): p. 1916-1923.

138. Boukari, H., Long, G.G., and Harris, M.T., *Polydispersity during the formation and growth of the Stöber silica particles from small-angle X-ray scattering measurements.* Journal of Colloid and Interface Science, 2000, 229(1): p. 129-139.

139. Fyfe, C.A. and Aroca, P.P., *Quantitative kinetic analysis by high-resolution 29Si NMR spectroscopy of the initial stages in the sol-gel formation of silica gel from tetraethoxysilane.* Chemistry of Materials, 1995, 7(10): p. 1800-1806.

140. Kimber, B.J. and Harris, R.K., *Measurement of spin-lattice relaxation-times in null-signal case.* Journal of Magnetic Resonance, 1974, 16(2): p. 354-356.

141. Rousseau, F., Poinsignon, C., Garcia, J., and Popall, M., *Polycondensation of aminosilanes in methanol.* Chemistry of Materials, 1995, 7(5): p. 828-839.

142. Bredereck, K., Effenberger, F., and Tretter, M., *Preparation and characterization of silica aquasols.* Journal of Colloid and Interface Science, 2011, 360(2): p. 408-414.

143. Harris, M.T., Brunson, R.R., and Byers, C.H., *The base-catalyzed hydrolysis and condensation reactions of dilute and concentrated TEOS solutions.* Journal of Non-Crystalline Solids, 1990, 121(1-3): p. 397-403.

144. Van Blaaderen, A., Van Geest, J., and Vrij, A., *Monodisperse colloidal silica spheres from tetraalkoxysilanes: Particle formation and growth mechanism.* Journal of Colloid and Interface Science, 1992, 154(2): p. 481-501.

145. in *CRC Handbook of Chemistry and Physics*, D.R. Lide, Editor. 2010. p. 6-148.

146. Sadasivan, S., Dubey, A.K., Li, Y.Z., and Rasmussen, D.H., *Alcoholic solvent effect on silica synthesis - NMR and DLS investigation.* Journal of Sol-Gel Science and Technology, 1998, 12(1): p. 5-14.

147. Park, J.S., Hah, H.J., Koo, S.M., and Lee, Y.S., *Effect of alcohol chain length on particle growth in a mixed solvent system.* Journal of Ceramic Processing Research, 2006, 7(1): p. 83-89.

148. Peace, B.W., Mayhan, K.G., and Montle, J.F., *Polymers from the hydrolysis of tetraethoxysilane.* Polymer, 1973, 14(9): p. 420-422.

149. Chen, K.C., Tsuchiya, T., and Mackenzie, J.D., *Sol-gel processing of silica .1. The role of the starting compounds.* Journal of Non-Crystalline Solids, 1986, 81(1-2): p. 227-237.

150. Xu, Y., Liu, R.L., Wu, D., Sun, Y.H., Gao, H.C., Yuan, H.Z., and Deng, F., *Ammonia-catalyzed hydrolysis kinetics of mixture of tetraethoxysilane with methyltriethoxysilane by Si-29 NMR.* Journal of Non-Crystalline Solids, 2005, 351(30-32): p. 2403-2413.

151. Hansen, C.M., *The universality of the solubility parameter.* Ind. Eng. Chem. Prod. Res. Dev., 1969, 8(1): p. 2-11.

152. Barton, A.F.M., *Handbook of Solubility Parameters*, 1983: CRC Press.

153. Yao, K.J., Song, M., Hourston, D.J., and Luo, D.Z., *Polymer/layered clay nanocomposites: 2 polyurethane nanocomposites.* Polymer, 2002, 43(3): p. 1017-1020.

154. Paul, D.R. and Robeson, L.M., *Polymer nanotechnology: Nanocomposites.* Polymer, 2008, 49(15): p. 3187-3204.

155. Pham, J.Q., Mitchell, C.A., Bahr, J.L., Tour, J.M., Krishanamoorti, R., and Green, P.F., *Glass transition of polymer/single-walled carbon nanotube composite films.* Journal of Polymer Science Part B: Polymer Physics, 2003, 41(24): p. 3339-3345.

156. Luong, N.D., Hippi, U., Korhonen, J.T., Soininen, A.J., Ruokolainen, J., Johansson, L.-S., Nam, J.-D., Sinh, L.H., and Seppala, J., *Enhanced mechanical and electrical properties of polyimide film by graphene sheets via in situ polymerization.* Polymer, 2011, 52(23): p. 5237-5242.

157. Dan, C.H., Lee, M.H., Kim, Y.D., Min, B.H., and Kim, J.H., *Effect of clay modifiers on the morphology and physical properties of thermoplastic polyurethane/clay nanocomposites.* Polymer, 2006, 47(19): p. 6718-6730.

158. Zha, W., Han, C.D., Moon, H.C., Han, S.H., Lee, D.H., and Kim, J.K., *Exfoliation of organoclay nanocomposites based on polystyrene-block-polyisoprene-block-poly(2-vinylpyridine) copolymer: Solution blending versus melt blending.* Polymer, 2010, 51(4): p. 936-952.

159. Saeed, K., Park, S.-Y., Lee, H.-J., Baek, J.-B., and Huh, W.-S., *Preparation of electrospun nanofibers of carbon nanotube/polycaprolactone nanocomposite.* Polymer, 2006, 47(23): p. 8019-8025.

160. Yilgor, E., Burgaz, E., Yurtsever, E., and Yilgor, I., *Comparison of hydrogen bonding in polydimethylsiloxane and polyether based urethane and urea copolymers.* Polymer, 2000, 41(3): p. 849-857.

161. Das, S., Cox, D.F., Wilkes, G.L., Klinedinst, D.B., Yilgor, I., Yilgor, E., and Beyer, F.L., *Effect of symmetry and H-bond strength of hard segments on the structure-property relationships of segmented, nonchain extended polyurethanes and polyureas.* Journal of Macromolecular Science Part B-Physics, 2007, 46(5): p. 853-875.

162. Lee, S., *Thermoplastic polyurethane markets in the EU: Production, Technology, Applications and Trends* 1998, UK: Rapra Technology Limited.

163. Choi, W.J., Kim, S.H., Jin Kim, Y., and Kim, S.C., *Synthesis of chain-extended organifier and properties of polyurethane/clay nanocomposites.* Polymer, 2004, 45(17): p. 6045-6057.

164. Potschke, P., Haussler, L., Pegel, S., Steinberger, R., and Scholz, G., *Thermoplastic polyurethane filled with carbon nanotubes for electrical dissipative and conductive applications.* Kgk-Kautschuk Gummi Kunststoffe, 2007, 60(9): p. 432-437.

165. Russo, P., Acierno, D., and Spena, P., *Rheological behaviour, mechanical properties and morphological aspects of thermoplastic polyurethane reinforced with multiwalled carbon nanotubes*, in *5th International Conference on Times of Polymers Top and Composites*, A. Damore, D. Acierno, and L. Grassia, Editors, Amer Inst Physics: Melville. p. 168-171.

166. Hunley, M.T., Potschke, P., and Long, T.E., *Melt dispersion and electrospinning of non-functionalized multiwalled carbon nanotubes in thermoplastic polyurethane.* Macromolecular Rapid Communications, 2009, 30(24): p. 2102-2106.

167. Barick, A.K. and Tripathy, D.K., *Preparation and characterization of carbon nanofiber reinforced thermoplastic polyurethane nanocomposites.* Journal of Applied Polymer Science, 124(1): p. 765-780.

168. Powers, D.S., Vaia, R.A., Koerner, H., Serres, J., and Mirau, P.A., *NMR characterization of low hard segment thermoplastic polyurethane/carbon nanofiber composites.* Macromolecules, 2008, 41(12): p. 4290-4295.

169. Jauregui-Beloqui, B., Fernandez-Garcia, J.C., Orgiles-Barcelo, A.C., Mahiques-Bujanda, M.M., and Martin-Martinez, J.M., *Thermoplastic polyurethane-fumed silica composites: influence of the specific surface area of fumed silica on the viscoelastic and adhesion properties.* Journal of Adhesion Science and Technology, 1999, 13(6): p. 695-711.

170. Petrovic, Z.S., Javni, I., Waddon, A., and Banhegyi, G., *Structure and properties of polyurethane-silica nanocomposites.* Journal of Applied Polymer Science, 2000, 76(2): p. 133-151.

171. Petrovic, Z.S., Javni, I., Waddon, A., and Soc Plast, E., *Polyurethane elastomers with nano-fillers*. Conference Proceedings at Antec '98: Plastics on My Mind, Vols I-3: Vol I; Processing, Vol Ii; Special Areas, Vol Iii; Materials. Vol. 44, 1998. 2390-2393.

172. Javni, I., Zhang, W., Karajkov, V., Petrovic, Z.S., and Divjakovic, V., *Effect of nano- and micro-silica fillers on polyurethane foam properties.* Journal of Cellular Plastics, 2002, 38(3): p. 229-239.

173. Gerard, J.F., Kaddami, H., and Pascault, J.P. Proceedings Eurofillers 97, . Vol. 97, 1997, Manchester.

174. Garrett, J.T., Siedlecki, C.A., and Runt, J., *Microdomain Morphology of Poly(urethane urea) multiblock copolymers.* Macromolecules, 2001, 34(20): p. 7066-7070.

175. McLean, R.S. and Sauer, B.B., *Tapping-Mode AFM Studies Using Phase Detection for Resolution of Nanophases in Segmented Polyurethanes and Other Block Copolymers.* Macromolecules, 1997, 30(26): p. 8314-8317.

176. Desper, C.R., Schneider, N.S., Jasinski, J.P., and Lin, J.S., *Deformation of microphase structures in segmented polyurethanes.* Macromolecules, 1985, 18(12): p. 2755-2761.

177. Lee, S.-I., Hahn, Y.B., Nahm, K.S., and Lee, Y.-S., *Synthesis of polyether-based polyurethane-silica nanocomposites with high elongation property.* Polymers for Advanced Technologies, 2005, 16(4): p. 328-331.

178. Hu, C.B., Ward, R.S., and Schneider, N.S., *A new criterion of phase separation: The effect of diamine chain extenders on the properties of polyurethaneureas.* Journal of Applied Polymer Science, 1982, 27(6): p. 2167-2177.

179. Sadeghi, M., Semsarzadeh, M.A., Barikani, M., and Ghalei, B., *Study on the morphology and gas permeation property of polyurethane membranes.* Journal of Membrane Science, 2011, 385(1-2): p. 76-85.

180. Xu, Y.J., Petrovic, Z., Das, S., and Wilkes, G.L., *Morphology and properties of thermoplastic polyurethanes with dangling chains in ricinoleate-based soft segments.* Polymer, 2008, 49(19): p. 4248-4258.

181. Huang, S.L. and Lai, J.Y., *Gas-permeability of cross-linked HTPB-H(12)MDI-based polyurethane membrane.* Journal of Applied Polymer Science, 1995, 58(10): p. 1913-1923.

182. Jafarzadeh, M., Rahman, I.A., and Sipaut, C.S., *Synthesis of silica nanoparticles by modified sol-gel process: the effect of mixing modes of the reactants and drying techniques.* Journal of Sol-Gel Science and Technology, 2009, 50(3): p. 328-336.

183. Jeon, H.T., Jang, M.K., Kim, B.K., and Kim, K.H., *Synthesis and characterizations of waterborne polyurethane-silica hybrids using sol-gel process.* Colloids and Surfaces a-Physicochemical and Engineering Aspects, 2007, 302(1-3): p. 559-567.

184. Kim, B.K., Seo, J.W., and Jeong, H.M., *Properties of waterborne polyurethane/nanosilica composite.* Macromolecular Research, 2003, 11(3): p. 198-201.

185. Bistri*ƒçiƒá*, L., Baranovi*ƒá*, G., Leskovac, M., and Bajsi*ƒá*, E.G., *Hydrogen bonding and mechanical properties of thin films of polyether-based polyurethane,Äìsilica nanocomposites.* European Polymer Journal, 46(10): p. 1975-1987.

186. Greenwood, J.A. and Williamson, J.B.P., *Contact of nominally flat surfaces.* Proceedings of the Royal Society of London. Series A. Mathematical and Physical Sciences, 1966, 295(1442): p. 300-319.

187. Tanaka, K., *Elastic/plastic indentation hardness and indentation fracture toughness: The inclusion core model.* Journal of Materials Science, 1987, 22(4): p. 1501-1508.

188. Yilgor, E., Eynur, T., Kosak, C., Bilgin, S., Yilgor, I., Malay, O., Menceloglu, Y., and Wilkes, G.L., *Fumed silica filled poly(dimethylsiloxane-urea) segmented copolymers: Preparation and properties.* Polymer, 2011, 52(19): p. 4189-4198.

189. Yilgor, I., Burgaz, E., Metin, B., Yurtsever, E., and Yilgor, E., *Influence of competitive hydrogen bonding between hard and soft segments on the properties of siloxane and polyether-based segmented copolymers.* Abstracts of Papers of the American Chemical Society, 1999, 218: p. 341-POLY.

190. Madathingal, R.R. and Wunder, S.L., *Confinement Effects of Silica Nanoparticles with Radii Smaller and Larger than R-g of Adsorbed Poly(ethylene oxide).* Macromolecules, 2011, 44(8): p. 2873-2882.

191. Waddon, A.J. and Petrovic, Z.S., *Spherulite crystallization in poly(ethylene oxide)-silica nanocomposites. Retardation of growth rates through reduced molecular mobility.* Polymer Journal, 2002, 34(12): p. 876-881.

192. Yilgor, I. and Yilgor, E., *Hydrophilic polyurethaneurea membranes: influence of soft block composition on the water vapor permeation rates.* Polymer, 1999, 40(20): p. 5575-5581.